Synthesis and Characterization of Polymers, and Development of Polymer Based Lipid-Nanodiscs

by

Nathaniel Zachary Hardin

A dissertation submitted in partial fulfillment
of the requirements for the degree of
Doctor of Philosophy
(Chemistry)
in the University of Michigan
2020

Doctoral Committee:

Professor Ayyalusamy Ramamoorthy, Chair
Professor Ryan Bailey
Assistant Professor Aaron Frank
Professor Adam Matzger
Assistant Professor Kevin Wood

Nathaniel Zachary Hardin

nathardi@umich.edu

ORCID iD: 0000-0002-4445-7956

Dedication

To Raeann, Leann, Graceann, Sheila, and Michael Hardin.

Acknowledgements

I would first like to thank my family for all the support they have given me. I would like to mention my three sisters, Raeann, Graceann, and my twin Leann. Their support and love has been a Godsend during my long graduate hours. I enjoyed the weekend game nights we were able to have together during my time here which provided great relief.

I would like to also extend my thanks to my father who started me at a young age learning about history and science. While when I was younger I may not have appreciated the "turn off the cartoons and put on X historical/science documentary", and the "get off the TV and help me with the car", both have proven instrumental at giving me the learning interests and mechanical skills that I have been able to use and appreciate thought my graduate career.

My mother has also provided me with support and love in excess of what was required. I am so thankful for your love and the wonderful support you have provided me. You and dad have been a positive force in my life and have provided a tremendous and wonderful area of my life for which I am grateful.

My graduate career would never have started without the advice and tutelage from my first academic advisor from undergrad, Professor Christine Chow. Without her lab and the amazing scientific role model she provided I would have never considered a furthering my studies in science and I would like to thank her for all the support she provided me.

Rams I would like to thank you for the opportunity to work in your group. Working in your group has given me an excellent environment of learning and support. I would also like to

thank you for your patience (I know it was hard at times) throughout my career and the growth I have gained through my research under you.

To all my friends, I have made in grad school (Adam, John, Kori, Andy, Ron, Brad, and Ted) a thank you for your help and support and I will miss our time together. Also to the Rams lab I would like to thank you for your support and putting up with me all these years.

Finally I would like to thank my partner in research Thiru. You were the best postdoc I could have asked for when I joined the Rams group. I thank you for your guidance as I moved from the beginning of the project to the growth into new areas. I will miss working with you on science and I believe as a scientist and partner you will never be beaten.

Table of Contents

List of Figures

List of Abbreviations

AFM	atomic force microscopy
butyl-PAA	butyl containing polyacrylic acid
CP-MAS	cross polarization – magic angle spinning
CD	circular dichroism
DLS	dynamic light scattering
DMPC	1,2-dimyristoyl-*sn*-glycero-3-phosphocholine
DNA	deoxyribonucleic acid
DOTA	1,4,7,10-Tetraazacyclododecane-1,4,7,10-tetraacetic acid
DSC	differential scanning calorimetry
FID	free induction decay
FT-IR	Fourier transform – infrared
hexyl-PAA	hexyl containing polyacrylic acid
HPLC	high performance liquid chromatography
Mn	number average molecular weight
MSP	membrane scaffold protein
Mw	weight average molecular weight
neopentyl-PAA	neopentyl containing polyacrylic acid
NMR	nuclear magnetic resonance
PAA	polyacrylic acid
PDI	polydispersity index

pentyl-PAA	pentyl containing polyacrylic acid
PRE	paramagnetic relaxation enhancement
RDC	residual dipolar coupling
SANS	small angle neutron scattering
SAXS	small angle x-ray scattering
SEC	size exclusion chromatography
SLS	static light scattering
SMA	styrene maleic acid
SMAd-A	styrene maleimide amine
SMA-EA	styrene maleic acid – ethanolamine
SMA-EA-DOTA	styrene maleic acid – ethanolamine 1,4,7,10-Tetraazacyclododecane-1,4,7,10-tetraacetic acid
SMA-ED	styrene maleic acid – ethylenediamine
SMALP	styrene maleic acid lipoparticle
SMAnh	styrene maleic anhydride
SMA-QA	styrene maleimide quaternary ammonium
SS-NMR	solid state nuclear magnetic resonance
STD	saturation transfer difference
T_1	spin-lattice relaxation time
T_2	spin-spin relaxation time
TEM	transmission electron microscopy
TFA	trifluoroacetic acid
UV	ultraviolet

Abstract

There is substantial interest in the development of membrane mimetics for use in membrane protein studies. Membrane proteins require a native like membrane environment for the study of their structure, dynamics, and function. This requirement of a membrane environment leads to some key challenges in their research. Membrane proteins can be insoluble in water without a lipid bilayer causing their research by the most common biophysical techniques (NMR, UV absorption, CD, etc.) to be nearly untenable. Common solubilization techniques such as detergents frequently disrupt the structure of the membrane proteins causing the study of membrane proteins, within detergent micelles, to be based on extensive experimental trials. To alleviate this problem various membrane mimetics for the solubilization and study of membrane proteins have been developed such as liposomes, bicelles, and nanodiscs. Nanodiscs are the newest of the field of membrane mimetics. Nanodiscs are discs shaped lipid bilayers surrounded by amphiphilic molecules such as proteins, peptides, or polymers. The protein and peptide based nanodiscs have been shown to be very useful in solubilization of membrane proteins however they have some significant drawbacks. Protein based nanodiscs still require detergents during the protein reconstitution process, have minimum size control, and have interfering spectral properties. Peptide nanodiscs are more versatile that protein based nanodiscs due to their size control and easier production, however they also have limited functionalization potential and still have disruptive spectral properties.

Polymers that assemble into lipid nanodiscs with membranes have been shown to be useful in forming a native like membrane mimetic. This is demonstrated by their ability to self-

assemble into a native like membrane environment, and their ability to extract membrane proteins from cellular membranes without the use of detergents. To achieve the formation of polymer-lipid nanodiscs the polymer with the proper characteristics must be used.

The focus on this thesis is on the development of polymers with various hydrophobic and hydrophilic modifications. The change of hydrophilic moieties into positive or zwitterionic charged polymers allowed for tunability of the nanodiscs solubilization stability. While the addition of an amino group as the hydrophilic moiety performed as expected, the zwitterionic form of the polymer precipitated from solution at neutral pH due to charge-charge interactions. This work was further expounded upon and a polymer with a quaternary ammonium hydrophilic group was developed. Polymer containing a quaternary ammonium (SMA-QA) showed solubilization stability in all biological relevant pH and metal ion conditions. Nanodiscs formed using SMA-QA also showed size control and mono-dispersion. While SMA-QA polymer nanodiscs were demonstrated to have a higher solubilization stability as compared to other polymers used to form nanodiscs, challenges still remain. SMA-QA polymers still are not applicable with membrane proteins with an overall opposite charge. The charge-charge attraction of SMA-QA (+) or SMA-EA (-) with opposing charged proteins causes inactivation of the incompatible system. Because of this more work on the development of non-ionic polymers is required.

The functionalization of a low molecular weight polyacrylic acid (PAA) with various anime hydrophobic groups that enabled the study and optimization of hydrophobic groups with regards to polymer-lipid nanodiscs formation were also investigated. The addition of several different hydrophobic groups to the PAA backbone showed that the hydrophobic group chosen had a large effect on the nanodiscs formation. Using butyl as the hydrophobic portion of the

nanodisc forming polymer cause a large decrease in nanodiscs forming ability due to the lower amount of amphiphilicity of the polymer. Upon the addition of the bulkier neopentyl or hexyl hydrophobic groups to the PAA the polymer was able to form nanodiscs, however because of the bulkiness of the neopentyl or hexyl groups the resulting nanodiscs' lipid bilayer exhibit a large disruption. The Pentyl-PAA nanodiscs were shown to be the optimized hydrophobic modified PAA polymer with the solubilization power needed to form nanodiscs with the minimum lipid bilayer disruption. These findings show that the addition of various hydrophobic groups does greatly affect the stability of the resulting polymer-lipid nanodiscs.

Finally the development of a novel Cu^{2+} chelated polymer for use in paramagnetic relaxation enhancement NMR studies is shown. NMR is an inherently low sensitivity technique which commonly requires isotopic labeling or long NMR acquisition times to achieve an adequate signal to noise ratio. Long NMR times however can lead to a variety of issues due to biomolecule instability. Paramagnetic relaxation enhancement (PRE) is one of the various methods that can lower the NMR experimental time. PRE uses unpaired electrons from either metal ions (in this case Cu^{2+}) or free radicals to increase the T1 relaxation rate of the nuclei of interest. By increasing the T1 relaxation rate PRE can decrease the recycle delay between scans, thereby allowing for the acquisition of more scans in the same amount of time. To achieve this for polymer nanodiscs a facile addition of an amino-DOTA to the SMA polymer was developed. This addition of DOTA to SMA-EA did not significantly affect the polymer solubilization properties, but it did allow for the chelation of Cu^{2+}. The reported metal chelated polymer was able to form polymer-lipid nanodiscs. We showed this metal-polymer system significantly increased the T_1 relaxation rate of protons of the polymer, lipid, and (proof of concept) DNA. The resulting polymer nanodiscs-PRE system is an exciting potential tool for fast NMR

applications. This research was supported by funds from NIH (GM084018 to A.R.).

Chapter 1 Introduction

Portions of this chapter are reproduced from: T. Ravula, N. Z. Hardin, G. M. Di Mauro, A. Ramamoorthy, European Polymer Journal 2018, 108, 597-602,

1.1 Importance and Challenges of Membrane Proteins

Proteins represent one of the basic building blocks necessary for life. While the study of proteins dates back to their first naming in 1838 the field has nonetheless exploded into becoming one of the most important fields in science and medicine.[1] One particularly important and notoriously difficult class of proteins that are being studied today are known as membrane proteins. Membrane proteins are a diverse group of proteins that play an intricate role in cellular homeostasis,[2] signaling,[3,4] membrane shuttling,[5] and drug metabolism.[6,7] While most organisms have 20-30% of their genome dedicated to membrane protein expression,[8-10] and 60% of drug

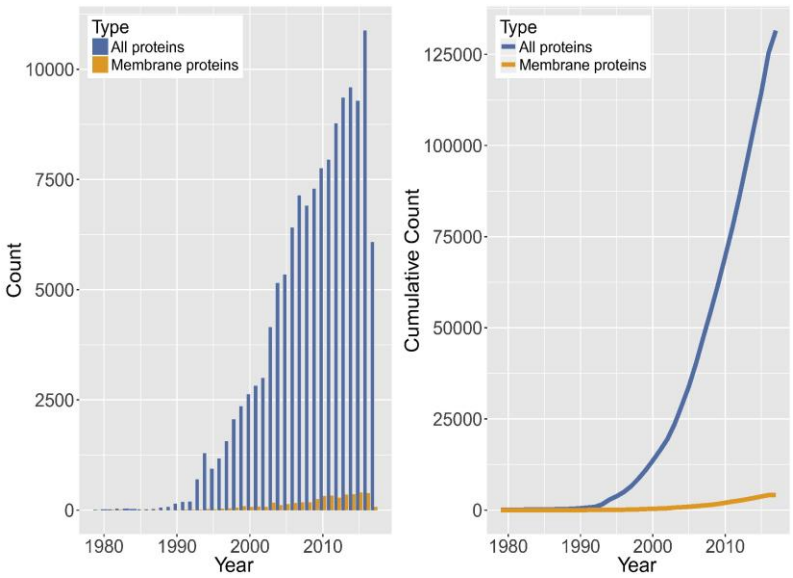

Figure 1-1: Number of PDB entries by year (Left). Total cumulative number of PDB entries (Right) by 2017. Reproduced from reference 14.

targets are membrane proteins in humans,[11,12] membrane proteins only represent only a fraction of solved atomic level protein structures (**Figure 1-1**) leaving a severe gap in our understanding.[13,14] This gap in our understanding is due to the hydrophobic nature of membrane proteins, which is necessary for their incorporation into the membrane, but also make them insoluble in water.[9] Because of this lack of structural understanding, and due to the majority of drugs targeting membrane proteins, there has been a hindrance in structural/drug relationship studies. To tackle the problem of the deficiency of knowledge of membrane proteins' structure, various types of membrane protein solubilization techniques have been developed.

1.2 Membrane Protein Solubilization Techniques

Because of membrane proteins innate lipophilicity, researchers have had to develop different systems that allows for the stable solubilization of membrane proteins for characterization and study. One common solubilization technique employed is the use of detergents. Detergents

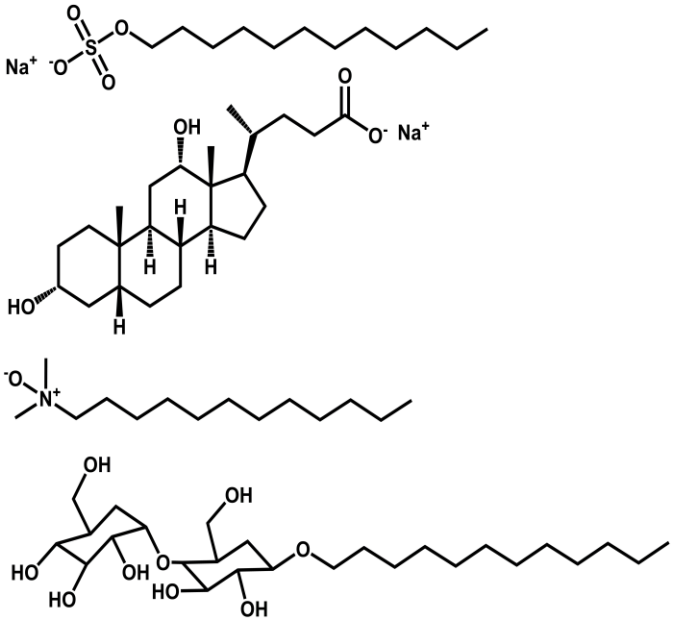

Figure 1-2 Structure of different common detergents from top to bottom: sodium dodecyl sulfate, sodium deoxycholate, n-dodecyl-N,N-dimethylamine-N-oxide, and n-dodecyl-β-D-maltoside.

are amphiphilic molecules that consist of a hydrophilic head group and a hydrophobic tail which at specific concentrations in water form micelles with the hydrophobic tales oriented inside and the hydrophilic heads oriented outside.[15] These detergents have grown to encompass a variety of molecules with a diversity of both hydrophobic and hydrophilic chemical moieties.[15] For perspective, some of the common detergents used are anionic sodium dodecyl sulfate, the bile salt, sodium deoxycholate, zwitterionic n-dodecyl-N,N-dimethylamine-N-oxide, and nonionic n-dodecyl-β-D-maltoside (**Figure 1-2**).[15] While many detergents have different molecular structures, they exhibit a similar mechanism to membrane protein solubilization. In short detergents extract a membrane protein by associating and hydrophobically inserting into the lipid bilayer. Upon insertion the detergent molecules solubilizes the lipid bilayer, and extracts and solubilizes the membrane proteins by association of the detergent hydrophobic tails with the hydrophobic regions of the membrane proteins.[16] Even though detergents have proven useful in a variety of studies, and have been shown to be able to solubilize membrane proteins for structural characterization and crystallization,[17] detergents are also denaturing. Because the hydrophobic tails directly interact with the hydrophobic regions of the membrane proteins, detergents frequently cause structural denaturing effects and thereby causes the membrane proteins to enter an inactive state less useful for characterization.[17]

To circumvent this problem a common membrane mimetic used in membrane protein research is the liposome.[18,19] Liposomes are vesicles that consist of lipids that spontaneously assembled into a bilayer (**Figure 1-3 A**). These are advantageous over detergents as the liposomal bilayer closely resembles the cellular membrane environment as compared to a detergent micelle.[17] The major drawback of liposomes as a membrane mimetic is their relative instability, their limited use in various biophysical characterization techniques, and the need for detergent inclusion in the

extraction process of membrane proteins.[20] Another common membrane mimetic used to study membrane proteins are bicelles,[21-24] which are disc-shaped phospholipid bilayers surrounded by a rim containing short chained detergent molecules. The advantages of bicelles over liposomes are that bicelles have no membrane curvature, higher stability, and size tunability. Particularly, the size tunability is achieved by changing the ratio of lipid to detergent (q-ratio).[25] By controlling the q-ratio, bicelles have been shown to align in the presence of a magnetic field at larger sizes (q>2.5). These large bicelles are anisotropic as they do not tumble fast enough in the NMR time scale.[26] Bicelles have also been used for solution NMR studies when formed at lower sizes (q < 0.5; also known as isotropic bicelles).[27,28] While advantageous over liposomes, bicelles still have the crucial problem of including detergents during the reconstitution of membrane proteins. The detergent molecules present in bicelles undergo diffusion from the rim to the planar lipid bilayer and also present in the form of toroidal pores within the planar lipid bilayer of the Bicelles.[29] The ability of the detergent molecule to diffuse into the lipid bilayer can denature an embedded protein.[16] To overcome these challenges researchers have developed nanodiscs to better simulate a native-like membrane environment for membrane protein research (**Figure 1-3 B**).[30]

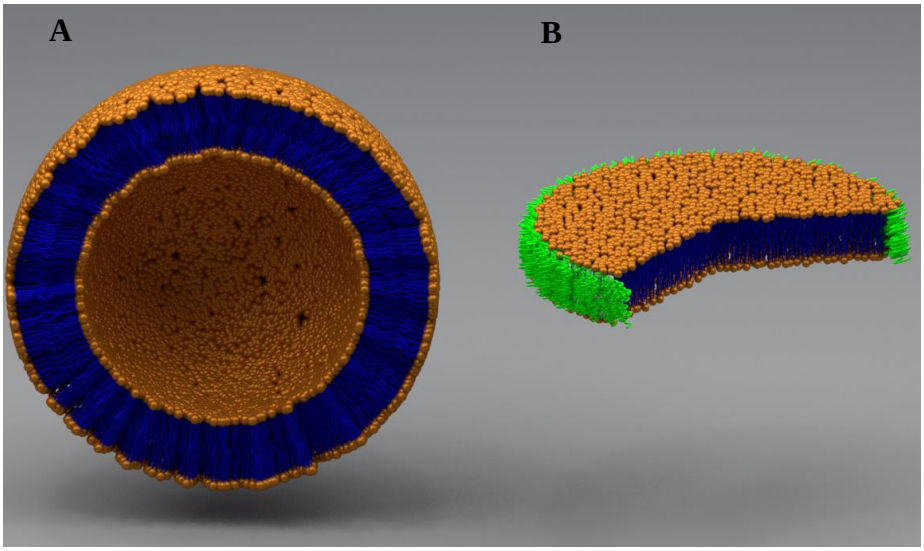

Figure 1-3: Model of a liposome (**A**) and nanodisc (**B**) shown.

1.3 Curvature-free lipid nanodiscs enabled structural studies of membrane proteins

Introduced by Sligar and co-workers in 2002, nanodiscs are non-covalent nanoparticles that consist of a disc shaped lipid bilayer stabilized by an amphiphilic membrane scaffold protein (MSP) that was inspired from high density lipid particles.[32] MSP nanodiscs can be made by mixing MSPs with detergent-solubilized protein and lipid.[28] Scaffold protein nanodiscs have been very successful in the study of several membrane proteins[30-38] and amyloid proteins.[39,40] The curvature-free nanodiscs have been demonstrated to be highly valuable to understand amyloid aggregation mechanism and to trap amyloid oligomers for high-resolution NMR based structural studies.[37] However, the process of incorporating proteins into MSP nanodiscs still requires the use of detergents during the reconstitution process.[28] MSP based nanodiscs also introduce interfering spectral properties during the study of reconstituted membrane proteins. Even though very recent studies reported the possibility of increasing the size of MSP-based nanodiscs,[34] which are otherwise small (typically <15 nm diameter), there are difficulties in reconstituting large-size membrane proteins or protein-protein complexes. Some of these difficulties have been overcome using short amphipathic peptides engineered from the MSP protein.[41,42] These peptides have been shown to self-assemble with lipids to form nanodiscs and enable the reconstitution of protein-protein complexes. These nanodiscs undergo collision and exchange lipid contents as demonstrated by a recent study using high-speed AFM and ^{31}P NMR experiment.[43-45] The peptide-based nanodiscs are useful for structural studies of membrane proteins using solution NMR,[39] SAXS,[46] solid-state NMR,[47] and also used for potential cancer immunotherapy.[48,49] While peptide-based nanodiscs are increasingly used, their interference with biophysical studies of the embedded protein of interest and other potential undesired effects for in-vivo applications are inherent limitations for further biological and biomedical applications. Therefore, to overcome these

limitations, there is significant interest in the development of different types of amphipathic molecules that can form nanodiscs.

1.4. Polymer based lipid-nanodiscs

Poly(Styrene-co-Maleic Acid), SMA, is an amphiphilic polymer that is obtained by hydrolyzation of the poly(Styrene-co-Maleic Anhydride) (**Figure 1-4)**, SMAnh.[50-52] SMA based nanodiscs are a promising technology that can be used for isolation, purification, structural and functional characterization of membrane proteins.[49,53] In 2009 SMA-lipid particles (SMALPs) were first reported to have the ability to form nanodiscs.[54] SMA also allows the direct extraction of

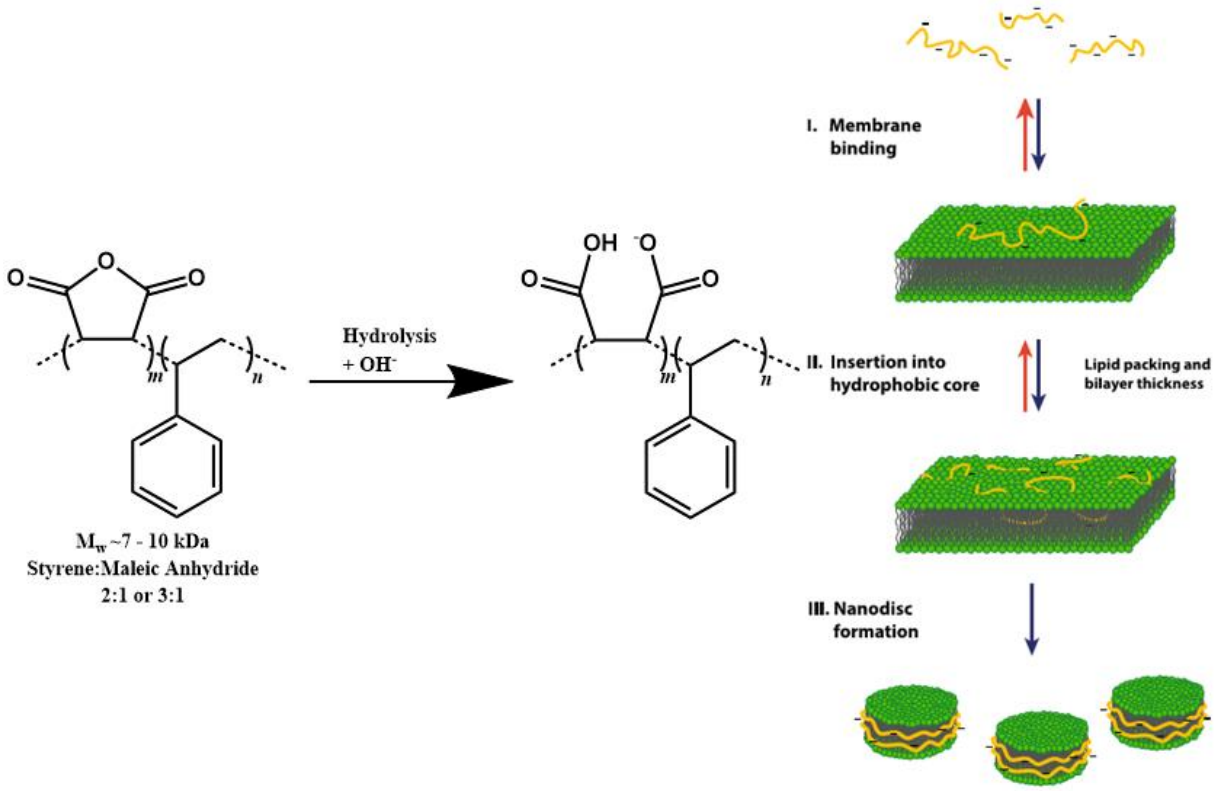

Figure 1-4: Left – Schematic of the hydrolysis of Styrene maleic anhydride to Styrene maleic acid (SMA) Right - Representation of membrane solubilization and nanodiscs formation by SMA type polymers. Reproduced from reference 65.

membrane proteins without removing them from their native lipid membrane environment and,

most importantly, this process is accomplished without the use of destabilizing detergents (**Figure 1-4)**.[51,55,56]

Most of the current SMA research has involved investigating several different molecular weights and styrene to maleic anhydride ratios, leading to a plethora of different polymers available commercially.[57,58] The advantages over micelles, liposomes, bicelles, and protein based nanodiscs allow polymer nanodiscs to be applied to a wider variety of membrane protein studies. Polymer nanodiscs in the form of SMALPs have been shown to have significant downsides to their use however. The original SMA polymers (~9.5 kDa) used in SMALPs did not allow for a large range of size control over the nanodiscs,[50] also all SMA based polymer nanodiscs are unstable to conditions that require low pH or the presence of divalent metal ions.[48,51] These limitations have restricted the applications of SMA based nanodiscs and do not allow for the active study of membrane proteins whose function require a low pH or require the presence of divalent metal ions such as Ca^{2+} or Mg^{2+}.[59-61] The instability of SMA is due to the presence of carboxylic acids as the hydrophilic portion of the polymer. SMA is only soluble in water at a high pH that allows for the formation of carboxylates, however carboxylates also strongly chelate with divalent metal ions, leading to SMAs instability.[48,51] The anhydride unit of SMAnh copolymers can be functionalized by amines via a nucleophilic ring opening reaction.[62] SMAnh can be customized in several different ways and our research has focused on the hydrophilic functionalization of SMA, while also imparting size control by employing a lower molecular weight SMA as our starting material.

SMA polymers have been very successful in the reconstitution of membrane proteins into nanodiscs. [49,51,63-70] SMA polymers have the unique advantage over other membrane mimetics in that SMA has been shown to directly extract membrane proteins from the cellular membrane by directly interacting and extracting the lipids.[49,51,53] SMA polymer nanodiscs have been shown to

form in a variety of lipids with a size range of 10-15 nm diameter.[51,71] A variety of biophysical studies reported the characterization of SMA based polymer nanodiscs.[72-74] NMR experiments have been used to show the formation of nanodiscs and to probe lipid dynamics.[75,76] Due to the lack of relative size control the current NMR applications of polymer nanodiscs are limited to solution NMR. In order to expand the NMR applications of polymer nanodiscs to both solution and solid-state NMR, more control over nanodiscs size is needed.[19,36,77] The hypothesis was that a lower molecular weight polymer would allow for size control of nanodiscs is based on the knowledge gained from the molecular weight (MW) difference between high MW MSPs, which do not allow for size control, and low MW peptide based nanodiscs which have been demonstrated to enable size control.[32,39] It was shown that using low molecular weight polymers achieved the necessary nanodiscs size control for various biophysical and structural biology studies.

1.5 Expanding nanodiscs size tunability by using SMA-EA.

The first functionalized SMA based polymer developed was styrene maleic anhydride – ethanol amine (SMA-EA) using the starting material poly(styrene-co-maleic anhydride) cumene terminated with an approximately 1.3:1 styrene:maleic anhydride molar ratio with a number average molecular weight of about ~1.6 kDa.[78] SMA-EA was synthesized by modifying the starting SMAnh via a nucleophilic ring opening reaction using ethanolamine. The resulting polymer was shown to form nanodiscs with a large range of sizes (10-60 nm diameter) by varying the lipid to polymer ratio. Small SMA-EA nanodiscs, with lipid:polymer (w/w) ~ 2, (<20 nm) were shown to be suitable for solution NMR experiments, whereas the larger sized nanodiscs (macro-nanodiscs) (lipid:polymer 1:1 w/w) aligned in the presence of an external magnetic field enabling structural studies of membrane proteins using solid-state NMR spectroscopy.[79-81] The use of nanodiscs in the study of membrane proteins using solution as well as solid state NMR were shown

using Cyt b_5 as an example. Uniformly-^{15}N-labeled Cytochrome-b_5 reconstituted in small nanodiscs (10 nm) exhibited well dispersed peaks in a 2D TROSY-HSQC (transverse relaxation optimized spectroscopy-heteronuclear single quantum correlation) spectrum suggesting that protein is well folded.[82] Cyt b_5 reconstituted in macro-nanodiscs were used in a 2D PISEMA (polarization inversion and spin exchange at magic angle) experiment.[78,83-85] The PISEMA spectrum revealed a characteristic wheel-like pattern of resonances showing the tilt of the helical transmembrane domain with respect to the lipid bilayer normal. The SMA-EA polymer was also shown to have an increased stability towards divalent metal ions (up to 21 mM for Ca^{2+} and 30 mM for Mg^{2+}), and an increased tolerance towards low pH (from pH 4.5 to pH 3.3 based on the lipid:polymer w/w ratio)) as compared to SMALP (pH ~ 6.3). While we demonstrated that SMA-EA polymer nanodiscs could be formed in a wide variety of sizes, the presence of carboxylic groups as the hydrophilic component still limited the application of SMA-EA nanodiscs.

1.6: Outline

As polymer based lipid-nanodiscs are a relatively new field there is much work to be done on optimizing and expanding the uses of this system. As a result, the work on this thesis encompasses the functionalization of different polymers for improved chemical stability and increasing the application of lipid-nanodiscs. Chapter 2 discusses the functionalization of low molecular weight SMA to yield various polymers with tunable pH stability not seen in standard SMA derivatives. Chapter 3 outlines the work we did with further improvements on the SMA based polymer for even better enhancement on its pH and metal ion solubility tolerance. Chapter 4 describes a novel functionalized polyacrylic acid based system which allowed for a systematic probing on the hydrophobic moiety of polymers and its effect on nanodiscs stability. Chapter 5 discuses a new SMA system which was engineered for an enhanced NMR application using

paramagnetic relaxation enhancement (PRE) resulting from a SMA-metal chelated polymer nanodisc system. Finally, Chapter 6 outlines the future potential work which will result in a broader impact in the field of polymer nanodiscs and the potential of polymer-lipid nanodiscs to be used not only in membrane protein research but in drug delivery applications as well.

1.7 Acknowledgements: This study was supported by funds from NIH (GM084018 to A.R.).

1.8 References

1. H. Hartley, *Nature* 1951, 168, 244.

2. Z. Cournia, T.W. Allen, I. Andricioaei, et al. *J Membrane Biol.* 2015, 248, 611-640.

3. R. Fredriksson, *Mol*. 2005, 67, 1414–1425

4. Li, E.; Hristova, K. *Biochem* 2006, 45, 6241–6251

5. B. Alberts, A. Johnson, J. Lewis, D. Morgan, M. C. Raff, K. Roberts, P. Walter, J. Wilson, T. Hunt, *Molecular biology of the cell*; Garland Science: New York, NY, 2015.

6. F. P. Guengerich, *Chem. Res. Toxicol.* 2008, *21*, 70–83.

7. U. M. Zanger, M. Schwab, *Pharmacol. Ther*. 2013, 138, 103–141.

8. K. Liszewski, *Genet. Eng. Biotechn. N.* 2015, 35.

9. E Wallin, G. V Heijne, *Protein Sci.* 2008, 7, 1029–1038.

10. E. P. Carpenter, K. Beis, A. D. Cameron, S. Iwata, *Curr. Opin. Struct. Biol*. 2008, 18 (5), 581–586.

11. J. P. Overington, B. Al-Lazikani, A. L. Hopkins, *Nat. Rev. Drug Discov.* 2006, 5 (12), 993–996.

12. I. Moraes, G. Evans, J. Sanchez-Weatherby, S. Newstead, P. D. S. Stewart, *BBA–Biomembranes* 2014, 1838, 78–87.

13. W. A. Hendrickson, *Nat. Struct. Mol. Biol.* 2016, 23, 464–467.

14. J. G. Almeida, A. J. Preto, P. I. Koukos, A. M. J. J. Bonvin, I. S. Moreira, *BBA–Biomembranes* 2017, 1859, 2021–2039.

15. M. A. Seddon, P. Curnow, P. J. Booth, *BBA–Biomembranes* 2004, 1666, 105-117,

16. A. Anandan, A. Vrielink, *Adv. Exp. Med. Biol.* 2016, 922, 13-28.

17. T. Arnold, D. Linke, *Curr. Protoc. Protein Sci.* 2008, 53: 4.8.1-4.8.30.

18. M.J. Parmar, M. Lousa Cde, S.P. Muench, A. Goldman, V.L. *Biochem. Soc. Trans.* 2016 44, 877-882.

19. J. L. Rigaud, D. Lévy, *Methods in Enzymo.* 2003, 372, 65–86.

20. J. L. Rigaud, M. T. Paternostre, A. Bluzat, *Biochemistry* 1988, 27, 2677–2688.

21. U. H. Durr, M. Gildenberg, A. Ramamoorthy, *Chem. Rev.* 2012, 112, 6054–6074.

22. C.R. Sanders, R.S. Prosser, *Structure*, 1998, 1227–1234.

23. C.R. Sanders, G.C. Landis, *Biochemistry* 1995, 4030–4040.

24. R. Soong, J. Xu, A. Ramamoorthy, *Nuclear Magnetic Resonance Spectroscopy of Liquid Crystals* 117–128.

25. M. Beaugrand, A. A. Arnold, J. Henin, D. E. Warschawski, P. T. Williamson, I., *Langmuir* 2014, 30, 6162–6170.

26. C. R. Sanders, J. P. Schwonek, *Biochemistry* 1992, 31, 8898–8905.

27. C. R. Sanders, B. J. K. P. Hare, J. H. Howard, *Prog. Nucl. Mag. Res. Sp.* 1994, 26, 421–444.

28. T. B. Cardon, P. C. Dave, G. A. Lorigan, *Langmuir* 2005, 21, 4291–4298.

29. K. Yamamoto, R. Soong, A. Ramamoorthy, *Langmuir* 2009, 25, 7010–7018.

30. I. G. Denisov, S. G. Sligar, *Nat. Struct. Mol. Biol*. 2016, 23, 481–486.

31. T. H. Bayburt, Y. V. Grinkova, S. G. Sligar, *Nano Lett*. 2002, 2, 853–856.

32. T. H. Bayburt, J. W. Carlson, S. G. Sligar, *J. Struct. Biol*. 1998, 123, 37–44.

33. A. Nath, W. M. Atkins, S. G. Sligar, *Biochemistry* 2007, 46, 2059–2069.

34. I. G. Denisov, S. G. Sligar, *Chem. Rev.* 2017, 117, 4669–4713.

35. F. Hagn, M. Etzkorn, T. Raschle, G. Wagner, *J. Am. Chem. Soc.* 2013, 135, 1919–1925.

36. M. L. Nasr, D. Baptista, M. Strauss, Z. J. Sun, S. Grigoriu, S. Huser, A. Pluckthun, F. Hagn, T. Walz, J.M. Hogle, G. Wagner, *Nat. Methods* 2017, 14, 49–52.

37. T. K. Ritchie, Y. V. Grinkova, T. H. Bayburt, I. G. Denisov, J. K. Zolnerciks, W. M. Atkins, S. G. Sligar, N. Düzgünes (Ed.), *Methods in Enzymology*, vol. 464, Academic Press, 2009, pp. 211–231.

38. F. Hagn, M. L. Nasr, G. Wagner, *Nat. Protoc*. 2018, 13, 79–98.

39. D. C. Rodriguez Camargo, K. J. Korshavn, A. Jussupow, K. Raltchev, D. Goricanec, M. Fleisch, R. Sarkar, K. Xue, M. Aichler, G. Mettenleiter, A. K. Walch, C. Camilloni, F. Hagn, B. Reif, A. Ramamoorthy, *Elife* 2017, 6, e31226.

40. A. Nath, A. D. Miranker, E. Rhoades, *Angew. Chem. Int. Ed. Engl*. 2011, 50, 10859–10862.

41. M. Zhang, R. Huang, R. Ackermann, S. C. Im, L. Waskell, A. Schwendeman, A. Ramamoorthy, *Angew. Chem. Int. Ed.* 2016, 128, 4497–4499.

42. T. Ravula, C. Barnaba, M. Mahajan, G. M. Anantharamaiah, S. C. Im, L. Waskell, A. Ramamoorthy, *Chem. Commun*. 2017, 53, 12798–12801.

43. T. Ravula, D. Ishikuro, N. Kodera, T. Ando, G. M. Anantharamaiah, A. Ramamoorthy, *Chem. Mater.* 2018, 30, 3204–3207.

44. C. Barnaba, B. R. Sahoo, T. Ravula, I. G. Medina-Meza, S. C. Im, G. M. Anantharamaiah, L. Waskell, A. Ramamoorthy, *Angew. Chem. Int. Ed. Engl.* 2018, 57, 3391–3395.

45. C. Barnaba, T. Ravula, I. G. Medina-Meza, S. C. Im, G. M. Anantharamaiah, L. Waskell, A. Ramamoorthy, *Chem. Commun*. 2018, 54, 6336–6339.

46. E. Prade, M. Mahajan, S. C. Im, M. Zhang, K. A. Gentry, G. M. Anantharamaiah, L. Waskell, A. Ramamoorthy, *Angew. Chem. Int. Ed. Engl.* 2018, 57, 8458–8462.

47. S. H. Park, S. Berkamp, G. A. Cook, M. K. Chan, H. Viadiu, S. J. Opella, *Biochemistry* 2011, 50, 8983–8985.

48. R. Kuai, L. J. Ochyl, K. S. Bahjat, A. Schwendeman, J.J. Moon, *Nat. Mater*. 2017, 16, 489–496.

49. R. Kuai, D. Li, Y. E. Chen, J. J. Moon, A. Schwendeman, *ACS Nano* 2016, 10, 3015–3041.

50. S. Scheidelaar, M. C. Koorengevel, C. A. van Walree, J. J. Dominguez, J. M. Dörr, A. J. Killian, *Biophys. J.* 2016, 111, 1974–1986.

51. J. M. Dörr, M. C. Koorengevel, M. Schäfer, A.V. Prokofyev, S. Scheidelaar, E. A. W. van der Cruijsen, T. R. Dafforn, M. Baldus, J. A. Killian, *PNAS.* 2014, 111, 18607–18612.

52. M. C. Orwick, P. J. Judge, J. Procek, L. Lindholm, A. Graziadei, A. Engel, G. Grobner, A. Watts, *Angew. Chem. Int. Ed. Engl*. 2012, 51, 4653–4657.

53. S. C. Lee, T. J. Knowles, V. L. Postis, M. Jamshad, R. A. Parslow, Y. P. Lin, A. Goldman, P. Sridhar, M. Overduin, S. P. Muench, T. R. Dafforn, *Nat. Protoc*. 2016, 11, 1149–1162.

54. T. J. Knowles, R. Finka, C. Smith, Y. P. Lin, T. Dafforn, M. Overduin, *J. Am. Chem. Soc*. 2009, 131, 7484–7485.

55. S. Rajesh, T. Knowles, M. Overduin, *New Biotechnol*. 2011, 28, 250–254.

56. M. Jamshad, Y. P. Lin, T. J. Knowles, R. A. Parslow, C. Harris, M. Wheatley, D. R. Poyner, R. M. Bill, O. R. Thomas, M. Overduin, T. R. Dafforn, *Biochem. Soc. Trans*. 2011, 39, 813–818.

57. Web link for polymer nanodisc: http://www.smalp.net/.

58. Z. Stroud, S. C. L. Hall, T. R. Dafforn, *Methods* 2018, 147, 106-117.

59. Z. Xie, S. Schendel, S. Matsuyama, J. C. Reed, *Biochemistry* 1998, 37, 6410–6418.

60. D. O. O'Keefe, V. Cabiaux, S. Choe, D. Eisenberg, R. J. Collier, *Proc. Natl. Acad. Sci. U.S.A* 1992, 89, 6202–6206.

61. Y. Xu, M. P. Bhate, A. E. McDermott, *Proc. Natl. Acad. Sci. U.S.A.* 2017, 114, 8788–8793.

62. B.C. Trivedi, B.M. Culbertson, *Maleic Anhydride*, Springer, 1982.

63. D. J. K. Swainsbury, S. Scheidelaar, R. van Grondelle, J. A. Killian, M. R. Jones, *Angew. Chem. Int. Ed. Engl.* 2014, 53, 11803–11807.

64. M. Tanaka, A. Hosotani, Y. Tachibana, M. Nakano, K. Iwasaki, T. Kawakami, T. Mukai, *Langmuir* 2015, 31, 12719–12726.

65. J. M. Dörr, S. Scheidelaar, M. C. Koorengevel, J. J. Dominguez, M. Schäfer, C. A. van Walree, J.A. Killian, *Eur. Biophys. J.* 2016, 45, 3–21.

66. K. A. Morrison, A. Akram, A. Mathews, Z. A. Khan, J. H. Patel, C. Zhou, D. J. Hardy, C. Moore-Kelly, R. Patel, V. Odiba, T. J. Knowles, M. U. H. Javed, N. P. Chmel, T. R. Dafforn, A. J. Rothnie, *Biochem. J.* 2016, 473, 4349–4360.

67. Z. Hu, J. C. S. Ho, M. Nallani, *Curr. Opin. Biotechnol*. 2017, 46, 51–56.

68. A. O. Oluwole, B. Danielczak, A. Meister, J. O. Babalola, C. Vargas, S. Keller, *Angew. Chem. Int. Ed. Engl.* 2017, 56, 1919–1924.

69. C. Sun, S. Benlekbir, P. Venkatakrishnan, Y. Wang, S. Hong, J. Hosler, E. Tajkhorshid, J. L. Rubinstein, R. B. Gennis, *Nature* 2018, 557, 123–126.

70. T. Laursen, J. Borch, C. Knudsen, K. Bavishi, F. Torta, H.J. Martens, D. Silvestro, N. S. Hatzakis, M. R. Wenk, T. R. Dafforn, C. E. Olsen, M. S. Motawia, B. Hamberger, B. L. Moller, J. E. Bassard, *Science* 2016, 354, 890–893.

71. K. A. Morrison, A. Akram, A. Mathews, Z. A. Khan, J. H. Patel, C. Zhou, D. J. Hardy, C. Moore-Kelly, R. Patel, V. Odiba, T. J. Knowles, M. U. Javed, N. P. Chmel, T. R. Dafforn, A. J. Rothnie, *Biochem. J*. 2016, 473, 4349–4360.

72. A. Grethen, A. O. Oluwole, B. Danielczak, C. Vargas, S. Keller, *Sci. Rep.* 2017, 7, 11517.

73. R. Cuevas Arenas, J. Klingler, C. Vargas, S. Keller, *Nanoscale* 2016, 8, 15016–15026.

74. S. C. L. Hall, C. Tognoloni, G. J. Price, B. Klumperman, K. J. Edler, T. R. Dafforn, T. Arnold, *Biomacromolecules* 2018, 19, 761–772.

75. R. Zhang, I. D. Sahu, A. P. Bali, C. Dabney-Smith, G. A. Lorigan, *Chem. Phys. Lipids* 2017, 203, 19–23.

76. D. Martinez, M. Decossas, J. Kowal, L. Frey, H. Stahlberg, E.J. Dufourc, R. Riek, B. Habenstein, S. Bibow, A. Loquet, *ChemPhysChem* 2017, 18, 2651–2657.

77. R. Puthenveetil, K. Nguyen, O. Vinogradova, *Nanotechnol Rev.* 2017, 6, 111–126.

78. T. Ravula, S. K. Ramadugu, G. Di Mauro, A. Ramamoorthy *Angew. Chem. Int. Ed. Engl.* 2017, 56, 11466–11470.

79. K. Yamamoto, M. Gildenberg, S. Ahuja, S.C. Im, P. Pearcy, L. Waskell, A. Ramamoorthy, *Sci. Rep*. 2013, 3, 2556.

80. A. Ramamoorthy, Y. Wei, D.-K. Lee, *Annual Reports on NMR Spectroscopy* 2004, 52, 1–52.

81. J. Radoicic, S. H. Park, S. J. Opella, *Biophys. J.* 2018, 115, 22–25.

82. K. Pervushin, R. Riek, G. Wider, K. Wüthrich, *PNAS*. 1997, 94, 12366-12371.

83. A. Gayen, J. R. Banigan, N. J. Traaseth, *Angew. Chem. Int. Ed. Engl*. 2013, 52, 10321–10324.

84. S. Wang, T. Gopinath, G. Veglia, *Methods* 2018, 138–139, 54–61.

85. E. S. Salnikov, G. M. Anantharamaiah, B. Bechinger, *Biophys. J.* 2018, 115, 467–477.

Chapter 2

pH Tunable and Divalent Metal Ion Tolerant Polymer Lipid Nanodiscs

Portions of this chapter are reproduced from: T. Ravula[+], N.Z. Hardin[+], S.K. Ramadugu, A. Ramamoorthy, *Langmuir* 2017, 33, 10655–10662.

2.1 Introduction

Membrane proteins play important roles in a variety of cellular functions and also on the pathology of many diseases.[1-5] High-resolution structural and functional studies on these membrane bound proteins are severely limited by the difficulties associated with their solubilization and reconstitution without a loss of their function.[6,7] Several membrane mimetics like liposomes,[8-9] bicelles,[10-13] micelles,[14-15] ampiphols,[16-17] and nanodiscs[18-20] have been developed in an attempt to study membrane proteins in native-like cell membrane environment. Recently lipid nanodiscs have been increasingly used in the structural and functional studies of membrane proteins and also in other nano biotechnological applications.[21-22] Nanodiscs are disc shaped lipid bilayers surrounded by an amphiphilic protein,[23] and are inspired from high-density lipoproteins.[24] Nanodiscs provide a near native lipid membrane environment and enables the study of membrane proteins in its active form.[25] Another possible application of nanodiscs is the potential use as a drug delivery system.[26-28] Recent advances in nanodiscs technology have allowed nanodiscs to be formed not only by scaffold proteins but also using amphiphilic peptides[29-32] or polymers[33-39]. The hydrolysed form of styrene maleic anhydride copolymer was the first amphiphilic polymer shown to form lipid

nanodiscs (also referred to as styrene-maleic acid copolymer-lipid nanoparticles or SMALPs)[40-42] and reconstitute proteins. The polymer based nanodiscs have attracted significant attention due to their ability to reconstitute membrane proteins from native cell membranes without the use of detergents.[43-44] In addition, styrene maleic acid and diisobutyl maleic acid copolymers have been used for extraction of membrane proteins.[37] While previously reported nanodiscs were limited by their small size (<20 nm diameter), we recently demonstrated the formation of polymer nanodiscs that vary in size from ~10 to ~60 nm diameter. Our study further demonstrated that the macro-nanodiscs (size >40 nm) have the ability to magnetically-align which has opened avenues for solid-state NMR applications for high-resolution structural studies on membrane proteins.[45]

Even though polymer nanodiscs are advantageous over protein/peptide based nanodiscs and their applications will continue to grow, tuning their stability under different pH conditions and in the presence of divalent metal ions is highly important.[46-47] The presence of carboxylic groups in SMA polymer makes them unstable under acidic conditions,[48-49] which disable the applications of polymer nanodiscs to study those membrane proteins that bind to the cell membrane or become active only under acidic conditions.[50-52] Another issue with SMA based polymers is that due to the presence of the carboxylate groups their stability in the presence of divalent metal cations such as Ca^{2+} or Mg^{2+} is greatly reduced.[35, 53] This phenomena limits the use of SMA-based polymer nanodiscs to study those membrane proteins that bind to such divalent metal ions.[47, 54-57]

In this study we report the synthesis and characterization of two different SMA analogs by modifying the maleic anhydride to form differing functional groups. Subsequent lipid nanodiscs were characterized using solid-state NMR, FT-IR, TEM, and DLS experiments. The pH dependence and metal ion stability of these nanodiscs were examined using static light scattering

and FT-IR experiments. The two newly synthesized polymer nanodiscs exhibit unique pH dependent stability based on the modified functional group and show high tolerance towards divalent metal ions. We also successfully demonstrate that these tunable new polymer nanodiscs can be used to encapsulate, and stabilize curcumin for potential biological and biomedical applications.

2.2 Material and Methods

Poly(Styrene-co-Maleic Anhydride) cumene terminated~1.3:1 (SMA M_n~1600 g/mol), anhydrous N-Methyl-2-Pyrrolidone (NMP), N-Boc-ethylenediamine, (2-Aminoethyl)trimethylammonium chloride hydrochloride, Triethylamine (Et_3N), phosphoric acid (H_3PO_4), acetic acid (HOAc), hydrochloric acid (HCl), sodium hydroxide (NaOH), trifluoracetic acid (TFA), citric acid, diethyl ether, calcium chloride ($CaCl_2$), magnesium chloride ($MgCl_2$), Dimethylformamide (DMF), Acetic Anhydride, and Sodium Acetate were purchased from Sigma-Aldrich®. 1,2-dimyristoyl-*sn*-glycero-3-phosphocholine (DMPC) was purchased from Avanti Lipids Polar, Inc®. All synthesized polymers were characterized by FT-IR and NMR experiments. All polymers were purified using 2000 kDa dialysis membranes in water before use.

Synthesis of various compounds: N-Boc-SMA-ED (1) (5 g, 3.125 mmol) of SMA was dissolved in 30 ml of anhydrous NMP. The solution was added to 10.1 g of N-Boc-Ethylenediamine dissolved in 10 ml NMP while stirring. After that, 3.16 g of triethyl amine was added, followed by incubation at 70 °C for 3 hrs while stirring. The reaction was then cooled to room temperature and the polymer was precipitated by the addition of ice cold 0.1 M HCl and pelleted by centrifugation. The polymer was washed with 0.1 M HCl several times by centrifugation to remove excess amounts of NMP, N-Boc-ethylenediamine, and Et_3N. The polymer was then lyophilized to give a white powder.

Synthesis and purification of SMA-ED (2): 2 g of **N-Boc-SMA-ED** was dissolved in 40 ml TFA, and 2 ml of water and was stirred for 3 hrs. The reaction solution was then precipitated in cold ether and then washed by centrifugation with cold ether.

Synthesis and purification of N-Boc-SMAd-A (3): 1 g (0.32 mmol) of **N-Boc-SMA-ED** was added to 20 ml acetic anhydride. 330 mg of sodium acetate and 100 mg of triethylamine were added and stirred to make a homogenous mixture. The reaction mixture was then heated to 80 °C and stirred overnight. The mixture was then precipitated in cold water and washed via centrifugation with cold water and freeze dried.

Synthesis and purification of SMAd-A (4): 470 mg of **N-Boc-SMAd-A** was dissolved in 40 ml TFA and 2 ml of water followed by stirring for 3 hrs. The reaction solution was then precipitated in cold ether and then washed by centrifugation with cold ether. The product was then dried under vacuum.

Formation of lipid nanodiscs: Nanodiscs used in this study were formed by the addition of 100 µl DMPC (10 mg/ml) and 100 µl **SMA-ED** or **SMAd-A** (10 mg/ml) in a 1.5ml tube and diluted to 1ml using water, 10 mM citric acid buffer pH 3.5, or 10 mM HEPES buffer pH 8.5.

2.3 Experimental

Static light scattering (SLS) experiments: The time dependent solubilization, pH stability, and metal ion stability experiments were carried out by measuring the scattered light at 90^{o} angle using Fluoro Fluorimeter under identical DMPC concentrations. 500 µl of nanodiscs or polymer were dispensed into a 2 ml cuvette under stirring. Then the solution was diluted to 2 ml with citric acid buffer, or HEPES buffer as required. pH titrations were performed using 1M HCl and NaOH. Metal ion titrations were performed using 5M $MgCl_2$, 5M NaCl, and 3.3M $CaCl_2$. The excitation and emission wavelengths were set at 400 nm and 404 nm, respectively. The slit was set to 2 nm.

All SLS experimental measurements were carried out using FluoroMax 4® from Horiba Scientific®.

Solid state NMR Spectroscopy: ^{31}P NMR spectra were acquired using an Agilent/Varian 400 MHz solid-state NMR spectrometer and using 5 mm triple-resonance and double-resonance NMR probes. 5 μs 90^0 pulse, 30 kHz continuous-wave decoupling of protons, 2000 scans, and a 6 s recycle delay were used in NMR experiments. ^{31}P NMR spectra were referenced by setting the ^{31}P chemical shift of 100 % H_3PO_4 sample to 0 ppm.

Samples for NMR measurements: Samples for NMR experiments were prepared using stock solutions of DMPC MLVs (10 mg/ml) in 10 mM citric acid buffer pH 3.5 and 10 mM HEPES buffer for pH 8.5. pH was adjusted using NaOH.

CPMAS solid-state NMR experiments: Carbon-13 CPMAS (cross-polarization magic angle spinning) experiments were carried on a Bruker 500 MHz solid-state NMR spectrometer operating at 500 MHz and 125.721 MHz for ^1H and ^{13}C, respectively, under 13 kHz MAS using a 3.2 mm triple-resonance MAS probe. The reported ^{13}C CPMAS NMR spectra were acquired using the following parameters: 3 μs 90° pulse, 2 ms CP contact time, 40 ms acquisition time, 2048 scans, 4 s recycle delay and a 50 kHz radio-frequency power applied to decouple protons during the acquisition of ^{13}C magnetization. ^{13}C chemical shifts were calibrated by setting the chemical shift of CH_2 resonance of adamantane powder sample to 28.5 ppm.

Formation of curcumin loaded nanodiscs for stability studies: 1mg/ml stock solution of curcumin was made by dissolving curcumin in methanol. 37 microliters of stock solution was added to 3.7 mg of DMPC. Methanol was removed under nitrogen gas, and the residual solvent was completely removed using high vacuum. To the resulting lipid film containing curcumin, 2 ml of 7.4 mg of SMAd-A or SMA-ED dissolved in 10 mM citric acid buffer at pH 3.5 was added.

The resulting solution was vortexed and freeze thawed to form lipid nanodiscs.

Stability of curcumin using UV-Vis spectroscopy: 2ml of curcumin encapsulated nanodiscs (a final concentration of ~50 micro molar curcumin) was placed into a 2ml standard UV quartz cuvette with a path length of 1cm. Curcumin stability in water was tested by placing 37 µl of curcumin methanol stock solution and diluted to 2ml with 10 mM citric acid buffer. Spectra were acquired every 5 mins for 2 hours. All UV-Vis spectra were recorded using Varian Cary 5000

Transmission Electron Microscopy (TEM): All TEM micrographs were obtained using a Technai® T-20® machine (FEI®, Netherlands) with a 80 kV operating voltage. A dilute solution was dropped on the carbon-coated copper grid and dried overnight at room temperature in a desiccator before using in the experiments.

Dynamic Light Scattering (DLS): All DLS experiments were performed using Wyatt Technology® DynaPro® NanoStar® using a 1 µL quartz MicroCuvette.

Fourier-Transform Infrared (FT-IR) Spectroscopy: The FT-IR spectra from 4000 cm^{-1} to 800 cm^{-1} were recorded using a Thermos scientific ATR-FTIR instrument. Water was removed by lyophilization from each of the samples before recording the spectrum.

^{31}P CSA: As shown in the main text, the parallel edge at 25.5 ppm and the perpendicular edge at -26.43 ppm to result in a CSA span for the ^{31}P powder patter to be ~50 ppm (**Figure 2-3E**, pH 6.0). On the other hand, the sample prepared at pH=8.5 exhibited the parallel edge at 27.2 ppm and the perpendicular edge at -21.4 ppm to result in a similar CSA span for the ^{31}P powder patter to be ~50 ppm (**Figure 3F**, pH=8.5).

Measuring the effect of divalent metal ions on SMA-EA nanodiscs: Nanodiscs were titrated using 3.3 M CaCl2 or 5 M MgCl2 in 10 mM citric acid buffer or 10 mM HEPES in low or high pH condition, respectively

Fourier-Transform Infrared (FT-IR) Spectroscopy: The FT-IR spectra from 4000 cm-1 to 800 cm-1 were recorded using a Thermos scientific ATRFTIR instrument. Water was removed by lyophilization from each of the samples before recording the spectrum.

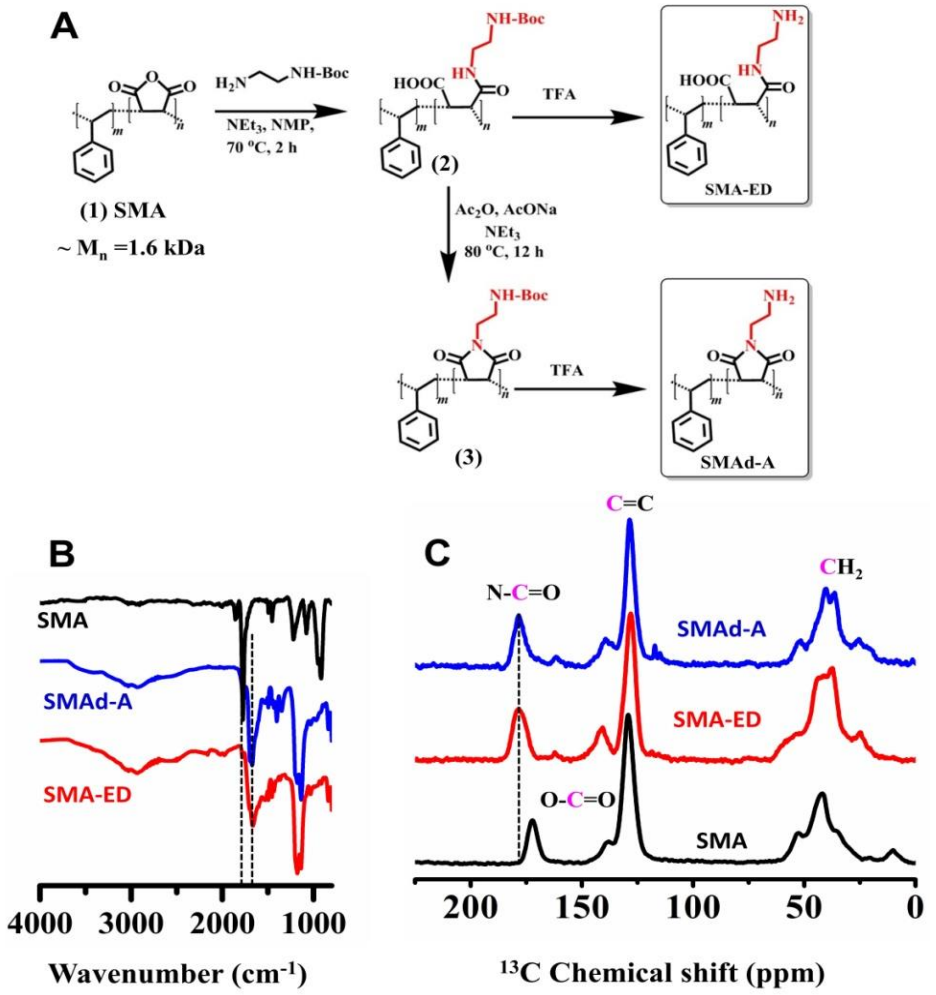

Figure 2-1: Synthesis and characterization of SMA-ED and SMAd-A polymers. (**A**) Reaction scheme showing the modifications of SMA polymer to synthesize zwitterionic SMA-ED and positively-charged SMAd-A polymers. FT-IR (**B**) and ^{13}C CPMAS solid-state NMR (**C**) spectra of SMA (black), SMA-ED (red) and SMAd-A (blue) polymers confirm the completion of the chemical reaction.

2.4 Results and Discussion

The overall schematics used for the synthesis of two different polymers, zwitterionic SMA-ED and positively-charged (except under neutral pH) SMAd-A, using low molecular weight SMA as

the starting material is shown in **Figure 2-1A**. The synthesis of SMA-ED was accomplished by first reacting SMA with N-Boc-ethylene diamine in the presence of triethylamine to form N-Boc-SMA-ED. Deprotection of N-Boc-SMA-ED was achieved with triflouroacetic acid followed by precipitation in ether.

The synthesized polymers were characterized by FT-IR (**Figure 2-1B**). The appearance of a broad peak in the 3000-3600 cm^{-1} region indicates the formation of carboxylic groups. The complete opening of the anhydride group was confirmed by the shift of C=O stretching frequency to lower wave numbers (~1772 cm^{-1} (SMA) to ~1690 cm^{-1} (SMA-ED)). Both polymers were further characterized by ^{13}C CPMAS solid-state NMR experiments. The observed shift of the carbonyl ^{13}Carbon peak around ~172 ppm, to a lower field region suggests the complete opening of the anhydride group and the presence of the newly formed amide carbonyls in SMA-ED (**Figure 2-1C**). SMAd-A was obtained by the dehydration of N-Boc-SMA-ED in acetic anhydride, followed by the deprotection step. The presence of a peak ~1696 cm^{-1} in the FT-IR spectrum (**in Figures 2-1B** and **2-2B**) confirms the formation of malimide group, while the appearance of a peak ~178 ppm in the ^{13}C CPMAS spectrum (**in Figure 2-1C**) confirms the presence of a carboxyl amide group in the SMAd-A. Because of similar carboxyl stretching frequency bands for SMA-ED and SMAd-A and overlapping NMR chemical shifts, FT-IR spectra were recorded under basic conditions. SMA-ED showed a carboxylate stretching frequency of ~1550 cm^{-1} suggesting the

presence of carboxylic groups whereas the absence of peaks for carboxylate stretching frequency in SMAd-A suggests the successful formation of malimide (**Figure 2-2**).

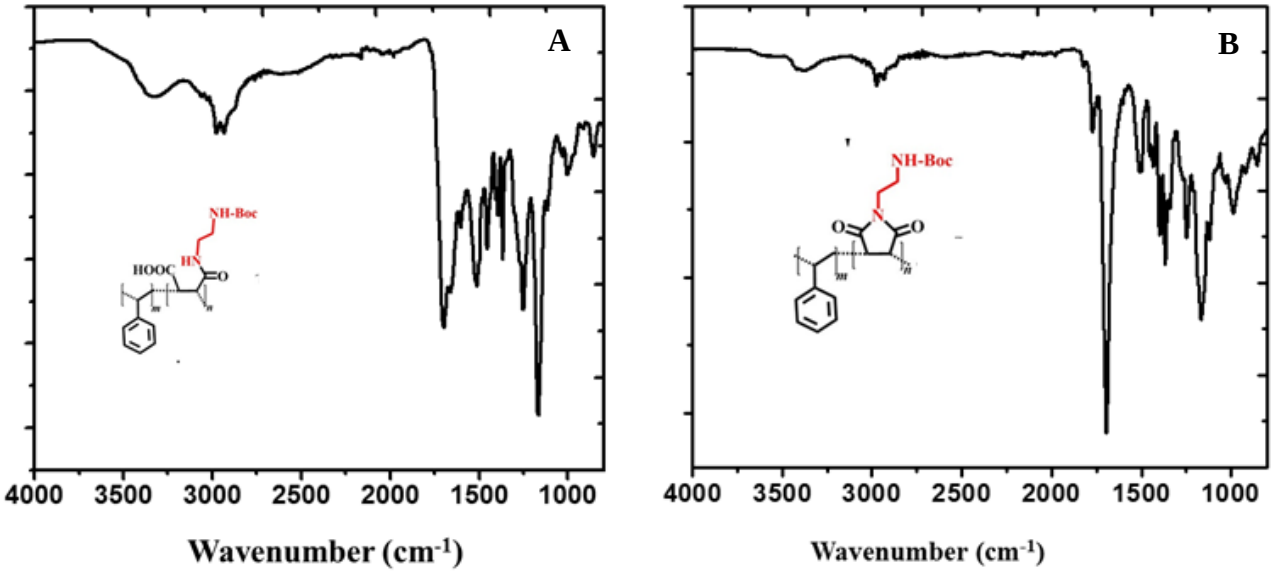

Figure 2-2: FT-IR of SMA intermediates. A) FT-IR of Boc protected SMA-ED. B) FT-IR of Boc protected SMA-dA

The ability of SMA-ED and SMAd-A to form lipid nanodiscs was tested by the addition of polymer solution to multilamellar vesicles (MLVs) of DMPC (1,2-dimyristoyl-sn-glycero-3-phosphocholine) in water. The polymer addition spontaneously changed the cloudy DMPC MLVs solution to a clear solution. The solubilization of MLVs was followed using SLS experiments. The significant decrease in SLS intensity after the addition of polymer suggests that both SMA-ED (**Figure 2-3A**) and SMAd-A (**Figure 2-3B**) can solubilize DMPC MLVs. The resulting solution was further characterized by DLS and TEM. DLS profiles show the size of nanodiscs and dependence on the lipid:polymer ratio (**Figure 2-3C and D**). The nanodiscs were further confirmed by TEM (**Figure 2-3E and F**).

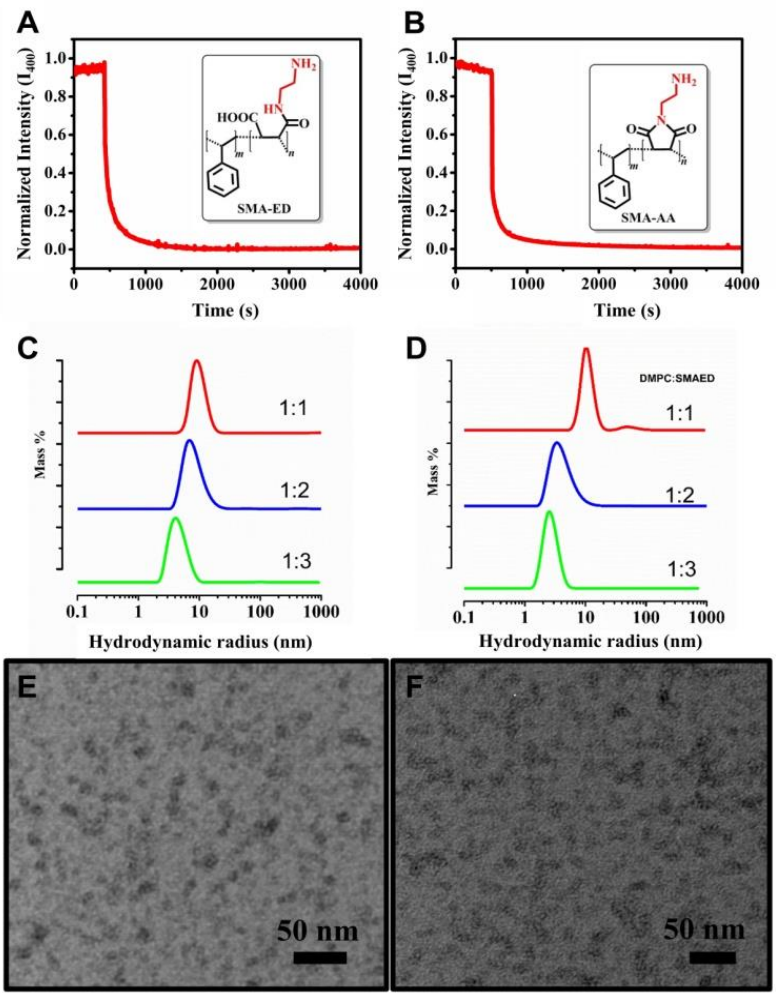

Figure 2-3: **Characterization of polymer based lipid nanodiscs.** SLS profiles for the formation of nanodiscs upon the addition of polymer SMA-ED (**A**) or SMAd-A (**B**). DLS profiles showing the different size nanodiscs obtained by varying the lipid to polymer weight ratio for SMA-ED (**C**) and SMAd-A (**D**). TEM micrographs of nanodiscs obtained by mixing 1:3 lipid to polymer weight ratio for SMA-ED (**E**) and SMAd-A (**F**).

Next, we examined the formation of polymer nanodiscs at pH 7.4 in phosphate buffer. Interestingly, SMA-ED showed nanodisc formation whereas SMAd-A did not form nanodiscs

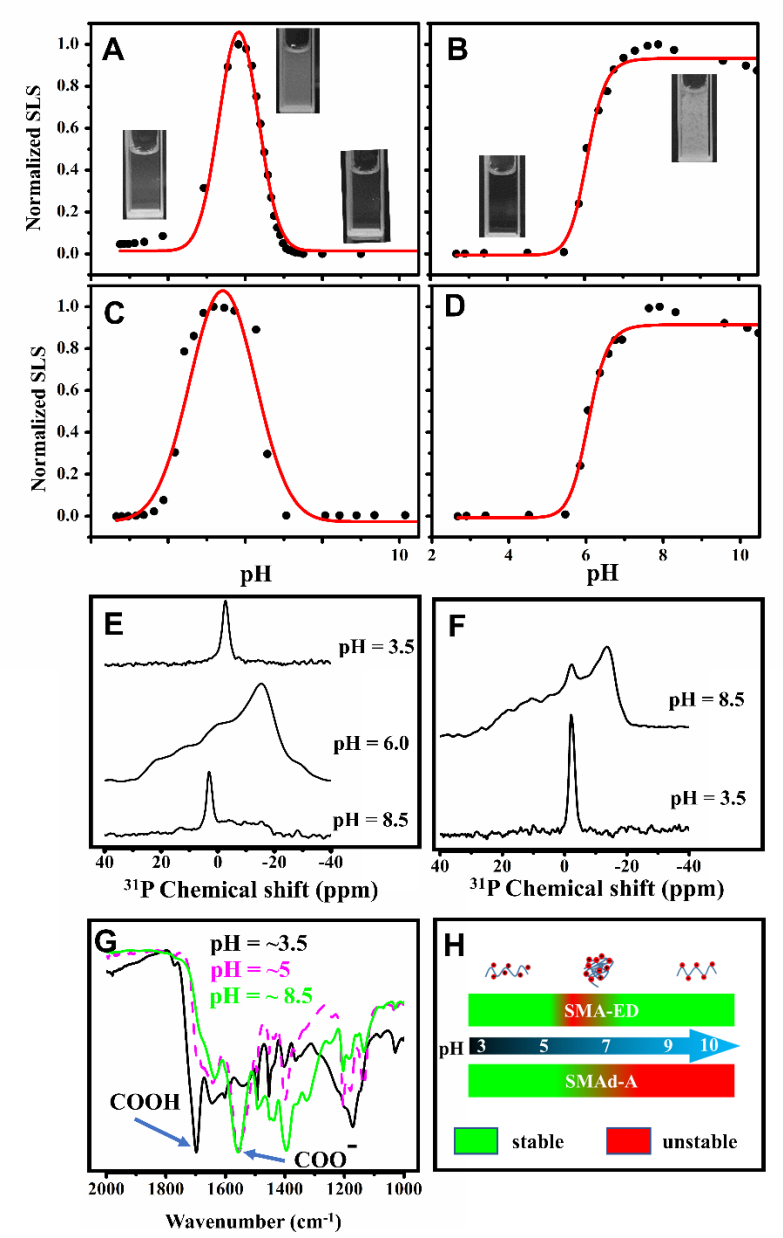

Figure 2-4: Stability of polymer nanodiscs vs pH. SLS profiles of SMA-ED nanodiscs (**A**), SMA-dA nanodiscs (**B**), SMA-dA polymer alone (**C**) and SMA-ED polymer (**D**) showing the stability against pH at 25 °C. The nanodiscs contained 1:1 polymer:DMPC weight ratio. Static 1D ^{31}P solid-state NMR spectra of SMA-ED (E) and SMAd-A (**F**) nanodiscs at the indicated pH value. (**G**) FT-IR spectra of SMA-ED polymer at the indicated pH. The observed bands at ~1550 cm^{-1} and ~1690 cm^{-1} for COO^- and COOH, respectively, confirm the protonated state of the carboxyl group of SMA-ED under different pH. (**H**) Schematic illustration explaining pH dependent stability of polymer-based nanodiscs.

under these conditions suggesting a pH dependent nanodisc formation. SLS experiments were performed to further investigate the pH dependent properties of SMA-ED and SMAd-A polymers

by measuring the SLS intensity which is proportional to the particle size and concentration. Experimental results obtained under different pH conditions were used to analyze the stability of nanodiscs formed by both polymers (see supporting information for experimental details). SMA-ED nanodiscs showed increased light scattering, and visible precipitate formation between pH 5 and 7 (**Figure 2-4A**). This observation suggests that SMA-ED is stable under all pH conditions except between 5 and 7. This is because the polymer is zwitterionic and forms hypercoils due to intramolecular charge-charge interactions, as confirmed by SLS and FT-IR experiments. SLS profiles for pH titrations of polymer alone are similar to that of the nanodiscs (Figure 3C), showing SMA-ED polymer aggregates and lowers its solubility due to hypercoiling. FT-IR spectra showed the presence of carboxylate formation at pH 5 suggesting the zwitterionic form of the SMA-ED polymer in the 5-7 pH range (**Figures 2-4G, H**). The stability of nanodiscs was also characterized by ^{31}P static solid-state NMR experiments. An isotropic peak observed close to 0 ppm at pH 3.5 and 8.5 suggest the formation of lipid nanodiscs that tumble rapidly on the NMR time scale (**Figure 2-4E**). On the other hand, a typical axially symmetric chemical shift anisotropy pattern observed at pH 6.0 suggests the inability of the polymer to form nanodiscs (**Figure 2-4E**); the appearance of a small peak at the isotropic chemical frequency in the powder pattern spectrum can be attributed to the presence of a small amount of isotropic nanodiscs. These observations complement the results obtained from SLS (**Figure 2-4A**).

The SLS intensity of SMAd-A nanodiscs (**Figure 2-4B**) was stable for pH<6. A steep increase in intensity and the formation of a visible precipitate was observed for pH>6. These results suggest that SMAd-A polymer nanodiscs are stable under acidic pH. A similar profile was also observed for SMAd-A polymer alone (**Figure 2-4D**). ^{31}P NMR spectra showed an isotropic peak under acidic pH indicating the presence of nanodisc whereas an axially symmetric powder pattern

at higher pH (**Figure 2-4F**) confirming the observations from SLS experiments. The SMAd-A polymer is positively charged under acidic conditions, soluble in water, and forms lipid nanodiscs. For pH>6, the solubility of the polymer is decreased due to deprotonation of the ammonium cation leading to polymer precipitation as experimentally observed.

The stabilities of SMA-ED and SMAd-A nanodiscs in the presence of different divalent cations were also examined using SLS. SMA-ED and SMAd-A tested at several concentrations

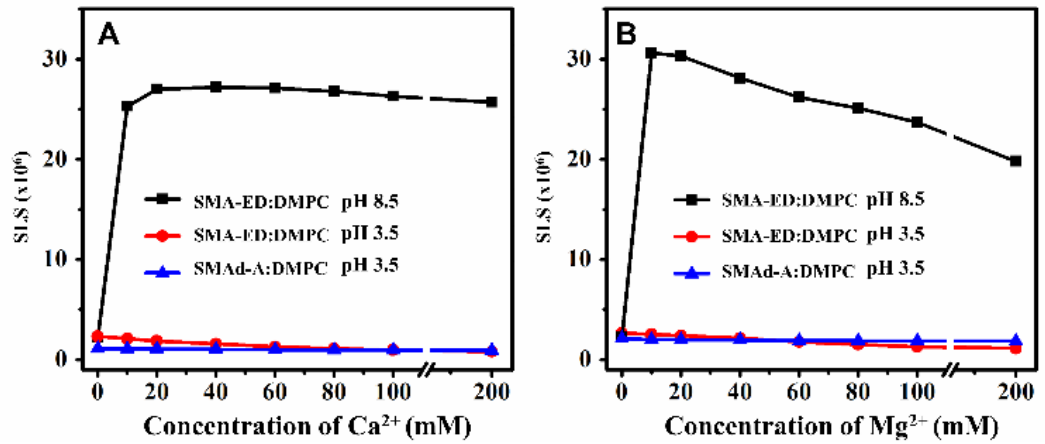

Figure 2-5*:* **Stability of polymer nanodiscs against divalent metal ions.** SLS profiles showing the stability of polymer nanodiscs against calcium (A) and magnesium (B) ions

(10-200 mM) of NaCl showed no substantial change in intensity (**Figure 2-6**). These results demonstrate the stability of both SMA-ED and SMAd-A based nanodiscs in high concentrations of a monovalent salt. The stability of SMA-ED and SMAd-A polymers and their lipid nanodiscs were also tested by varying the concentration (10 to 200 mM) of $MgCl_2$ and $CaCl_2$ at pH 3.5. Both SMA-ED and SMAd-A nanodiscs were found to be tolerant to Ca^{2+} and Mg^{2+} for all the tested

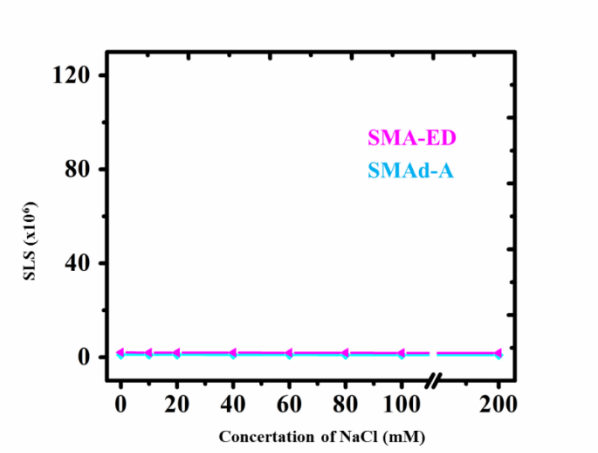

Figure 2-6: SLS of SMA-ED and SMAd-A polymers ad different NaCl concentrations

concentrations (**Figure 2-5**). However, at pH 8.5 soluble nanodiscs (SMA-ED) had no tolerance to Ca^{2+} or Mg^{2+} due to the presence of COO^- group that can interact with the metal ions.

Due to the amphiphilic nature of nanodiscs we theorized that the polymer nanodiscs system could be a good candidate for encapsulating and stabilizing hydrophobic drugs in water. To this end, curcumin, a known biologically active molecule with poor water solubility and stability,[58-60] was chosen as a model system for hydrophobic drug encapsulation.[61] The UV-Vis spectra of curcumin in water showed decreasing of absorption over time at ~420 nm (**Figure 2-7**), suggesting instability in water, whereas curcumin encapsulated nanodiscs showed stable absorption over time suggesting curcumin is stable in the presence of nanodiscs. These results suggest nanodiscs not only solubilized the curcumin but also greatly increased its stability in water.

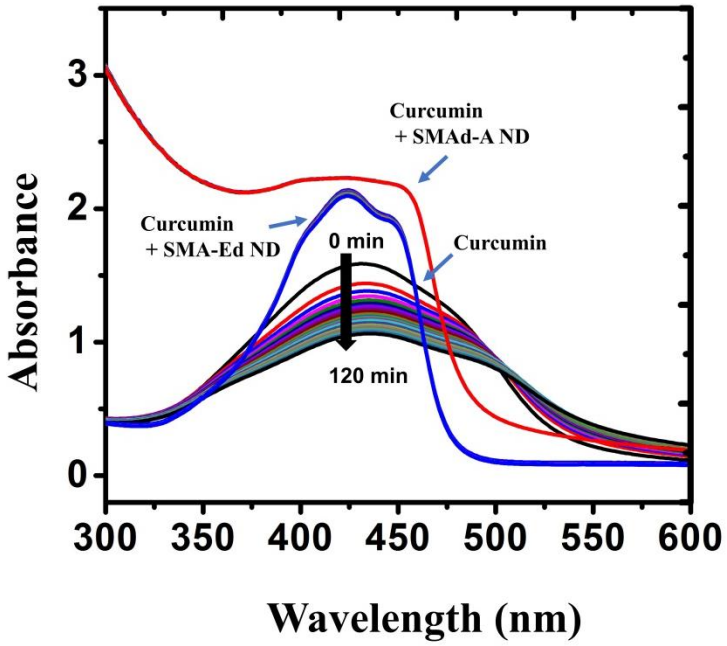

Figure 2-5: Stability of curcumin is enhanced by polymer nanodiscs. UV-Vis absorbance of Curcumin, Curcumin SMA-dA, and Curcumin SMA-ED.

2.5 Conclusions

In this study, we have synthesized two new SMA polymer analogues that show unique pH stability dependence and divalent metal ion stability. Characterization using SLS, DLS, TEM and solid-

state NMR experiments revealed the abilities of both zwitterionic (SMA-ED) and positively-charged (SMAd-A) polymers to form lipid nanodiscs. The SLS and ^{31}P solid-state NMR experimental results revealed the high stability of polymer nanodiscs formed by both of the polymers under acidic conditions, and the tolerance of these nanodiscs to monovalent and divalent cations. The results reported in this study also show the significant role of the charge of the polymer in the formation of nanodiscs One potential application of these nanodiscs was proven by the ability of both polymer nanodiscs to solubilize and stabilize one of the well-studied naturally occurring small molecule, curcumin, that is found in turmeric and has been reported to exhibit numerous biological activities including anticancer and antibiotic. We expect that the nanodiscs can also be used to stabilize other polyphenolic compounds such as EGCG that are used to inhibit amyloid aggregation[62-63] Therefore, we expect that the reported polymers and the findings will broaden the applications of polymer based nanodiscs in general and in particular to study those membrane proteins that are functional under acidic environments. The unique pH selective nanodisc formation of SMAd-A and SMA-ED polymer can potentially be utilized in drug delivery and other biotechnological applications. In addition, we expect that these polymer-based lipid nanodiscs to expand the applications of sophisticated solid-state NMR techniques to study atomic-resolution structure, dynamics and membrane topology of membrane proteins.[45,65]

2.6 Acknowledgements: This study was supported by funds from NIH (GM084018 to A.R.).

2.7 References

1. A. Engel, H. E. Gaub, *Annu. Rev. Biochem.* 2008, 77, 127-148.

2. R. Koebnik, K. P. Locher, P. Van Gelder, *Mol. Microbiol.* 2000, 37, 239-253.

3. M. S. Almén, K. J. V. Nordström, R. Fredriksson, H. B. Schiöth, *BMC Biology* 2009, *7*, 50-64.

4. C. Barnaba, K. Gentry, N. Sumangala, A. Ramamoorthy, *F1000Research* 2017, 6-17.

5. Y. Miao, T. A. Cross, *Curr. Opin. Struct. Biol.* 2013, 23, 919-928.

6. S. Kalipatnapu, A. Chattopadhyay, *IUBMB Life* 2005, *57,* 505-512.

7. G. G. Privé, *Methods* 2007, 41, 388-397.

8. J.-L. Rigaud, D. Lévy, *Methods Enzymol.* 2003, 372, 65-86.

9. J. Knol, K. Sjollema, B. Poolman, *Biochemistry* 1998, 37, 16410-16415.

10. C. R. Sanders, B. J. Hare, K. P. Howard, J. H. Prestegard, *Prog. Nucl. Magn. Reson. Spectrosc.* 1994, 26, 421-444.

11. C. R. Sanders, R. S. Prosser, *Structure* 1998, 6, 1227-1234.

12. U. H. N. Dürr, M. Gildenberg, A. Ramamoorthy, *Chem. Rev.* 2012, 111, 6054-6074.

13. L. Czerski, C. R. Sanders, *Anal. Biochem.* 2000, 284, 327-333.

14. A. M. Seddon, P. Curnow, P. J. Booth, *BBA-Biomembranes* 2004, 1666, 105-117.

15. S. Hiller, R. G. Garces, T. J. Malia, V. Y. Orekhov, M. Colombini, G. Wagner, *Science* 2008, 321, 1206-1210.

16. C. Tribet, R. Audebert, J.-L. Popot, *Proc. Natl. Acad. Sci. U.S.A.* 1996, 93, 15047-15050.

17. P. Bazzacco, E. Billon-Denis, K. S. Sharma, L. J. Catoire, S. Mary, C. Le Bon, E. Point, J.-L. Banères, G. Durand, F. Zito, B. Pucci, J.-L Popot, *Biochemistry* 2012, 51, 1416-1430.

18. A. Nath, W. M. Atkins, S. G. Sligar, *Biochemistry* 2007, 46, 2059-2069.

19. Z .Hu, J. C. S. Ho, M. Nallani, *Curr. Opin. Biotechnol.* 2017, 46, 51-56.

20. F. Hagn, M. Etzkorn, T. Raschle, G. Wagner, *J. Am. Chem. Soc.* 2013, 135, 1919-1925.

21. I. G. Denisov, S. G. Sligar, *Nat. Struct. Mol. Biol.* 2016, 23, 481-486.

22. I. G. Denisov, S. G. Sligar, *Chem. Rev.* 2017, 117, 4669-4713.

23. I. G. Denisov, Y. V. Grinkova, A. A. Lazarides, S. G. Sligar, *J. Am. Chem. Soc.* 2004, 126, 3477-3487.

24. J Borch, T. Hamann, *Biol. Chem.* 2009, 390, 805.

25. J. M. Dorr, M. C. Koorengevel, M. Schafer, A. V. Prokofyev, S. Scheidelaar, E. A. van der Cruijsen, T. R. Dafforn, M. Baldus, J. A. Killian, *Proc. Natl. Acad. Sci. U.S.A.* 2014, 111, 18607-12.

26. T. Murakami, *Biotechnol. J.* 2012, 7, 762-767.

27. R. O. Ryan, *Expert Opin. Drug Deliv.* 2008, 5, 343-351.

28. R. Kuai, L. J. Ochyl, K. S. Bahjat, A. Schwendeman, J. J. Moon, *Nat. Mater.* 2017, 16, 489-496.

29. M. Zhang, R. Huang, R. Ackermann, S. C. Im, L. Waskell, A. Schwendeman, A. Ramamoorthy, *Angew. Chem. Int. Ed.* 2016, 128, 4497-4499.

30. S. R. Midtgaard, M. C. Pedersen, J. J. K. Kirkensgaard, K. K. Sorensen, K. Mortensen, K. J. Jensen, L. Arleth, *Soft Matter* 2014, 10, 738-752.

31. S. T. Reddy, M. Navab, G. M. Anantharamaiah, A. M. Fogelman, *Curr. Opin. Lipidol.* 2014, 25, 304-308.

32. S. H. Park, S. Berkamp, G. A. Cook, M. K. Chan, H. Viadiu, S. J. Opella, *Biochemistry* 2011, 50, 8983-8985.

33. S. K Scheidelaar, C. Martijn J. D. Pardo, J. D. Meeldijk, E. Breukink, J. A. Killian, *Biophys. J.* 2015, 108, 279-290.

34. J. M. Dörr, S. Scheidelaar, M. C. Koorengevel, J. J. Dominguez, M. Schäfer, C. A. van Walree, J. A. Killian, *Eur. Biophys. J.* 2016, 45, 3-21.

35. S. C. Lee, T. J. Knowles, V. L Postis, M. Jamshad, R. A. Parslow, Y. P. Lin, A. Goldman, P. Sridhar, M. Overduin, S. P. Muench, T. R. Dafforn, *Nat. Protoc.* 2016, 11, 1149-62.

36. M. C Orwick, P. J. Judge, J. Procek, L. Lindholm, A. Graziadei, A. Engel, G. Grobner, A. Watts, *Angew. Chem. Int. Ed. Engl.* 2012, 51, 4653-7.

37. A. Oluwole, B. Danielczak, A. Meister, J. Babalola, C. Vargas, S. Keller, *Angew. Chem. Int. Ed. Engl.* 2017, 56, 1919-1924.

38. J. J. Dominguez Pardo, J. M. Dörr, A. Iyer, R. C. Cox, S. Scheidelaar, M. C. Koorengevel, V. Subramaniam, J. A. Killian, *Eur. Biophys. J.* 2017, 46, 91-101.

39. I. D. Sahu, R. Zhang, M. M. Dunagan, A. F. Craig, G. A. Lorigan, *J. Phys. Chem. B* 2017, 121, 5312-5321.

40. R. Zhang, I. D. Sahu, L. Liu, A. Osatuke, R. G. Comer, C. Dabney-Smith, G. A Lorigan, *Biochim. Biophys. Acta.* 2015, 1848, 329-333.

41. A. F. Craig, E. E. Clark, I. D. Sahu, R. Zhang, N. D. Frantz, M. S. Al-Abdul-Wahid, C. Dabney-Smith, D. Konkolewicz, G. A. Lorigan, *BBA-Biomembranes* 2016, 1858, 2931-2939.

42. M. Orwick-Rydmark, J. E. Lovett, A. Graziadei, L. Lindholm, M. R. Hicks, A. Watts, *Nano Lett.* 2012, 12, 4687-4692.

43. T. J. Knowles, R. Finka, C. Smith, Y.-P. Lin, T. Dafforn, M. Overduin *J. Am. Chem. Soc.* 2009, 131, 7484-7485.

44. D. J. K. Swainsbury, S. Scheidelaar, R. van Grondelle, J. A. Killian, M. R. Jones, *Angew. Chem. Int. Ed. Engl.* 2014, 53, 11803-11807.

45. T. Ravula, S. Ramadugu, G. Di Mauro, A. Ramamoorthy, *Angew. Chem. Int. Ed. Engl* 2017, 56, 11466-11470.

46. A. Ladokhin, *Toxins* 2013, 5, 1362.

47. W. Kuhlbrandt, *Nat. Rev. Mol. Cell Biol.* 2004, 5, 282-295.

48. S. Scheidelaar, M. C. Koorengevel, C. A. van Walree, J. J. Dominguez, J. M. Dörr, J. A. Killian, *Biophys. J.* 2016, 111, 1974-1986.

49. M. Tanaka, A. Hosotani, Y. Tachibana, M. Nakano, K. Iwasaki, T. Kawakami, T. Mukai, *Langmuir* 2015, 31, 12719-12726.

50. D. O. O'Keefe, V. Cabiaux, S. Choe, D. Eisenberg, R. J. Collier, *Proc. Natl. Acad. Sci. U.S.A.* 1992, 89, 6202-6206.

51. O. A. Andreev, A. G. Karabadzhak, D. Weerakkody, G. O. Andreev, D. M. Engelman, Y. K. Reshetnyak, *Proc. Natl. Acad. Sci. U.S.A.* 2010, 107, 4081-4086.

52. Z. Xie, S. Schendel, S. Matsuyama, J. C. Reed, *Biochemistry* 1998, 37, 6410-6418.

53. K. A. Morrison, A. Akram, A. Mathews, Z. A. Khan, J. H. Patel, C. Zhou, D. J. Hardy, C. Moore-Kelly, R. Patel, V. Odiba, T. J. Knowles, M. H. Javed, N. P. Chmel, T. R. Dafforn, A. J. Rothnie, *Biochem. J.* 2016, 473, 4349-4360.

54. A. Caputo, E. Caci, L. Ferrera, N. Pedemonte, C. Barsanti, E. Sondo, U. Pfeffer, R. Ravazzolo, O. Zegarra-Moran, L. J. V. Galietta, *Science* 2008, 322, 590-594.

55. T. Dudev, C. Lim, *J. Am. Chem. Soc.* 2013, 135, 17200-17208.

56. M. F. M. Sciacca, M. Pappalardo, D. Milardi, D. M. Grasso, C. L. Rosa, *Arch. Biochem. Biophys.* 2008, 477, 291-298.

57. G. Di Natale, G. Pappalardo, D. Milardi, M. F. M. Sciacca, F. Attanasio, F. D. La Mendola, E. Rizzarelli, *J. Phys. Chem. B* 2010, 114, 13830-13838.

58. B. B. Aggarwal, K. B. Harikumar, *Int. J. Biochem. Cell Biol.* 2009, 41, 40-59.

59. Y. J. Wang, M. H. Pan, A. L. Cheng, L. I. Lin, Y. S. Ho, C. Y. Hsieh, J. K. Lin, *J. Pharm. Biomed. Anal.* 1997, 15, 1867-1876.

60. P. Anand, A. B. Kunnumakkara, R. A. Newman, B. B. Aggarwal, *Mol. Pharm.* 2007, 4, 807-818.

61. J. Barry, M. Fritz, J. R. Brender, P. E. S Smith, D. K. Lee, Ramamoorthy, A., *J. Am. Chem. Soc.* 2009, 131, 4490-4498.

62. R. Ahmed, B. VanSchouwen, N. Jafari, X. Ni, J. Ortega, G. Melacini, *J. Am. Chem. Soc.* 2017, 139, 13720-13734.

63. N. Popovych, J. R. Brender, R. Soong, S. Vivekanandan, K. Hartman, V. Basrur, P. M. Macdonald, A. Ramamoorthy, *J. Phys. Chem. B* 2012, 116, 3650-3658.

64. B. Bersch, J. M. Dorr, A. Hessel, J. A. Killian, P. S Schanda, *Angew. Chem., Int. Ed.* 2017, 56, 2508−2512.

Chapter 3

Formation of pH-Resistant Monodispersed Polymer-Lipid Nanodiscs

Portions of this chapter are reproduced from: T. Ravula[+], N.Z. Hardin[+], S.K. Ramadugu, S.J. Cox, A. Ramamoorthy, *Angew. Chem. Int. Ed.* 2018, 57,1342–1345. (Co-first author)

3.1 Introduction

Controlled molecular self-assembly in the formation of soft nanomaterials has been a challenge in bio-nanotechnology.[1, 2] Nanodiscs, lipid bilayers surrounded by an amphiphilic belt, are engineered soft nanomaterials that have been inspired from biological systems such as high-density lipo-particles (HDL).[3] These nanodiscs provide a lipid bilayer environment that is nearly like a native membrane, and they have been used to study the structure and function membrane proteins.[3-5] Recent developments have expanded the formation of nanodiscs using different types of amphiphilic systems such as proteins,[6-10] peptides,[11] and polymers.[12-15] Polymer nanodiscs exhibit significant advantages over conventional protein-based nanodiscs, such as detergent-free membrane protein extraction,[16] and they are devoid of interferences from the belt-forming protein or peptide.[17]

Currently, no polymer nanodisc systems have been able to demonstrate precise control of size and morphology over a wide range of sizes or tolerance towards a broad range of pH and divalent metal ions.[16] These unique properties are needed to greatly expand the applicability of nanodisc technology. Herein we report the directed self-assembly of covalently modified styrene

maleic acid copolymer with lipid bilayers to form monodispersed nanodiscs that show ultra-stability towards a broad range of pH and divalent metal ion concentration. We also demonstrate the ability to control the size of the self-assembled nanodiscs and size-dependent unique magnetic alignment properties.

3.2 Material and Methods

Poly(Styrene-co- Maleic Anhydride) cumene terminated ~1.3:1 (SMA Mn ~1600 g/mol), (2Aminoethyl)trimethylammonium chloride hydrochloride, Triethylamine (Et_3N), phosphoric acid (H_3PO_4), sodium phosphate, sodium chloride, hydrochloric acid (HCl), sodium hydroxide (NaOH), trifluoracetic acid (TFA), 4-(2-hydroxyethyl)-1-piperazineethanesulfonic acid (HEPES), diethyl ether (Ether), calcium chloride ($CaCl_2$), magnesium chloride ($MgCl_2$), Dimethylformamide (DMF), Acetic Anhydride, and Sodium Acetate were purchased from Sigma-Aldrich®. 1,2dimyristoyl-sn-glycero-3-phosphocholine (DMPC) was purchased from Avanti Lipids Polar, Inc®.

Synthesis of SMA-QA: 1 g of SMA was dissolved in 30 ml of anhydrous DMF dried over molecular sieves. 1.3 g of (2aminoethyl)trimethylammonium chloride hydrochloride was then added to the solution and to this mixture 5 ml of trimethylamine was added causing the solution to turn dark yellow. The reaction mixture was then stirred at 100 °C for 12 hours. The solution was cooled to room temperature and precipitated with diethyl ether. The precipitate was washed 3 times with diethyl ether and dried under vacuum. The dried intermediate was then added to 30 ml acetic anhydride. 660 mg of sodium acetate and 200 mg of triethylamine were then added. The reaction mixture was heated at 100 °C overnight and precipitated in ether. The precipitate was washed 3 times with ether and dried under vacuum. The product was then dissolved in water and passed

through a saphadex LH-20 column. The product was collected and then lyophilized to give a 850 mg brown powder.

Formation of nanodiscs: Nanodiscs of differing sizes were prepared using DMPC (10 mg/ml) in 20 mM sodium phosphate buffer containing 50 mM NaCl at pH 7.4. 10 mg/ml of polymer stock solutions were made in the same buffer solution. The required amount of polymer solution was added to the DMPC mixture and incubated for 4 hr at 35 °C. The samples made using DMPC:SMA-QA weight ratios of 1:0.25 and 1:0.5 were prepared using three freeze thaw cycles alternating between liquid nitrogen temperature and 35 °C. After the freeze thaw cycles the samples were further incubated at 35 °C for 4 hrs.

SLS experiments: The pH stability and metal ion stability experiments were carried out by measuring the intensity of scattered light at a 90° angle using a Fluro-Fluorimeter under identical DMPC concentrations. 500 ul of nanodiscs were dispensed into a 2 ml cuvette under stirring. Then the solutions were diluted to 2 ml with buffer. pH titrations were performed using 1M HCl and NaOH. Metal ion titrations were performed using 5M $MgCl_2$, 5M NaCl, and 3.3M $CaCl_2$. The excitation and emission wavelengths were set at 400 nm and 404 nm respectively. The slit opening was set to 2 nm. All SLS experimental measurements were carried out using a FluoroMax 4® from Horiba Scientific®. Time Dependent solubilization studies were run using the same fluorimeter settings as noted above using indicated polymer to lipid ratios.

Solid state NMR Spectroscopy: Phosphorous-31 NMR spectra were acquired using an Agilent/Varian 400 MHz solid-state NMR spectrometer and a 5 mm triple-resonance probe with 31P and 1H resonance frequencies of 161.974 MHz and 400.114 MHz, respectively. 5µs 900 pulse, 30 kHz ^{1}H continuous-wave decoupling, 2,000 scans, and a 4 s recycle delay were used to acquire

^{31}P NMR spectra. ^{31}P chemical shifts were referenced by setting the ^{31}P chemical shift of 100 % H_3PO_4 sample to 0 ppm.

CPMAS solid-state NMR experiments: Carbon-13 CPMAS experiments were carried on a Bruker 500 MHz solid-state NMR spectrometer under 12 kHz MAS using a 2.5 mm triple-resonance MAS probe operating at 500.112 MHz and 125.721 MHz for ^{1}H and ^{13}C, respectively. The reported CPMAS spectra (Figure 1 of the main text) were acquired using the following parameters: 3 µs 90° pulse, 2 ms CP contact time, 40 ms acquisition time, 4096 number of scans, 4s recycle delay and a 50 kHz radio-frequency decoupling of protons during the acquisition of ^{13}C magnetization. ^{13}C chemical shifts were calibrated by setting the chemical shift of CH_2 resonance of adamantane powder sample to 28.5 ppm.

^{14}N NMR Experiments: Nitrogen-14 NMR spectra were acquired using an Agilent/Varian 400 MHz solid-state NMR spectrometer and a 5 mm triple-resonance probe operating at the ^{14}N resonance frequency of 29.910 MHz. ^{14}N NMR spectra were recorded using the quadrupole-echo pulse sequence with a 90° pulse length of 5 µs and an echo-delay of 1.1 ms. ^{14}N magnetization was acquired using 25 ms acquisition time, 10000 scans and a recycle delay of 1.5 s with no ^{1}H decoupling.

Fourier-Transform Infrared (FT - IR) Spectroscopy: The FT-IR spectra from 4000 cm^{-1} to 800 cm^{-1} were recorded using a Thermos scientific ATR-FTIR instrument.

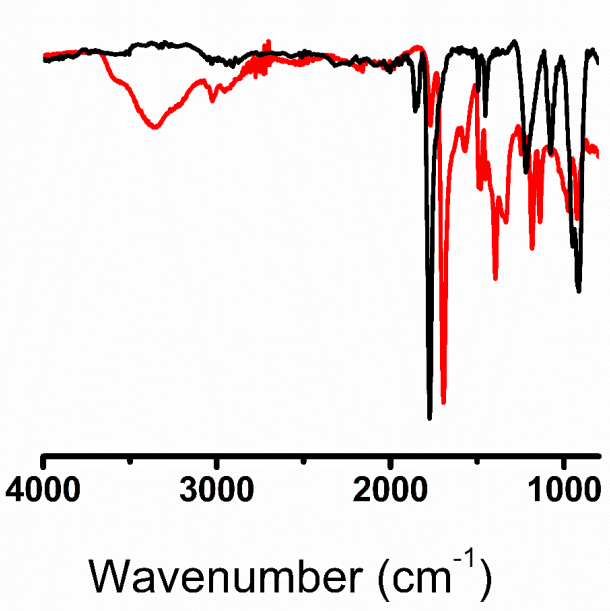

Figure 3-1: FTIR spectra of SMA (black) and the newly synthesized SMA-QA (red) polymers.

Water was removed by lyophilization from each of the samples before recording the spectrum (**Figure 3-1**).

Dynamic Light Scattering (DLS): All DLS experiments were performed using Wyatt Technology® DynaPro® NanoStar® using a 1 µL quartz MicroCuvette.

Transmission Electron Microscopy (TEM): All TEM micrographs were obtained using a Technai® T - 20® machine (FEI®, Netherlands) with a 80 kV operating voltage. A dilute solution was dropped on a carbon-coated copper grid and dried overnight at room temperature in a desiccator before using in experiments.

Size exclusion chromatography: Polymer-lipid nanodiscs were purified by size exclusion chromatography (SEC), using Superdex 200 Increase 300/10 GL column operated on an AKTA purifier (GE Healthcare, Freiburg, Germany). The elution profiles of polymer nanodisc contained two peaks one corresponding to nanodisc and other to the free polymer. All nanodisc samples were subjected to SEC to remove the free polymer.

Nitrogen-14 Quadrupole coupling: The ^{14}N quadrupole coupling is an axially symmetric tensor for the ^{14}N of choline group in DMPC lipid. Hence, the observed quadrupolar splitting is a direct measurement of the molecular order parameter of the Cβ-N (CN) bond of the choline moiety.

3.3 Results and Discussion

Synthesis of SMA-QA (styrene maleimide quaternary ammonium) was achieved by the treatment of a low-molecular-weight SMA (ca. 1.6 kDa) with (2-aminoethyl)trimethylammonium chloride hydrochloride in anhydrous dimethylformamide while heating in the presence of excess triethylamine. Maleimide formation was accomplished by a dehydration reaction using acetic anhydride, sodium acetate, and triethylamine (**Figure 3-2 a**). The newly synthesized SMA-QA

polymer was characterized using FTIR spectropscopy and ^{13}C-CPMAS (cross-polarization magic-angle spinning) solid-state NMR experiments. FTIR spectrum of SMA-QA exhibits a shift in carbonyl C=O stretching frequency from 1774 cm^{-1} to 1693 cm^{-1}, showing the successful formation of maleimide (**Figure 3-1**). The formation of SMA-QA was further confirmed by a ^{13}C CPMAS NMR spectrum (**Figure 3-2 b**): the peaks appearing at about 32 ppm and about 40 ppm are from the CH_2 group, and the peaks at about 53 ppm and about 62 ppm are from the methyl carbons associated with quaternary ammonium and methylene carbons, respectively. The observed change in the chemical shift of the carbonyl carbon from about 172 (from the reactant SMA polymer) to about 178 ppm (from the product SMA-QA polymer) confirms the presence of maleimide carbonyls and completion of the reaction and product formation (**Figure 3-2 b**).

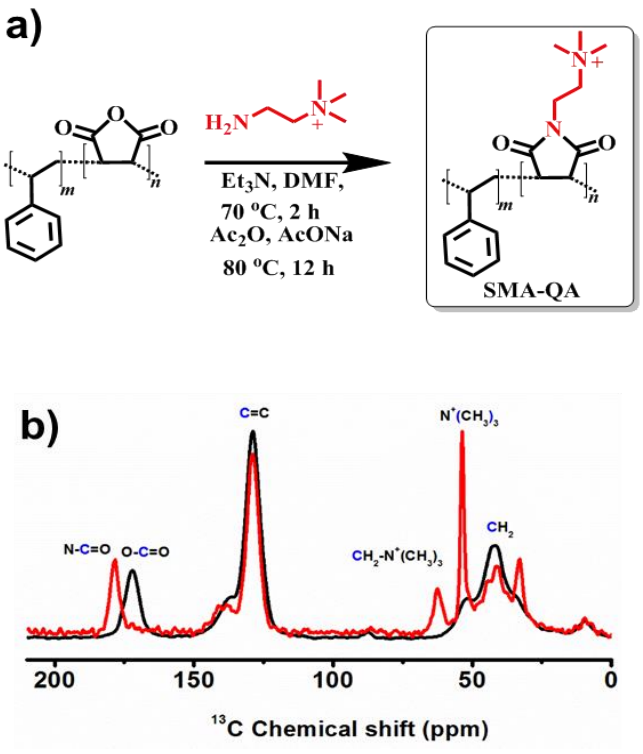

Figure 3-2: Synthesis and characterization of SMA-QA polymer. (a) Reaction scheme showing the modifications of SMA polymer to synthesize SMA-QA. (b) ^{13}C CPMAS solid-state NMR spectra of SMA (black) and SMA-QA (red) polymers confirm the formation and successful completion of the chemical reaction.

Next, we characterized the ability of SMA-QA to form lipid bilayer nanodiscs. Upon the addition of an aqueous solution of SMA-QA to a turbid solution of DMPC (1,2-dimyristoyl-sn-glycero-3-phosphocholine) multilamellar vesicles (MLVs), the turbid solution spontaneously became clear, indicating an efficient solubilization of MLVs by the polymer. The solubilization kinetics was followed by static light scattering (SLS) measurements. (**Figure 3-3 b**) shows the SLS profiles of DMPC MLVs for different lipid to polymer weight ratios. As shown in (**Figure 3-3 b**), the large intense scattering observed for DMPC MLVs dramatically decreased upon the addition

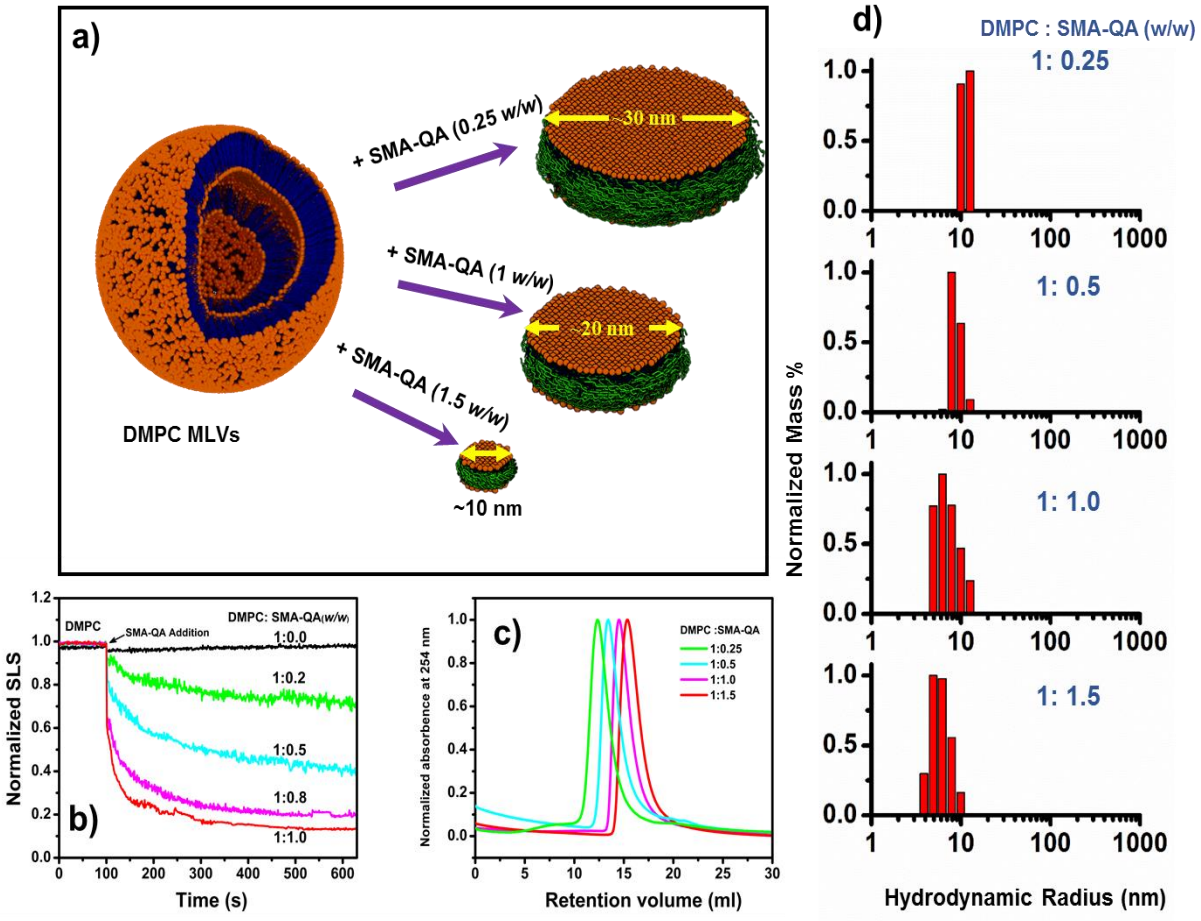

Figure 3-3: Formation and size tunability of SMA-QA lipid nanodiscs. a) Schematic illustrating the formation of SMA-QA nanodiscs of varying size. **b**) SLS profiles showing the kinetics of DMPC MLVs solubilization. **c**) Size exclusion profiles of nanodiscs made by varying the DMPC:SMA-QA weight ratio**. d**) DLS profiles of purified DMPC:SMA-QA nanodiscs demonstrate the formation of different size nanodiscs by varying the weight ratio of DMPC:SMA-QA.

of SMA-QA polymer, demonstrating the solubilization of large DMPC MLVs into small size polymer–lipid nanodiscs. Our results further demonstrate that the kinetics of solubilization of MLVs by the polymer was found to depend on the ratio of DMPC:SMA-QA (**Figure 3-3 b**). The rate of solubilization of MLVs was accelerated by the increase of the amount of SMA-QA.

The lipid nanodiscs formed by the SMA-QA polymer were subjected to size exclusion chromatography (SEC) to remove the free polymer. The SEC retention volume of purified nanodiscs was found to be dependent on the lipid:polymer ratio used in the nanodisc formation as

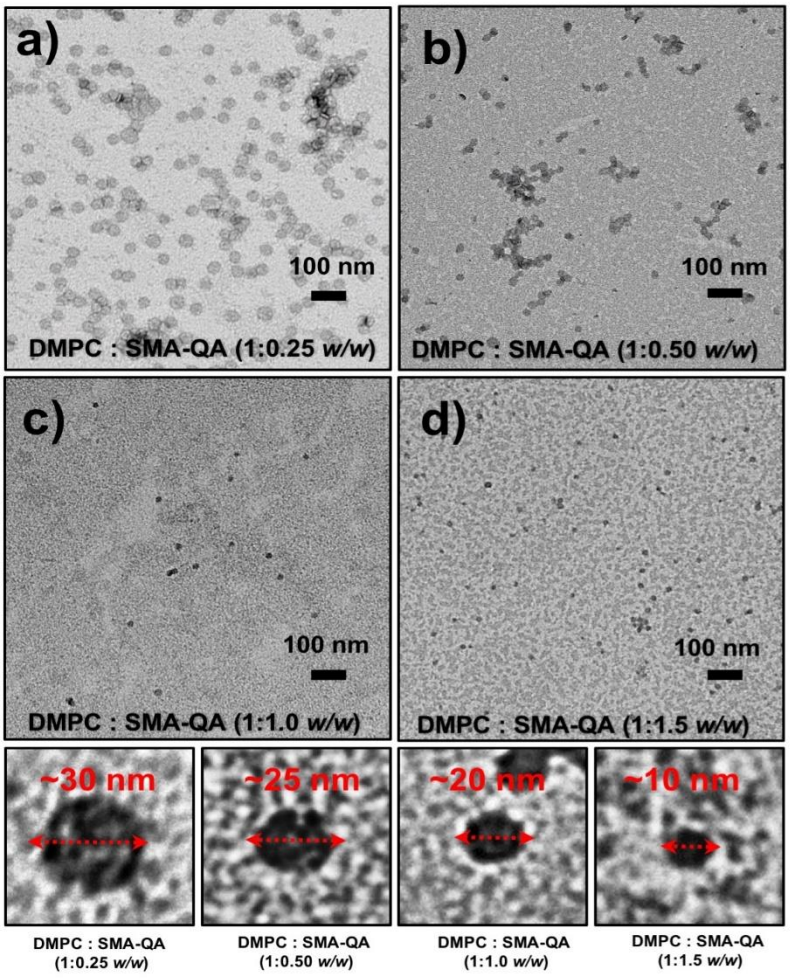

Figure 3-4: Remarkably monodispersed and circular shaped polymer nanodiscs revealed by TEM. (a-d) TEM images of DMPC:SMA-QA nanodiscs formed with the indicated lipid to polymer ratio. Expanded images of nanodiscs showing the remarkable disc shape of the nanodisc for different sizes (bottom most row).

shown (**Figure 3-3 c**). The resulting nanodisc solutions were further characterized using dynamic light scattering (DLS) experiments. The DLS profiles showed the presence of monodispersed nanodiscs of varying hydrodynamic radii (ca. 5 to ca. 13 nm) that were dependent on the ratio of DMPC to SMA-QA (**Figure 3-3 d**). Then, the size and morphology of the resulting nanodiscs were characterized using transmission electron microscopy (TEM) images. The TEM images of DMPC:SMA-QA nanodiscs confirmed the presence of disc-shaped, monodispersed particles as

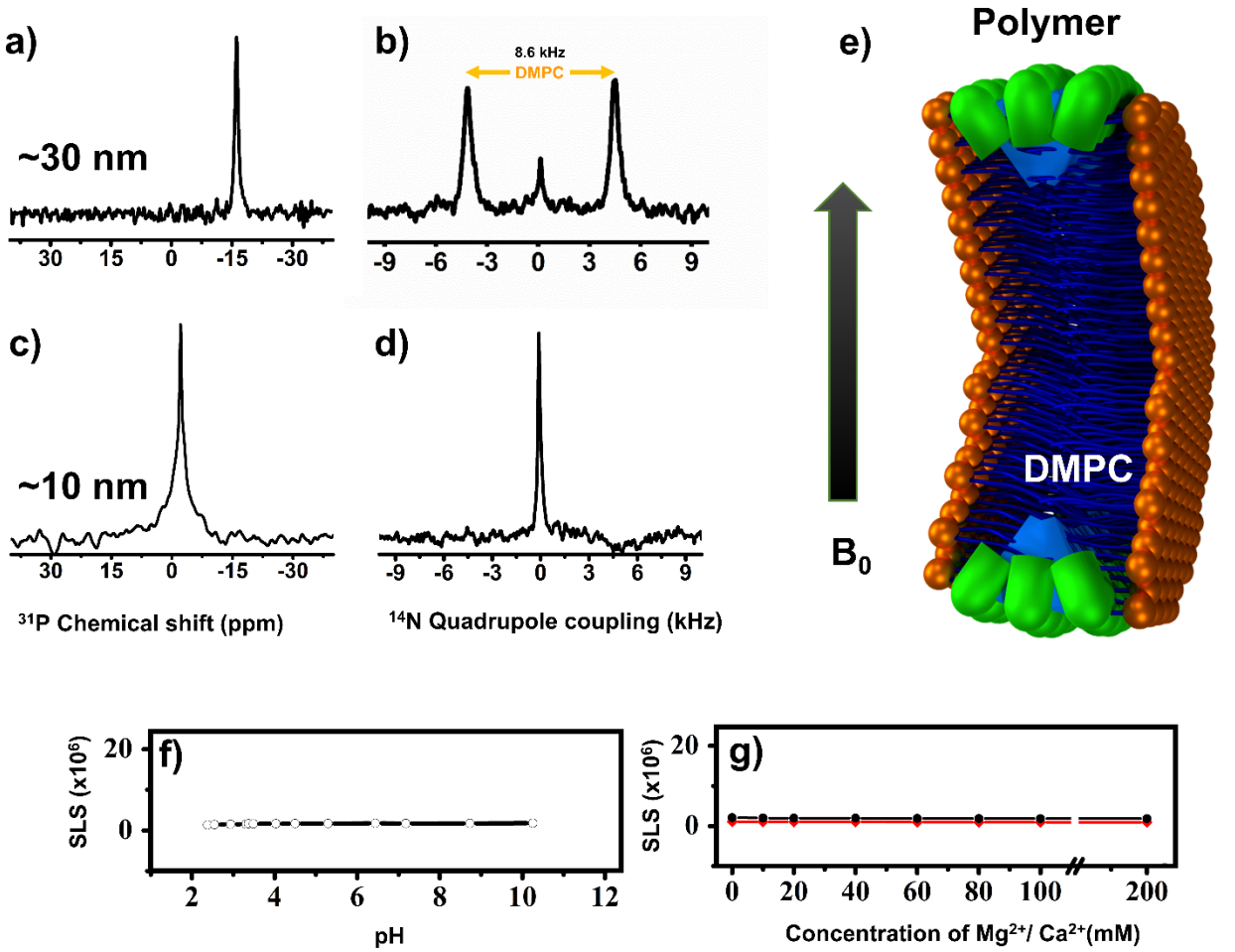

Figure 3.5: SMA-QA nanodiscs exhibit magnetic alignment and remarkable tolerance to pH and divalent metal ions. a) ^{31}P and **b**) ^{14}N NMR spectra of magnetically aligned large-size (ca. 30 nm diameter) nanodiscs made from DMPC:SMA-QA (1:0.25 w/w). **c**) ^{31}P and **d**) ^{14}N NMR spectra of isotropic nanodiscs (ca. 10 nm diameter) made from DMPC:SMA-QA (1:1.5 w/w). **e**) A nanodisc illustrating the orientations of the lipid head group and polymer in magnetically aligned nanodiscs. **f**), **g**) SLS profiles of DMPC:SMAQA (1:1 w/w) nanodiscs showing remarkable stability towards pH (**f**) and the presence of Mg^{2+} and Ca^{2+} ions (**g**).

shown (**Figure 3-4**). The expanded images shown (**Figure 3-4** (bottom most row)) show the size of individual nanodiscs and their remarkable circular shape.

The precise control over the size of nanodiscs for a wide range of sizes (ranging from 10 nm to 30 nm) inspired us to test their magnetic-alignment properties using solid-state NMR experiments under static conditions. The ^{31}P (spin=1/2) and ^{14}N (spin=1) spectra obtained from polymer nanodiscs are shown in (**Figure 3-5**). The ^{31}P NMR spectrum of DMPC:SMA-QA (1:0.25 *w/w*) shows a single narrow peak at about −16 ppm (**Figure 3-5 a**) demonstrating the magnetic alignment of polymer nanodiscs with the bilayer normal perpendicular to the magnetic field direction (**Figure 3-5 a**).[14] Owing to the large size (ca. 30 nm diameter), the slow tumbling of nanodiscs (the large nanodiscs are also called macro-nanodiscs[14]) allows the magnetic alignment in an external magnetic field. On the other hand, a narrow peak was observed at the isotropic chemical shift frequency (ca. −2 ppm) for small nanodiscs (ca. 10 nm), demonstrating their fast tumbling in the NMR timescale (**Figure 3-5 c**).

The ^{14}N NMR spectra of SMA-QA nanodiscs (ca. 30 nm) show three peaks corresponding to quadrupolar coupling values of about 8.6 (**Figure 3-5 b**). The magnitude of the observed quadrupolar coupling is dependent on the orientation of the quaternary ammonium C^{β}–N bond vector with respect to the magnetic field direction. The observed quadrupolar coupling magnitude of about 8.6 kHz arises from the choline group of DMPC. The observed quadrupolar couplings of a magnitude of about 2.9 kHz and about 14 kHz are from the quaternary ammonium group of the SMA-QA polymer. The observed 0 kHz quadrupolar coupling is likely to be from the quaternary ammonium group of the SMA-QA polymer. The SMA-QA polymer belt completely surrounds the lipid bilayer as shown in Figure 4e, which is similar to the orientations of detergent molecules in aligned bicelles.[18] As expected, the ^{14}N NMR spectrum of small nanodiscs (ca. 10 nm diameter)

showed a single narrow peak at the isotropic chemical shift value (0 ppm) suggesting the fast tumbling nature of isotropic nanodiscs in agreement with ^{31}P NMR data.

The major disadvantages of SMA and other polymers used to form nanodiscs is their poor stability towards pH and metal ions.[19] This instability is attributed to the presence of carboxylic/carboxylate groups that form the hydrophilic region of the amphiphilic polymer.[16] SMA-QA was specifically engineered and synthesized with a quaternary ammonium group as the hydrophilic portion of the polymer to increase the tolerance to pH and metal ions. The stability of the SMA-QA nanodiscs against pH and metal ion concentration was examined using SLS measurements (**Figure 4 f and g**). The SLS profiles of the DMPC:SMA-QA (1:1 w/w) nanodiscs showed no change in the scattering intensity over a wide range of pH (from about 2.5 to 10) and in the presence of metal ion concentrations up to 200 mM. These results signify the ultrahigh stability of DMPC:SMA-QA nanodiscs, further expanding the applicability of nanodisc technology to a wider range of biological and biomedical applications.

3.4 Conclusion

In conclusion, the newly developed SMA-QA polymer allows for the formation of monodispersed lipid nanodiscs with a precise size control and ultrahigh stability against pH (2.5–10) and metal ion concentrations up to 200 mM. The formation and stability of DMPC:SMA-QA nanodiscs were characterized using various biophysical experiments including solid-state NMR spectroscopy. The macro-nanodiscs (>20 nm diameter) showed magnetic alignment properties that can be utilized in the structural studies of membrane proteins by solid-state NMR techniques.[14, 20-23] Because of these unique properties of SMA-QA polymer nanodiscs, SMA-QA is a robust membrane mimetic tool that offers significant advantages over all currently reported nanodisc

systems, and therefore we foresee a significant expansion in the applicability of nanodisc technology. We expect direct and immediate impacts in the structural biology studies of those membrane proteins that are sensitive to pH and divalent metal ions[24-28] and amyloid proteins that self-assemble at the membrane interface.[29, 30]

3.5 Acknowledgements: This study was supported by funds from NIH (GM084018 to A.R.).

3.6 References

1. G. Whitesides, J. Mathias, C. Seto, *Science* 1991, 254, 1312– 1319.

2. M. Sarikaya, C. Tamerler, A. K. Y. Jen, K. Schulten, F. Baneyx, *Nat. Mater.* 2003, 2, 577– 585.

3. I. G. Denisov, S. G. Sligar, *Nat. Struct. Mol. Biol.* 2016, 23, 481– 486.

4. I. G. Denisov, S. G. Sligar, *Chem. Rev.* 2017, 117, 4669– 4713.

5. S. C. Lee, N. L. Pollock, *Biochem. Soc. Trans.* 2016, 44, 1011– 1018.

6. T. H. Bayburt, Y. V. Grinkova, S. G. Sligar, *Nano Lett.* 2002, 2, 853– 856.

7. M. L. Nasr, D. Baptista, M. Strauss, Z. J. Sun, S. Grigoriu, S. Huser, A. Pluckthun, F. Hagn, T. Walz, J. M. Hogle, G. Wagner, *Nat. Methods* 2017, 14, 49– 52.

8. F. Hagn, M. Etzkorn, T. Raschle, G. Wagner, *J. Am. Chem. Soc.* 2013, 135, 1919– 1925.

9. F. Hagn, G. Wagner, *J. Biomol. NMR* 2015, 61, 249– 260.

10. T. H. Bayburt, S. G. Sligar, *FEBS Lett.* 2010, 584, 1721– 1727.

11. M. Zhang, R. Huang, R. Ackermann, S. C. Im, L. Waskell, A. Schwendeman, A. Ramamoorthy, *Angew. Chem. Int. Ed.* 2016, 55, 4497– 4499.

12. A. Oluwole, B. Danielczak, A. Meister, J. Babalola, C. Vargas, S. Keller, *Angew. Chem. Int. Ed.* 2017, 56, 1919– 1924.

13. M. C. Orwick, P. J. Judge, J. Procek, L. Lindholm, A. Graziadei, A. Engel, G. Gröbner, A. Watts, *Angew. Chem. Int. Ed.* 2012, 51, 4653– 4657.

14. T. Ravula, S. K. Ramadugu, G. Di Mauro, A. Ramamoorthy, *Angew. Chem. Int. Ed.* 2017, 56, 11466– 11470.

15. I. D. Sahu, R. Zhang, M. M. Dunagan, A. F. Craig, G. A. Lorigan, *J. Phys. Chem. B* 2017, 121, 5312– 5321.

16. S. C. Lee, T. J. Knowles, V. L. G. Postis, M. Jamshad, R. A. Parslow, Y.-p. Lin, A. Goldman, P. Sridhar, M. Overduin, S. P. Muench, T. R. Dafforn, *Nat. Protoc.* 2016, 11, 1149– 1162.

17. J. M. Dörr, M. C. Koorengevel, M. Schafer, A. V. Prokofyev, S. Scheidelaar, E. A. van der Cruijsen, T. R. Dafforn, M. Baldus, J. A. Killian, *Proc. Natl. Acad. Sci. USA* 2014, 111, 18607– 18612.

18. S. V. Dvinskikh, K. Yamamoto, U. H. Durr, A. Ramamoorthy, *J. Magn. Reson.* 2007, 184, 228– 235.

19. T. Ravula, N. Z. Hardin, S. K. Ramadugu, A. Ramamoorthy, *Langmuir* 2017, 33, 10655– 10662.

20. S. H. Park, S. Berkamp, G. A. Cook, M. K. Chan, H. Viadiu, S. J. Opella, *Biochemistry* 2011, 50, 8983– 8985.

21. U. H. Dürr, M. Gildenberg, A. Ramamoorthy, *Chem. Rev.* 2012, 112, 6054– 6074.

22. H. Qin, Y. Miao, T. A. Cross, R. Fu, *J. Phys. Chem. B* 2017, 121, 4799– 4809.

23. E. S. Salnikov, C. Aisenbrey, F. Aussenac, O. Ouari, H. Sarrouj, C. Reiter, P. Tordo, F. Engelke, B. Bechinger, *Sci. Rep.* 2016, 6, 20895-20902.

24. V. Postis, S. Rawson, J. K. Mitchell, S. C. Lee, R. A. Parslow, T. R. Dafforn, S. A. Baldwin, S. P. Muench, *Biochim. Biophys. Acta Biomembr.* 2015, 1848, 496– 501.

25. L. S. Brown, V. Ladizhansky, *Protein Sci.* 2015, 24, 1333– 1346.

26. D. P. Staus, R. T. Strachan, A. Manglik, B. Pani, A. W. Kahsai, T. H. Kim, L. M. Wingler, S. Ahn, A. Chatterjee, A. Masoudi, A. C. Kruse, E. Pardon, J. Steyaert, W. I. Weis, R. S. Prosser, B. K. Kobilka, T. Costa, R. J. Lefkowitz, *Nature* 2016, 535, 448– 452.

27. Y. Gao, E. Cao, D. Julius, Y. Cheng, *Nature* 2016, 534, 347– 351.

28. N. Das, D. T. Murray, T. A. Cross, *Nat. Protoc.* 2013, 8, 2256– 2270.

29. D. C. Rodriguez Camargo, K. J. Korshavn, A. Jussupow, K. Raltchev, D. Goricanec, M. Fleisch, R. Sarkar, K. Xue, M. Aichler, G. Mettenleiter, A. K. Walch, C. Camilloni, F. Hagn, B. Reif, A. Ramamoorthy, *eLife* 2017, 6, e31226.

30. R. Ahmed, B. VanSchouwen, N. Jafari, X. Ni, J. Ortega, G. Melacini, *J. Am. Chem. Soc.* 2017, 139, 13720– 13734.

Chapter 4

Hydrophobic Functionalization of Polyacrylic Acid as a Versatile Platform for the Development of Polymer Lipid Nanodiscs

Portions of this chapter are reproduced from: N.Z Hardin, T. Ravula, G. M. Di Mauro, A. Ramamoorthy, *Small* 2019, *15*, 1804813

4.1 Introduction

Polymer nanodiscs have emerged as a new native-like membrane mimetic in recent years and are routinely being used for the study of membrane proteins.[1-3] A major advantage of using polymers is that they can directly extract membrane proteins from their native environment as shown by the styrene-maleic acid copolymers (SMA).[1, 2, 4-6] Despite the great potential, polymer nanodiscs have suffered from some major drawbacks due to the intrinsic chemical properties of SMA inherent to its hydrophobic and hydrophilic units.[2, 7]. Several studies have already shown an enhancement of SMA's stability by the modification of hydrophilic functional units.[7-12] The most common hydrophobic group used in SMA polymer nanodiscs is the styrene moiety. It is known that styrene has a strong absorption in the UV region that can interfere with various biophysical techniques, and can also have nonspecific interactions with other aromatic groups from the protein.[13, 14] Recently, two styrene-free polymers (Diisobutylene Maleic Acid co-polymer,[14] DIBMA, and Polymethacrylate[13]) have been shown to form nanodiscs; however there has been no systematic investigation comparing the effects of varying the hydrophobic functional groups used in the formation of nanodiscs. In this study, we employed a simple and robust modification method to vary the hydrophobic

groups on a commercially available low molecular weight PAA which allowed us to observe how alkyl-PPA affected the formation, stability, and other properties of nanodiscs.

4.2 Materials and Methods

Poly(acrylic acid) (PAA) average M_w 1800, (catalog 323667 Aldrich), 4-(2-hydroxyethyl)-1-piperazineethanesulfonic acid (HEPES), diethyl ether (Ether), calcium chloride ($CaCl_2$), magnesium chloride ($MgCl_2$), sodium chloride ($NaCl_2$), phosphoric acid (H_3PO_4) and potassium phosphate, were purchased from Sigma-Aldrich®. N-(3-Dimethylaminopropyl)-N′-ethylcarbodiimide hydrochloride (EDC), Pentylamine, Butylamine, Hexylamine, Neopentylamine, Tetrahydrofuran (THF), Hydrochloric acid (HCl), Sodium hydroxide (NaOH) were purchased from Thermo Fisher Scientific®. 1,2- dimyristoyl-sn-glycero-3-phosphocholine (DMPC) was purchased from Avanti Lipids Polar, Inc®. SMA-3000 was a kind gift from Polyscope. Precision Plus Protein™ Prestained Standards, Mini-PROTEAN® TGX™ Precast Protein Gels were obtained from BioRAD.

Synthesis of Akyl-PAA: All polymers were synthesized using the same PAA, Alkylamine, EDC, and solvent ratios. In general PAA (average M_w 1800, 25 acrylic acid groups per chain) was dissolved in THF. 2 eq EDC per acrylic acid group is added to solution and stirred. ddH_2O was added to the stirring solution until all the EDC was dissolved. 0.5 eq of alkyl amine per acrylic acid unit is added to the reaction mixture and the pH is adjusted to ~6.5 if needed. The mixture is diluted with THF and water to yield a final ratio of 70:30 THF:Water solution. The final solution is stirred overnight at room temperature. After completion, THF is removed using rotary evaporation and the cloudy mixture is diluted with an excess 1M NaOH and heated to 80 °C and stirred for 2 hours to hydrolyze any potential anhydrides formed during the reaction. The clear solution is precipitated using 1M HCl, centrifuged, washed 3 times with ddH_2O and lyophilized.

Example: 4 g PAA was dissolved in 160 mL of THF. 22 g EDC was added to the solution followed by 100 mL of ddH_2O and stirred until dissolved. 2.42 g (3.22 mL) of pentylamine was added to the solution and stirred (pH ~6.6). 40 mL of THF was added and the reaction was stirred overnight. The THF was removed using rotary evaporation at 40 °C. The cloudy mixture was diluted with 100 mL 1M NaOH and stirred for 2 hours at 80 °C. The solution was then cooled and precipitated with 1M HCl and centrifuged at 3500 g. The resulting precipitate was suspended in ddH_2O and centrifuged again (repeated 3 times). The final washed product was lyophilized until dry. The overall reaction yielded 4.5 g of final polymer.

Nanodiscs formation: DMPC (10 mg/mL) was suspended in 10 mM potassium phosphate buffer (pH 7.4) to form multilamellar vesicles (MLV). Alkyl-PAA stock solutions of 20 mg/mL were made by dissolving polymer with a minimum amount of 0.1M NaOH and diluting to the necessary concentration using potassium phosphate buffer. The resulting stock solutions where then added together at appropriate weight ratios and diluted to 1 mL using buffer. The resulting solutions were incubated at 35 °C overnight. Free polymer was removed either using SEC or centrifugation filtration using a 10 kDa filter.

^{1}H-NMR spectroscopy: 4 mg of dried polymer was dissolved in 600 µl of 0.1 M NaOD solution in D_2O. NMR spectra were acquired using an Inova 500 MHz NMR spectrometer. 40-168 scans were acquired with a recycle delay of 1s, processed and integrated using VNMRJ software.

Fourier-Transform Infrared (FT-IR) Spectroscopy: The FT-IR spectra from 4000 to 800 cm^{-1} were recorded using a Thermos scientific ATR-FTIR instrument. Lyophilized powder samples of polymers were used to record the spectra.

CP-MAS solid-state NMR experiments: Carbon-13 CPMAS experiments were carried out on a Bruker 500 MHz solid-state NMR spectrometer under 12 kHz MAS using a 3.2 mm triple-resonance MAS probe operating at 500.112 MHz and 125.721 MHz for ^{1}H and ^{13}C,

respectively. Sample was loaded into a 3.2 mm zirconium oxide rotor. The reported ^{13}C CP-MAS spectra were acquired using the following experimental parameters: 3 µs 90° pulse, 2 ms CP contact time, 20 ms acquisition time, 3072 number of scans, 3 s recycle delay and a 58 kHz radio-frequency decoupling of protons during the acquisition of ^{13}C magnetization. ^{13}C chemical shifts were calibrated by setting the chemical shift of CH_2 resonance of adamantane powder sample to 28.5 ppm.

Dynamic Light Scattering (DLS): All of the DLS experiments were performed using Wyatt Technology® DynaPro® NanoStar® using a 1 µL quartz MicroCuvette.

Transmission Electron Microscopy (TEM): All TEM micrographs were obtained using a Technai® T - 20® machine (FEI®, Netherlands) with a 80 kV operating voltage. A dilute solution was dropped on a carbon-coated copper grid and dried overnight at room temperature under vacuum before using in experiments.

Size exclusion chromatography (SEC): Polymer-lipid nanodiscs were purified by size exclusion chromatography (SEC), using self-packed Superdex 200 Increase 300/10 GL column operated on an AKTA purifier (GE Healthcare, Freiburg, Germany). Samples were monitored at 214 nm.

Static Light Scattering (SLS) solubilization experiments: The time dependent solubilization of DMPC MLVs was monitored by the intensity of scattered light at 90° angle. 1 mg/mL DMPC stock solutions were taken in a 4 mL cuvette (1 cm optical path) under continuous stirring at 20°C. Then the solution was equilibrated for 5 min before the addition of the Alkyl-PAA polymers. Excitation wavelength was set at 400 nm while the emission wavelength was set at 404 nm and the slit was set to 2 nm. All SLS experimental measurements were carried out using a FluoroMax-4® Spectrofluorometer from Horiba Scientific®.

SLS metal ion titrations: Nanodiscs stability was tested by titrating a 1 mg/mL solution of Alkyl-PAA:DMPC (1:1 w:w) nanodiscs in 10 mM HEPES buffer at pH = 7.4 with 2M $CaCl_2$ and 2M $MgCl_2$, and 4M NaCl. Results are shown below in Figures S3 and S4.

pH stability measurement using SLS experiments: To study pH stability of PAA based lipid nanodiscs, a solution made by 1 mg/mL Alkyl-PAA:DMPC (1:1 w:w) nanodiscs was titrated both with 1M HCl and 1M NaOH. Results are shown in Figure S5.

DSC experiments: NanoDSC (TA instruments) was used to determine the phase transition temperature of the PAA based lipid nanodiscs. Nanodiscs stock solutions were made according to above procedure with an additional 3 times of freeze thaw cycles; free polymer was removed using centrifugation filtration using a 10 kDa filter and diluting with 10 mM potassium phosphate buffer. The stock solutions were then centrifuged at 11,000 g and filtered through a 0.2 micron filter. The samples were vacuum degassed before loading. 300 µl of sample was loaded into the sample cell and 10 mM potassium phosphate buffer was loaded into the reference cell. The temperature was cycled from 5 to 60 °C three times.

Phosphorous-31 NMR: Spectra were acquired using an Agilent/Varian 400 MHz solid-state NMR spectrometer and a 5 mm triple-resonance probe with ^{31}P and ^{1}H resonance frequencies of 161.974 MHz and 400.114 MHz, respectively. 200 µl of sample was inserted using a 3.2 mm glass tube. 5µs 90° pulse, 25 kHz ^{1}H continuous-wave decoupling, 1024 scans, and a 2 s recycle delay were used to acquire ^{31}P NMR spectra. ^{31}P chemical shifts were referenced by setting the ^{31}P chemical shift of 100 % H_3PO_4 sample to 0 ppm.

^{14}N-NMR Experiments Nitrogen-14 NMR spectra were acquired using an Agilent/Varian 400 MHz solid-state NMR spectrometer and a 5 mm double-resonance probe operating at the ^{14}N resonance frequency of 29.910 MHz. ^{14}N-NMR spectra were recorded using the quadrupole-echo pulse sequence with a 90° pulse length of 8 µs and an echo-delay of 80 µs. ^{14}N

magnetization was acquired using 28.9 ms acquisition time (without ^{1}H decoupling), 20,000 scans and a recycle delay of 0.9 s.

Solubilization of native *E. coli* membranes: *E. coli* BL21(DE3) was obtained as described previously (Prade et al. *Angew. Chem. Int. Ed.* **2018**, *57*, 8458.). Cell pellets were re suspended in a 10-fold volume of ice-cold buffer (50 mM potassium phosphate buffer, 2 mM EDTA, 200 mM NaCl, pH 7.4) and subjected to ultrasonication. The cell lysate was subjected centrifugation for 1 h at 4 °C and 20,000 g and washed three times with buffer to remove soluble proteins. Membrane pellets were re-suspended in 50 mM potassium phosphate buffer, 200 mM NaCl, pH 7.4 to a final concentration of 50 mg/mL. Solubilization of the pellet was conducted by treating 500 µl of cell lysate with 250 µl of polymer solution (50 mg/mL). The samples were incubated overnight at room temperature while shaking. The resulting solutions were centrifuged at 11,000 g for 30 min. The supernatant was separated and analyzed using SDS PAGE gel. To remove the polymer and lipids, proteins were precipitated from polymer-containing samples with $CH_3OH/CHCl_3/H_2O$. 100 µL aliquot of ice-cold supernatant was mixed with 400 µL ice-cold methanol, then 100 µL ice-cold chloroform was added, and the sample was mixed. 300 µL ice-cold water was then added and the sample was thoroughly mixed and centrifuged at 2,000 g for 5 mins and 11,000 g for 10 mins at 4 °C. The top aqueous layer was carefully removed and 400 µL of ice cold methanol was added and mixed thoroughly. The resulting precipitate was pelleted at 2,000 g for 5 mins and 11,000 g for 10 mins at 4 °C. The resulting pellet was washed two times with 800 µL of ice cold methanol. Resulting pellet was dried under N_2 for 10 minutes and then under high vacuum for 3 hrs. The dry pellet was suspended in SDS buffer, heated to 100 °C for 10 mins with shaking and subjected to a SDS-PAGE

SDS-PAGE: Samples from above were loaded onto a precast gel. A constant voltage of 170 V was applied for 40 min at 50 W. Gels were fixed in 10% (v/v) acetic acid and 40% (v/v) ethanol,

stained with 0.025% (w/v) Coomassie brilliant blue in 10% (v/v) acetic acid, and de-stained with 10% (v/v) acetic acid. Finally, gels were photographed using slandered digital camera.

4.3 Results and Discussion

In the past hydrophobically modified PAAs were shown to act as amphipols which have the ability to form pores in a membrane and solubilize membrane proteins.[15, 16] We hypothesized that modifying a short chain PAA with relatively short alkyl groups (4-6 carbons), as compared to the long alkyl groups (>8 carbons) used in the formation of amphipols,[17] would produce an amphiphilic polymer with the ability to form nanodiscs. To test this hypothesis, we used a low molecular weight (M_w = 1800 Da) PAA as the starting material. Different hydrophobic groups (butyl, pentyl, hexyl, and neopentyl) were chosen to functionalize PAA. To achieve this, we applied a simple condensation reaction scheme to PAA using N-(3-Dimethylaminopropyl)-N-ethylcarbodiimide hydrochloride (EDC) as our coupling reagent and the appropriate alkyl amine as the reactant (**Figure 4-1a**). The resulting polymer was characterized using Fourier transform infrared spectroscopy (FT-IR), proton–nuclear magnetic

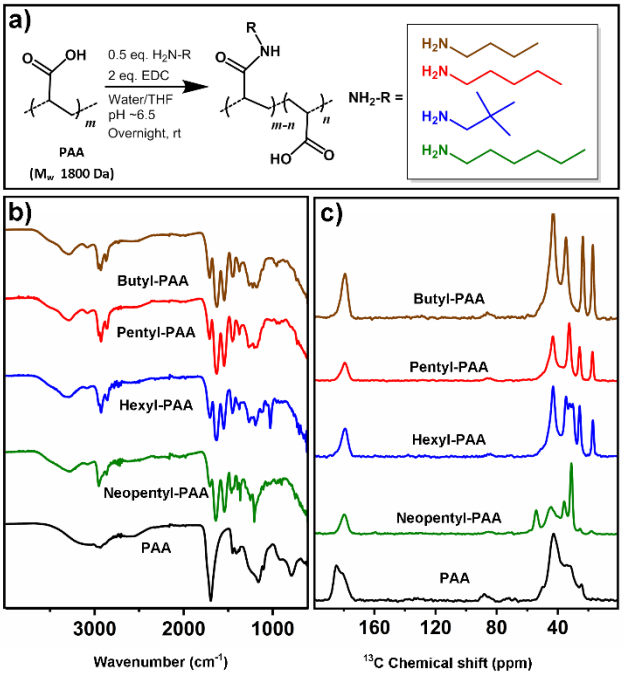

Figure 4-1: Synthesis and characterization of polyacrylic acid polymers. a) General reaction schematic of PAA functionalization. b) FT-IR and c) ^{13}C-CPMAS solid-state NMR spectra of functionalized alkyl-PAA

resonance spectroscopy (^{1}H-NMR), and carbon-13–cross polarization magic angle spinning (^{13}C-CPMAS) solid-state NMR experiments. FT-IR spectra show amide stretching frequency (~1640 cm^{-1}) for the products confirming the successful completion of the coupling reaction (**Figure 4-1b**). This was further confirmed by the carbonyl carbon resonance (~185-180 ppm) and the appearance of new peaks in the aliphatic region (CH_2 ~32 ppm, CH_3 ~17 ppm and quaternary C~54 ppm) in ^{13}C-CPMAS NMR spectra of the synthesized polymers as compared to PAA starting material (**Figure 4-1c**). ^{1}H-NMR spectra were used to estimate the extent of functionalization by integration (**Figure 4-2)** to be ~40-50%, within the range of optimal hydrophobic to hydrophilic ratio as seen previously for nanodiscs.[13]

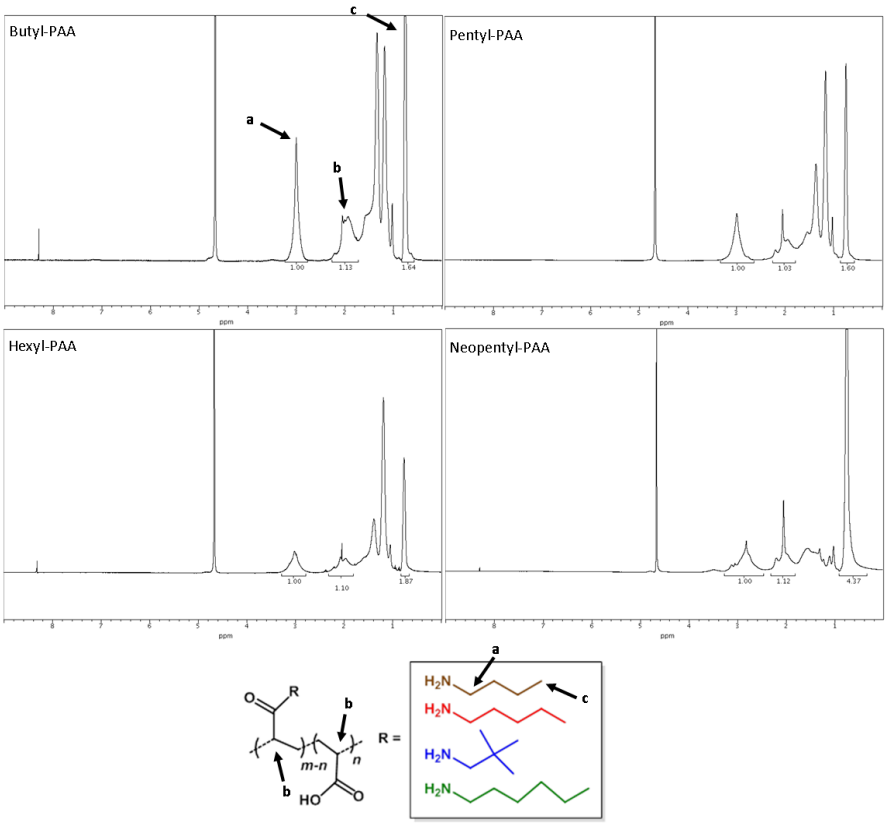

Figure 4-2: ^{1}H NMR spectra of alkyl-PAA polymers. Peaks labeled with a, b and c belong to alpha-CH_2, CH of the polymer backbone and CH_3 of the alkyl chain, respectively. Peak integration was done by setting the area of alpha CH_2 peak to 1.0.

The resulting polymers were mixed with 1,2-dimyristoyl-sn-glycero-3-phosphocholine (DMPC) at different polymer:lipid weight ratios (0.25:1, 0.5:1, 1:1). Static light scattering (SLS) measurements were used to monitor the solubilization of DMPC multilamellar vesicles (MLVs). While the Pentyl-PAA, Neopentyl-PAA, and Hexyl-PAA were found to solubilize DMPC vesicles into small particles, the Butyl-PAA needed a much higher amount of polymer to achieve solubilization (>1:1) and therefore was not used in further studies (**Figure 4-3**).

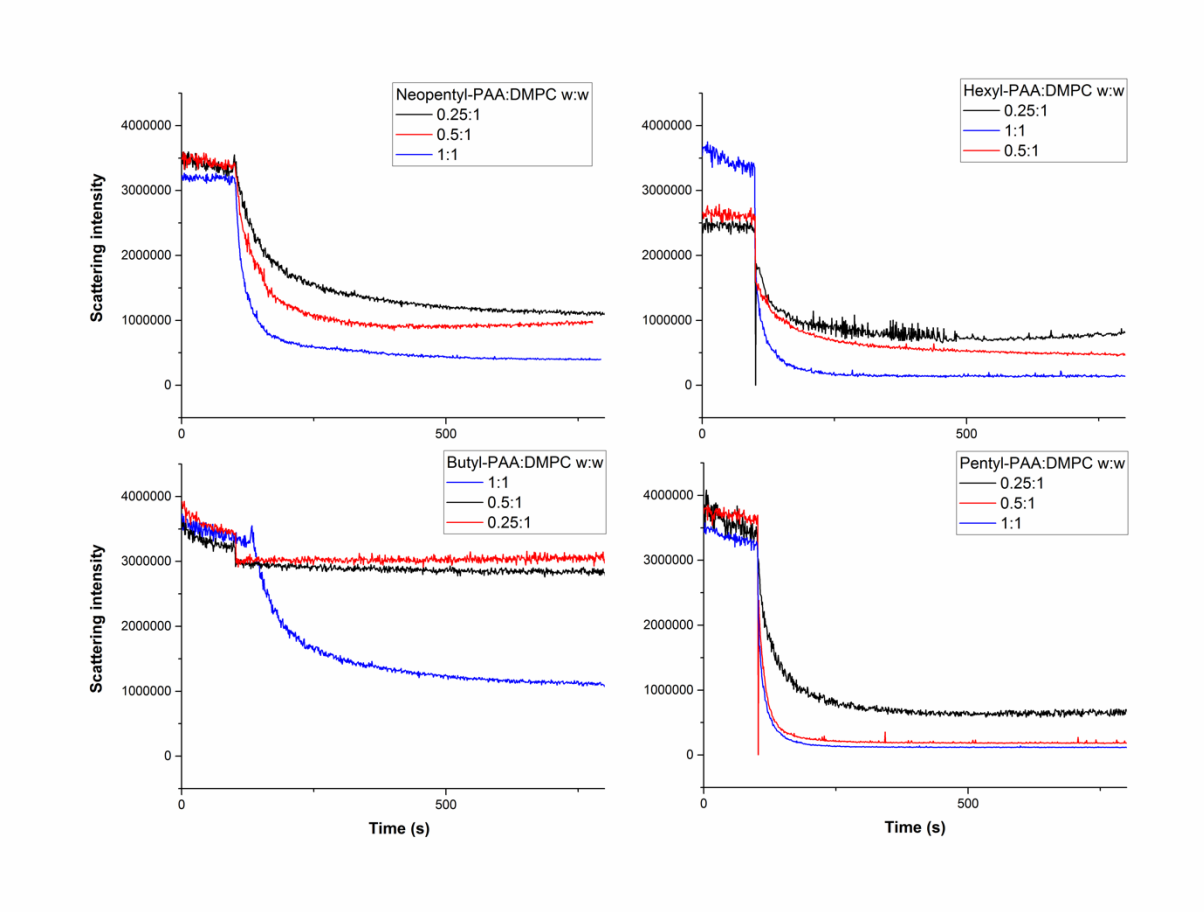

Figure 4-3: SLS profiles of nanodisc formation by the dissolution of DMPC multilamellar vesicles after the addition of alkyl-PAA polymers.

In order to investigate the size distribution of the polymer nanodiscs, we used size exclusion chromatography (SEC) and dynamic light scattering (DLS) (**Figure 4-4**). Polymers were mixed with DMPC MLVs at appropriate weight ratios and then incubated overnight at 32 °C. SEC chromatograms showed the presence of two peaks: nanodiscs eluted within the region of 9-12 mL whereas the free polymer eluted at 15-20 mL. All three polymers showed size tunability

by varying the polymer:lipid ratio. We concluded this by the observation of a shift in the retention volume of the nanodisc's peak and no shift in the retention volume of the free polymer peak in the SEC profiles. Neopentyl-PAA and Pentyl-PAA nanodiscs showed a major increase in the intensity of the polymer peak only at high polymer:lipid ratios. Hexyl-PAA showed the presence of new peaks (8.5 mL and 14.3 mL) and no shift in the nanodisc's peak at high polymer:lipid ratio, suggesting a saturation point in the polymer:lipid ratio needed to form nanodiscs was reached (**Figure 4-4 a-c**). The corresponding DLS profiles showed size variation as a function of polymer:lipid ratio (**Figure 4-4 (d-f), Table 1**) and were in good agreement with SEC observations similar to previous observations using SMA derivatives.[7, 8]

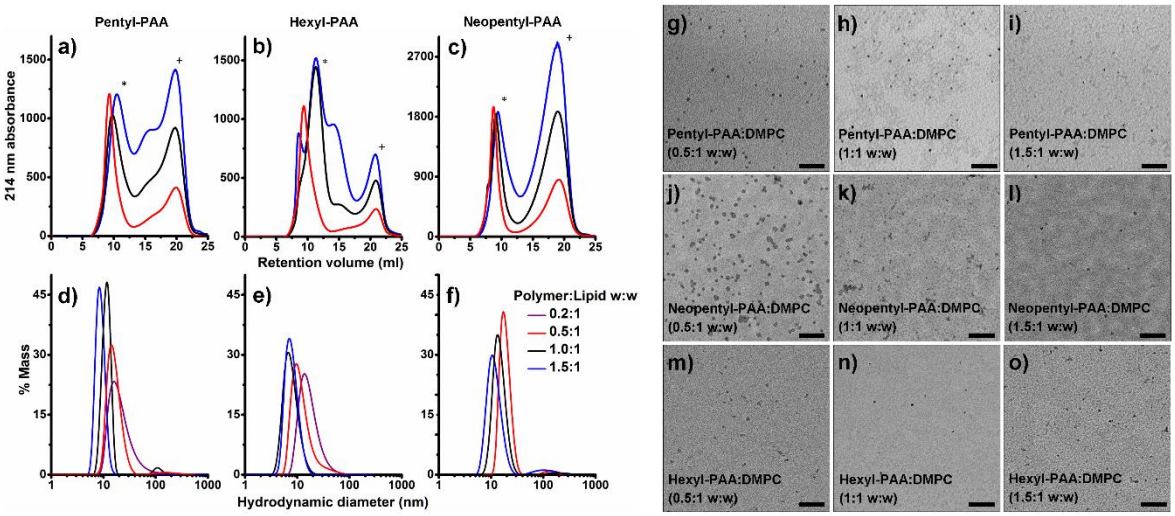

Figure 4-4: **Characterization of PAA polymer nanodiscs**. SEC (a-c) and DLS (d-f) profiles of nanodiscs prepared at the indicated polymer:lipid ratios. (*) denotes nanodiscs fractions collected and (+) denotes free polymer fraction. TEM images (g-o) of samples prepared at the specified polymer:lipid ratio; scale bar represents 200 nm.

The polymer nanodiscs were further characterized using transmission electron microscopy (TEM). The TEM images of the polymer nanodiscs with differing weight ratios clearly showed the presence of disc shaped particles of varying sizes complementary to SEC and DLS results (**Figure 4-4 g-o)**. These results confirmed that these polymers can form nanodiscs and the size of nanodiscs can be controlled by varying the polymer:lipid ratio.

The stability of the nanodiscs to the presence of divalent metal ions and pH were tested using SLS. Akyl-PAA polymers were found to have very similar stability properties towards pH and metal ions as compared to SMALP due to the presence of carboxylic groups as the hydrophilic functional group (**Table 1, Figure 4-5**).

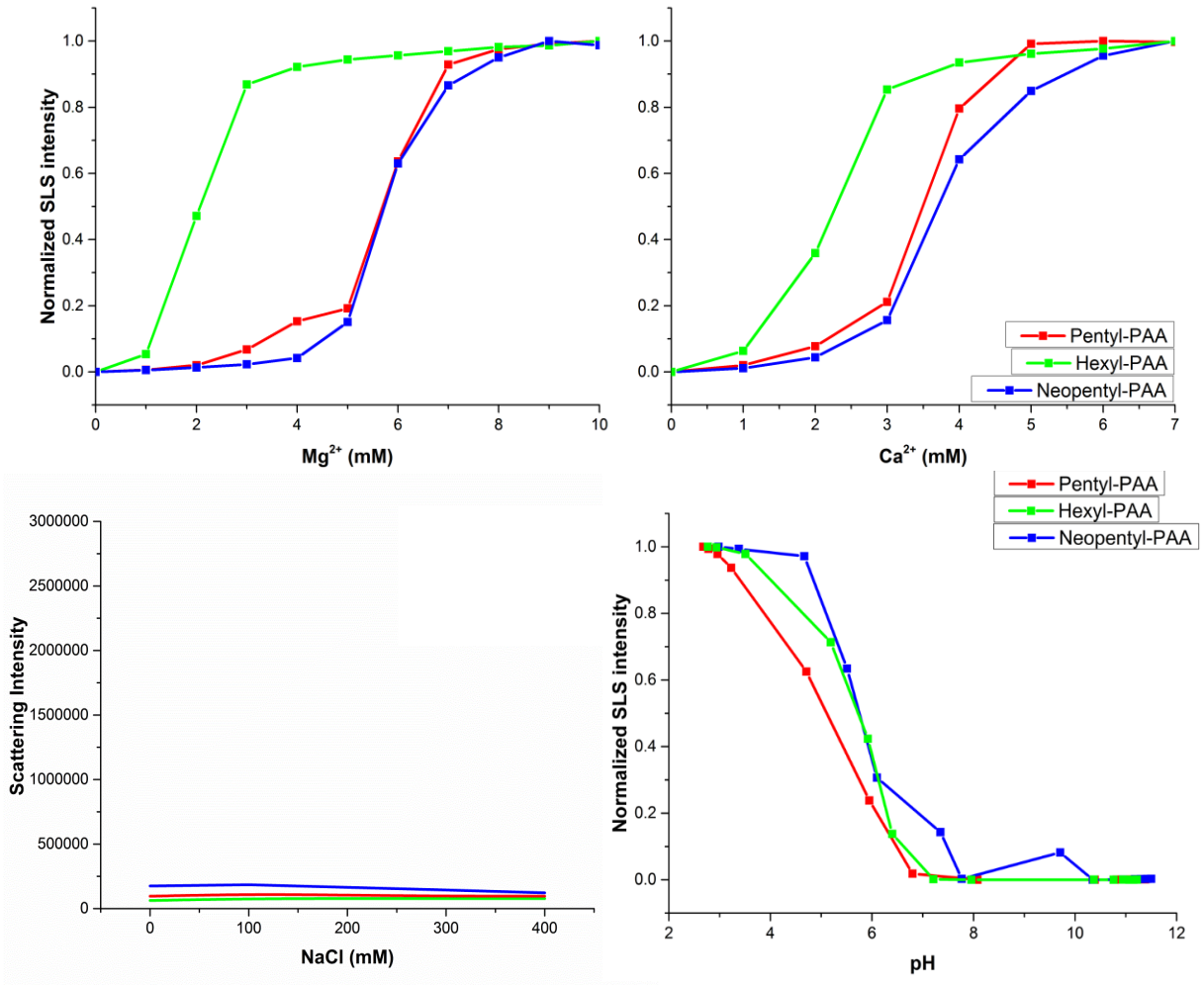

Figure 4-5: SLS profiles showing the stability of alkyl-PAA polymer DMPC-nanodiscs as a function of divalent metal ion concentration (Top), NaCl concentration (Bottom Left), and pH (Bottom Right).

Due to the absence of aromatic moieties, the akyl-PAA polymers showed no absorbance at 254 nm (**Figure 4-6**). The effect of polymer hydrophobic group on lipid bilayer properties was studied using differential scanning calorimetry (DSC) experiments. The DSC profiles of most polymer-DMPC-nanodiscs showed a typical gel to liquid crystalline phase transition

temperature (T_m) in the range of ~25-27 °C, which is very close to pure DMPC's T_m=24±1 °C, suggesting the preservation of lipid dynamics upon the formation of nanodiscs (**Table 1, Figure 4-7**). Pentyl-PAA showed only a 1°C change in the phase transition temperature between the low (0.2:1 w:w) and high (1:1 w:w) polymer:lipid ratios, signifying only a minor perturbation of the lipid bilayer. Neopentyl-PAA nanodiscs were seen to have both a similar major transition temperature (~26 °C) and a minor lower transition temperature at ~19 °C. This observation may be interpreted as Neopentyl-PAA increasing the disorder of those lipids located close to the polymer-belt of the nanodiscs. Hexyl-PAA at a low polymer:lipid ratio exhibited a similar behavior to that observed for Pentyl-PAA, whereas at a higher polymer:lipid ratio the transition temperature is shifted from ~26 to ~22 °C and is significantly broadened. This change is likely due to a strong perturbation of the lipid bilayer by the longer alkyl chain.

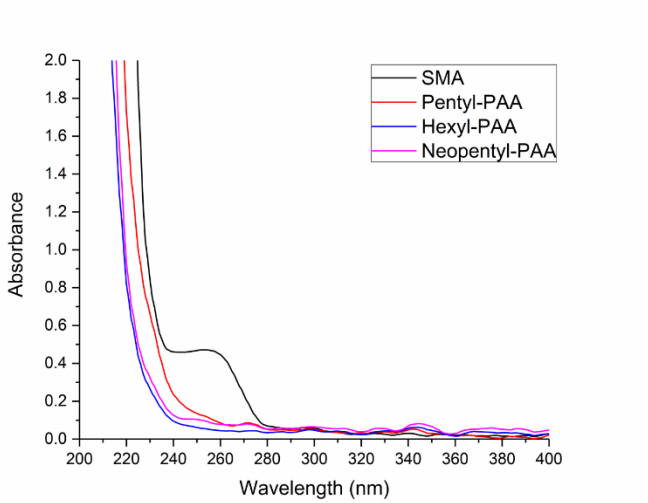

Figure 4-6: UV absorption spectra of alkyl-PAA and SMA polymers

Hydrophobic group	Polymer/Lipid (w/w)	Size[a] (nm)	PDI	Elution volume (mL)	pH stability [b]	Mg^{2+}, Ca^{2+} stability[c] (mM)	DSC transition temperature (°C)
Pentyl	0.2, 0.5, 1, 1.5	16, 14, 12, 8	1.7, 0.25, 0.11, 0.14	nd, 9.3, 9.7, 10.5	>6	5.5, 3.5	26, nd, 25, nd
Hexyl	0.2, 0.5, 1, 1.5	14, 10, 7, 7	1.0, 0.63, 0.31, 0.27	nd, 9.3, 11.3, 11.3	>6	2, 2	26, nd, 22, nd
Neopentyl	0.3, 0.5, 1, 1.5	nd, 17, 13, 10	nd, 0.39, 0.23, 0.27	nd, 8.7, 9.1, 9.5	>6.5	5.5, 2	28, nd, 26, nd

Table 4-1: Properties of alkyl-PAA-DMPC-nanodiscs. **a**, hydrodynamic diameter from DLS. **b, c** measured from SLS. nd denotes not determined. polydispersity index (PDI) from DLS

Since the size of PAA polymer based nanodiscs were easily tunable, we prepared macro-nanodiscs and examined their ability to spontaneously align in the presence of a magnetic field. All three types of polymer macro-nanodiscs were tested with the lowest polymer:lipid ratio possible (**Table 1**) using ^{31}P and ^{14}N static solid-state NMR experiments. The ^{31}P-NMR spectra were recorded at different temperatures ranging from 280 to 320 K. ^{31}P-NMR showed the appearance and disappearance of two main peaks at ~-1.5 ppm and in the ~-12 to ~-14 ppm region as a function of temperature. The peak at ~-1.5 ppm is due to the fast tumbling of isotropic nanodiscs, whereas the peak at ~-12 to ~-14 ppm is indicative of macro-nanodiscs with the lipid phosphate head groups aligned perpendicular to the magnetic field axis. Pentyl-PAA macro-nanodiscs showed an isotropic peak (~-1.5 ppm) at 280 K. Partial alignment of the nanodiscs was seen (~-12 ppm) at 285-290 K, and complete alignment above 295 K (**Figure 4-8a)**. Hexyl-PAA macro-nanodiscs showed alignment similar to Pentyl-PAA macro-nanodiscs, however, they required a higher temperature (300 K) to fully align, and at 320 K a small isotropic peak was observed. Neopentyl-PAA macro-nanodiscs had similar

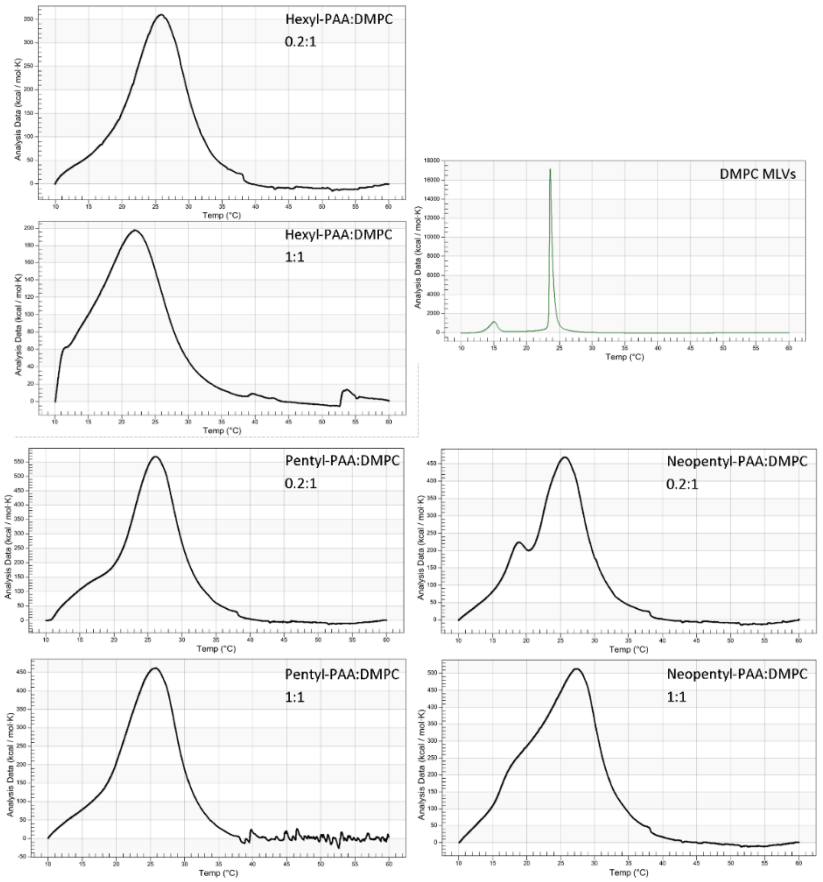

Figure 4-7: Gel-to-liquidcrystalline phase transition profiles obtained from differential scanning calorimetry (DSC) experiments on alkyl-PAA polymer DMPC nanodiscs for two different w:w ratios as indicated.

characteristics of Pentyl-PAA macro-nanodiscs at lower temperatures (<310 K) above which a large isotropic signal was observed suggesting less stability at higher temperature as compared to Pentyl-PAA. A similar trend was observed using ^{14}N-NMR. The quadrupolar coupling of ^{14}N nuclei is a direct measurement of the orientation of choline group (C-N bond vector) relative to the magnetic field direction. While at low temperature ^{14}N peaks were isotropic, at higher temperatures a quadrupolar coupling of 7-8 kHz was observed further confirming the magnetic-alignment of macro-nanodiscs with lipid bilayer normal oriented perpendicular to the magnetic field. (**Figure 4-8b**).

To demonstrate that these new polymers can be used for direct membrane protein

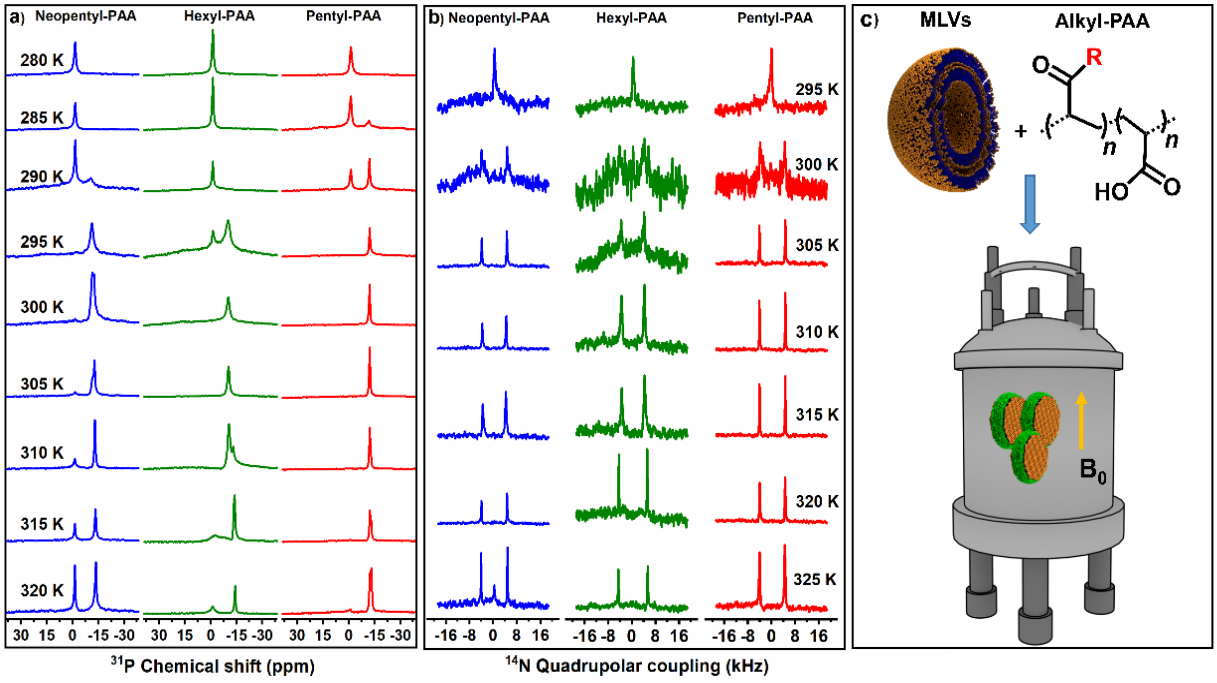

Figure 4-8: Magnetic-alignment of PAA based macro-nanodiscs. ^{31}P (**a**) and ^{14}N (**b**) NMR spectra of macro-nanodiscs prepared from Neopentyl-PAA:DMPC (0.3:1 w/w), Hexyl-PAA:DMPC (0.2:1 w/w), and Pentyl-PAA:DMPC (0.2:1 w/w) at the indicated temperatures. (c) Schematic representation of magnetic-alignment of macro-nanodiscs.

extraction from cellular membranes, we incubated the polymer with cell lysate following a published protocol[2] All three PAA polymers showed similar efficacy as compared to SMALP as evident from the SDS-PAGE gel (**Figure S8)**. These observations suggest that the hydrophobic modifications of PAA have the ability to extract membrane proteins from their native environment.

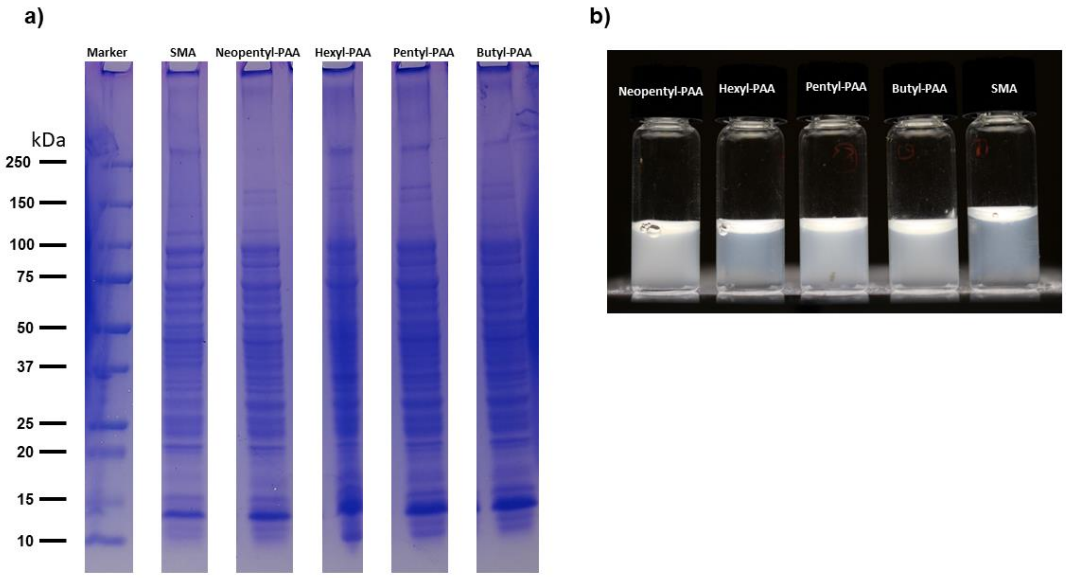

Figure 4-9: **Extraction of membrane proteins directly from *E.coli* lysate by polymers. a**) SDS-page gel showing membrane proteins extracted using different polymers. **b**) Photograph of the vials showing the cell lysate incubated with different polymers. The near-clear solution of a mixture of Hexyl-PAA and cell lysate indicates its excellent solubilizing potency, which is in good agreement with the least amount of polymer required to form nanodiscs.

4.4 Conclusion

In conclusion, we have successfully demonstrated the facile functionalization of PAA with differing hydrophobic groups that form nanodiscs at varying sizes. By using a variety of techniques (SLS, DLS, SEC, TEM, DSC and NMR) we have shown that the method of functionalization proved robust with multiple different sidechains that form nanodiscs. This allowed us to systematically probe the important effects of differing hydrophobic functionalization on the intrinsic properties polymer nanodiscs, which have yet to be seen. We show that the choice of hydrophobic group can have a noticeable effect on the polymer solubilization properties. Using these polymers we can control the extent of lipid bilayer perturbation which is vital for ensuring a more native like membrane environment. Due to this robust, tunable chemical synthesis method, PAA is an exciting platform for future optimization of the hydrophobic, hydrophilic, or direct purposed functionalization's for polymer nanodiscs.

4.5 Acknowledgements: This study was supported by funds from NIH (GM084018 to A.R.).

4.6 References

1. Z. Stroud, S. C. L. Hall, T. R. Dafforn, *Methods* 2018, 147, 106-117.

2. S. C. Lee, T. J. Knowles, V. L. Postis, M. Jamshad, R. A. Parslow, Y. P. Lin, A. Goldman, P. Sridhar, M. Overduin, S. P. Muench, T. R. Dafforn, *Nat. Protoc.* 2016, 11, 1149-1162.

3. J. M. Dörr, M. C. Koorengevel, M. Schäfer, A. V. Prokofyev, S. Scheidelaar, E. A. W. van der Cruijsen, T. R. Dafforn, M. Baldus, J. A. Killian, *Proc. Natl. Acad. Sci. U.S.A.* 2014, 111, 18607-18612.

4. K. A. Morrison, A. Akram, A. Mathews, Z. A. Khan, J. H. Patel, C. Zhou, D. J. Hardy, C. Moore-Kelly, R. Patel, V. Odiba, T. J. Knowles, M.-u.-H. Javed, N. P. Chmel, T. R. Dafforn, A. J. Rothnie, *Biochem. J.* 2016, 473, 4349-4360.

5. Z. Hu, J. C. S. Ho, M. Nallani, *Curr. Opin. Biotechnol.* 2017, 46, 51-56.

6. J. M. Dörr, S. Scheidelaar, M. C. Koorengevel, J. J. Dominguez, M. Schäfer, C. A. van Walree, J. A. Killian, *Eur. Biophys. J.* 2016, 45, 3-21.

7. T. Ravula, N. Z. Hardin, S. K. Ramadugu, S. J. Cox, A. Ramamoorthy, *Angew. Chem. Int. Ed. Engl*. 2018, 57, 1342-1345.

8. T. Ravula, S. K. Ramadugu, G. Di Mauro, A. Ramamoorthy, *Angew. Chem. Int. Ed. Engl.* 2017, 56, 11466-11470.

9. T. Ravula, N. Z. Hardin, S. K. Ramadugu, A. Ramamoorthy, *Langmuir* 2017, 33, 10655-10662.

10. S. Lindhoud, V. Carvalho, J. W. Pronk, M. E. Aubin-Tam, *Biomacromolecules* 2016, 17, 1516-1522.

11. M. C. Fiori, Y. Jiang, G. A. Altenberg, H. Liang, *Sci. Rep.* 2017, 7, 7432-7442.

12. S. C. L. Hall, C. Tognoloni, J. Charlton, E. C. Bragginton, A. J. Rothnie, P. Sridhar, M. Wheatley, T. J. Knowles, T. Arnold, K. J. Edler, T. R. Dafforn, *Nanoscale* 2018, 10, 10609-10619.

13. K. Yasuhara, J. Arakida, T. Ravula, S. K. Ramadugu, B. Sahoo, J. I. Kikuchi, A. Ramamoorthy, *J. Am. Chem. Soc.* 2017, 139, 18657-18663.

14. A. O. Oluwole, B. Danielczak, A. Meister, J. O. Babalola, C. Vargas, S. Keller, *Angew. Chem. Int. Ed. Engl.* 2017, 56, 1919-1924.

15. F. Vial, A. G. Oukhaled, L. Auvray, C. Tribet, *Soft Matter* 2007, 3, 75-78.

16. Y. Gohon, F. Giusti, C. Prata, D. Charvolin, P. Timmins, C. Ebel, C. Tribet, J. L. Popot, *Langmuir* 2006, 22, 1281-1290.

17. J. L. Popot, T. Althoff, D. Bagnard, J. L. Baneres, P. Bazzacco, E. Billon-Denis, L. J. Catoire, P. Champeil, D. Charvolin, M. J. Cocco, G. Cremel, T. Dahmane, L. M. de la Maza, C. Ebel, F. Gabel, F. Giusti, Y. Gohon, E. Goormaghtigh, E. Guittet, J. H. Kleinschmidt, W. Kuhlbrandt, C. Le Bon, K. L. Martinez, M. Picard, B. Pucci, J. N. Sachs, C. Tribet, C. van Heijenoort, F. Wien, F. Zito, M. Zoonens, *Annu. Rev. Biophys.* 2011, 40, 379-408.

Chapter 5

Metal-Chelated Polymer Nanodiscs for NMR Studies

Portions of this chapter are reproduced from: N. Z. Hardin[+], V. Kocman[+], G. M. Di Mauro, T. Ravula, A. Ramamoorthy, *Angew. Chem. Int. Ed.* 2019, 58, 17246—17250

5.1 Introduction

Nanodiscs are comprised of a discoidal lipid bilayer stabilized by an amphiphilic belt comprised of either peptidic based or polymer based molecules.[1-4] The introduction of amphiphilic polymers that form lipid nanodiscs has most notably contributed to the study of membrane proteins and allows for their functional and structural study in a tunable native-like membrane environment.[5-10] While polymer nanodiscs are the youngest of the nanodisc field, they are showing great potential due to the simplicity of their synthesis, their diverse chemical tunability, and their ability to directly extract membrane proteins from their cellular environment at practical cost.[5-7, 9, 11-22] Nanodiscs are a useful tool for NMR spectroscopy since their size can be tuned to conditions favorable to both solution and solid-state NMR. Additionally, nanodiscs were shown to align in the presence of the magnetic field which can provide additional useful structural information.[8, 19, 23] Despite these advantages the fundamental challenges related to poor NMR sensitivity still remain, requiring long acquisition times and high sample concentrations.[24] In this study we focused on the synthesis of a nanodisc-forming metal-chelated polymer and its use as a paramagnetic relaxation enhancement (PRE) system. We show that the polymer was able to decrease

longitudinal relaxation times (T_1) of nanodisc and DNA with a minimum adverse transverse relaxation shortening (T_2), which is ideal for fast NMR data acquisition.[25-30] We sought a simple method of preparing polymer nanodiscs modified with a stable metal chelator, 2-Aminoethyl-mono-amide-DOTA (DOTA, **Figure 5-1 a**), attached to the polymer belt for use as a system for T_1 relaxation enhancement. Designing polymer nanodiscs in such a way has two major advantages over previously reported lipid-chelator methods.[26-27] First, the position of the chelator on the nanodisc belt removes potentially detrimental effects of interacting DOTA-metal complexes in very close proximity to membrane associated biomolecules, while leaving a native like membrane environment. Secondly, the facile polymer preparation allows for exploitation of the paramagnetic effects of metal ions complexed nanodiscs without the need for costly metal complexed lipids. This strategy would also enable the use of PRE in the structural studies of membrane proteins [28, 31-32].

5.2 Materials and Methods

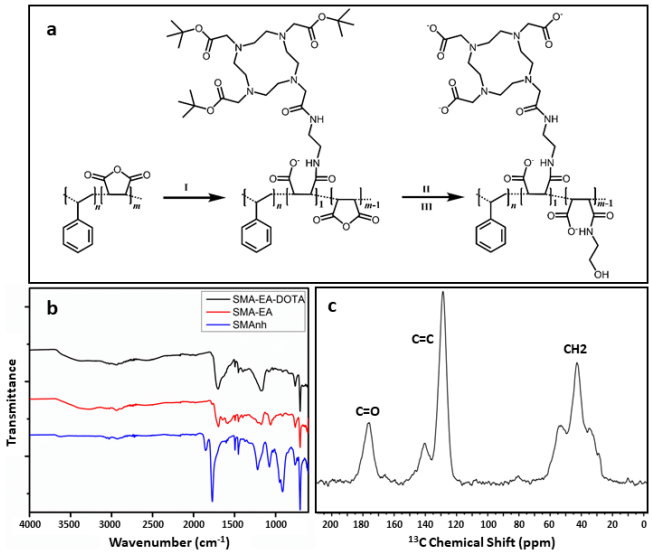

Figure 5-1: a) Reaction scheme of SMA-EA-DOTA synthesis I; 2-aminoethyl-mono-amide-DOTA-tris(t-Butyl ester), NMP, Triethylamine, II; Ethanolamine, Triethylamine, III; TFA deprotection. b) FT-IR spectra of polymers. c) ^{13}C CP-MAS solid-state NMR spectrum of SMA-EA-DOTA polymer. FT-IR and NMR spectra were recorded with polymer powder samples

Poly(Styrene-co-Maleic Anhydride) cumene terminated ~1.3:1 styrene-to-maleic anhydride molar ratio (SMAnh, M_n ~1600 g/mol), Triethylamine (Et_3N), potassium chloride (KCl), potassium phosphate monobasic (KH_2PO_4) and potassium phosphate dibasic (K_2HPO_4) , sodium chloride (NaCl), hydrochloric acid (HCl), sodium hydroxide (NaOH), trifluoracetic acid (TFA), diethyl ether (Ether), N-methyl-2-pyrrolidone (NMP) were purchased from Sigma-Aldrich®. 2-Aminoethyl-mono-amide-DOTA-tris(t-Butyl ester) was purchased from Macrocyclics®, 1,2-dimyristoyl-sn-glycero-3-phosphocholine (DMPC) was purchased from Avanti Lipids Polar, Inc®, DNA was purchased from Integrated DNA Technologies, Inc.

Synthesis of SMA-EA-DOTA: 1 g of SMAnh was dissolved in 40 mL of NMP then 435 mg (1 eq per chain) of 2-Aminoethyl-mono-amide-DOTA-tris(t-Bu ester) was added to the solution, then 1 mL of trimethylamine was added. The reaction mixture was then stirred at 80 °C for 2 hours. Then 0.4 mL of ethanolamine and another 1 mL trimethylamine was added to the solution and the solution was heated at 80 °C for 2 hours. The solution was cooled to room temperature, precipitated with HCl and washed 3x with water. The resulting compound was deprotected using 30 ml TFA for 2 hours at room temperature and precipitated using diethyl ether. The precipitate was washed 3 times with diethyl ether and dried under vacuum.

Nanodiscs preparation and purification: 20 mg DMPC was suspended in 10 mM potassium phosphate, 100 mM potassium chloride buffer (pH 7.4). 60 mg SMA-EA-DOTA was added and the solution was diluted to 3 mL and incubated overnight at 32 °C. The nanodiscs solution was then purified using self-packed Superdex 200, 10/600 GL column operated on an AKTA purifier (GE Healthcare, Freiburg, Germany). Samples were monitored at 254 nm and the first peak was collected (Figure 1a) and concentrated to 1 mL for use in NMR studies.

Static light scattering (SLS): SLS experiments were performed by observing scattered radiation at 90° through a 1 cm quartz cuvette using an excitation wavelength of 400 nm and emission wavelength of 404 nm at 25 °C. All SLS experiments were obtained on a FluoroMax-4® Spectrofluorometer from Horiba Scientific®.

pH stability measurements: A solution made by 1 mg/mL SMA-EA-DOTA:DMPC (1:1 w/w) nanodiscs was titrated both with 1M HCl and 1M NaOH and results were monitored with SLS . Results are shown in Figure S2.

SLS metal ion titrations: Nanodiscs stability was tested by titrating a 1 mg sample of 1:1 w/w nanodiscs in pH 7.4, 10 mM HEPES buffer with 2 M $CuCl_2$.

Transmission Electron Microscopy (TEM): TEM data was acquired on a Technai® T - 20® machine (FEI®, Netherlands) using an operating voltage of 80 kV.

Dynamic Light Scattering (DLS): DLS was performed using a Wyatt Technology® DynaPro® NanoStar® using a 1 µL quartz MicroCuvette.

Fourier-Transform Infrared (FT-IR) Spectroscopy: The FT-IR spectra from 4000 to 800 cm^{-1} were recorded using a Thermos scientific ATR-FTIR instrument. Lyophilized powder samples of polymers were used to record the spectra SMA-EA was obtained as previously reported.[1]

CPMAS solid-state NMR experiments: Carbon-13 CPMAS experiments were carried out on a Bruker 500 MHz solid-state NMR spectrometer under 12 kHz MAS using a 3.2 mm triple-resonance MAS probe operating at 500.112 MHz and 125.721 MHz for ^{1}H and ^{13}C nuclei, respectively, and using a 3.2 mm zirconia (ZrO_2) rotor. The reported ^{13}C CPMAS spectra were acquired using 3 µs 90° pulse, 2 ms CP contact time, 20 ms acquisition time, 3072 scans, 3 s

recycle delay and a 58 kHz radio-frequency decoupling of protons during acquisition. ^{13}C chemical shifts were calibrated using adamantine.

Spin Inversion Recovery ^{1}H NMR: NMR spectra were recorded using a 500 MHz NMR spectrometer equipped with a Bruker TXI probe. A basic inversion recovery experiment using an excitation sculpting employing soft selective pulses as described elsewhere.[2] Experiments were run using 16 scans per FID for nanodiscs samples and 256 scans for samples containing DNA, and between 11 and 15 FIDs were used for a single T_1 experiment. Spectral width was ~6,000 Hz for nanodiscs without DNA and ~10,000 Hz for all DNA containing samples. 90° pulses were set between 9 and 11 μs with a RF power level of ~15 W. The transmitter frequency was set to the bulk water-proton resonance.

NMR DNA sample preparation and purification: The oligonucleotide wtTel23 with the oligonucleotide sequence 5'-TAGGG(TTAGGG)$_3$-3' was purchased from Integrated DNA Technologies, Inc. Samples were purified and desalted with the use of a 3 kDa centrifugation filter to give a stock solution with the concentration of 0.6 mM per strand. An NMR sample with concentration of 0.1 mM per strand and in the presence of 100 mM KCl with a pH value of about 7 was prepared.

NMR Data analysis: NMR data were analyzed and plotted using Bruker® Topspin® version 3.5 pl 6 and Mestrelab Research® S.L. MestReNova® version 12.0.4-22023.

5.3 Results and discussion

Here we report the synthesis of a modified poly(styrene-co-maleic acid (SMA) derivative called SMA-EA-DOTA which is engineered with a metal chelator and forms lipid-nanodiscs. SMA-EA-DOTA polymer was synthesized similarly to SMA-EA polymer, which has been previously

reported to form stable nanodiscs and is used as a comparative system in this study. To synthesize the polymer, we used a low molecular weight (M_n ~ 1600 g/mol) poly(styrene-co-maleic anhydride) (SMAnh) as the starting material.[19] The chemical modification of the SMAnh includes on average one DOTA chelator molecule per polymer chain modification (**Figure 1a**).

The successful polymer modification was confirmed using FT-IR and ^{13}C-CP-MAS solid-state NMR on polymer powders (**Figure 5-1 b and c**). The FT-IR spectrum shows a clear C=O stretching frequency shift from ~1770 cm^{-1} to 1702 cm^{-1} indicating a change from an anhydride to an amide, which is further confirmed by the ^{13}C C=O NMR signal at 176 ppm. The ability of the polymer to form lipid nanodiscs with DMPC was established using dynamic light scattering (DLS), static light scattering (SLS), size-exclusion chromatography (SEC), and transmission electron microscopy (TEM) (**Figure 5-2**).

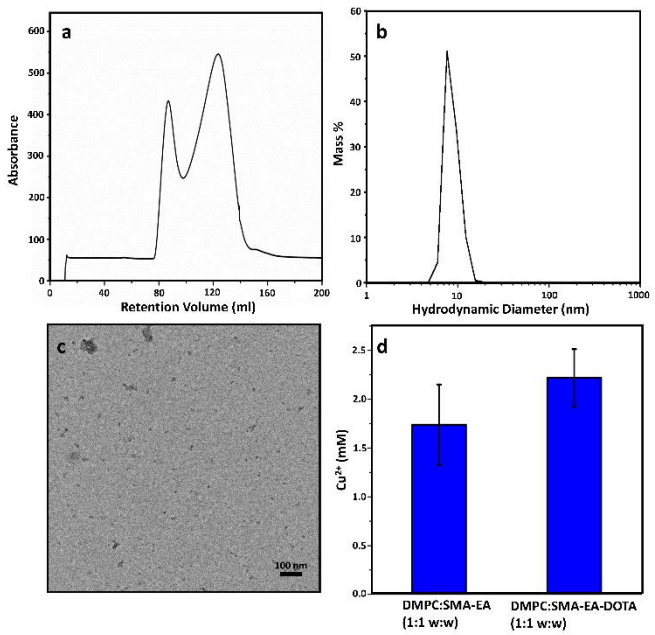

Figure 5-2: Nanodiscs prepared using 3:1 w/w polymer:lipid for (a) to (c) and 1:1 w/w for (d). a) SEC profile of SMA-EA-DOTA nanodiscs. b) DLS profile of purified nanodiscs. c) TEM micrograph showing small nanodiscs; scale bar represents 100 nm. d) SMA-EA and SMA-EA-DOTA nanodiscs tolerance/precipitation in the presence of differing Cu^{2+} concentrations.

The nanodiscs were shown to be size tunable at differing weight ratios (from 1:1 to 3:1 w/w) of polymer to DMPC by the shift in elution volume in SEC of the nanodiscs peak from 65 to 87 ml (**Figures 5-2a** and **5-3**). DLS shows the formation of small particles of ~8 nm diameter which is further confirmed by the presence of small disc-shaped particles in TEM (**Figure 5-2b** and **c**). These results show that the addition of DOTA-units to the SMA-EA polymer does not significantly change its nanodisc formation ability. To further establish the addition of the DOTA-units to the polymer we compared the metal ion stability of the SMA-EA-DOTA to previously studied SMA-EA by monitoring polymer nanodiscs precipitation upon the addition of copper(II) ions (**Figure 5-2d**). The resulting metal ion stability showed the expected increase in the Cu^{2+} tolerance as compared to SMA-EA nanodiscs due to the addition of the DOTA-units sequestering the Cu^{2+} ions. Furthermore, the polymer SMA-EA-DOTA showed similar size control and pH stability properties as compared to SMA-EA indicating that the addition of roughly one DOTA chelator per chain did not introduce any significant change in the lipid-nanodiscs forming properties of the polymer (**Figure 5-4**)

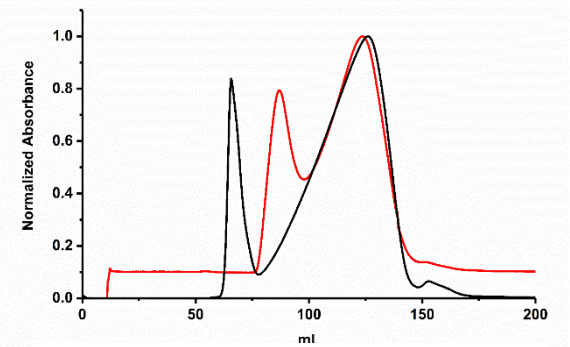

Figure 5-3: Size exclusion profiles of SMA-EA-DOTA nanodiscs. Black line represents nanodiscs prepared with a polymer:DMPC weight ratio of 1:1, red line is nanodiscs prepared with a polymer:DMPC weight ratio of 3:1.

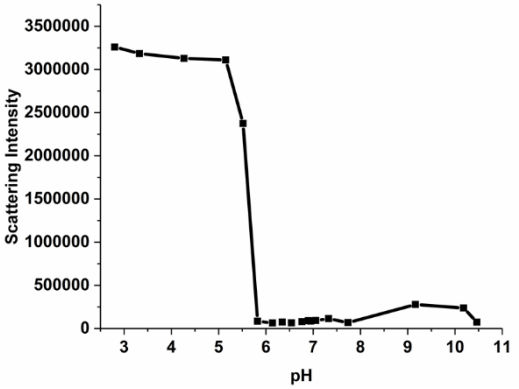

Figure 5-4: Scattering intensity of a SMA-EA-DOTA nanodiscs at different pH values.

NMR samples were prepared using a polymer:DMPC ratio of 3:1 w:w (6 mg:2 mg) to form nanodiscs of size ~ 8 nm (diameter) as observed from DLS results. The resulting nanodiscs were purified using SEC and concentrated to 1 mL using a 10 kDa filter. As shown (**Figure 3**), most of the peaks in the proton NMR spectrum of the functionalized nanodiscs were assigned.

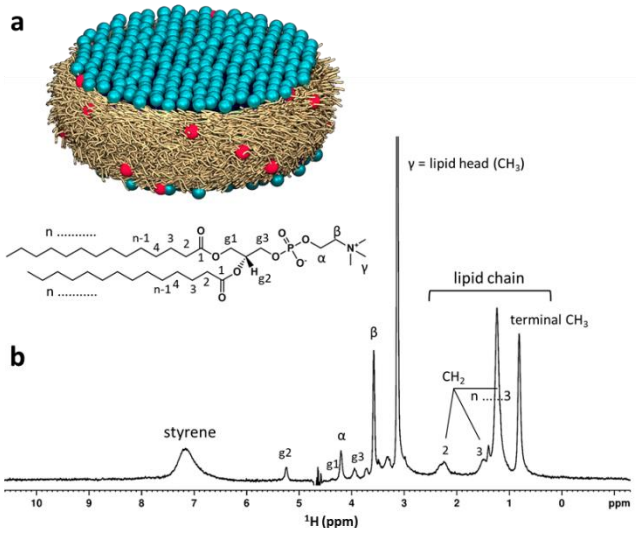

Figure 5-5: a) Schematic of SMA-EA-DOTA polymer-nanodiscs with lipid head, DOTA functional groups, and polymer represented in blue, red, and brown, respectively. A chemical structure of a lipid molecule with assignment is shown. **b**) ^{1}H NMR spectrum of a polymer nanodiscs recorded on a 500 MHz NMR spectrometer at 25 °C with assignment of lipid and styrene protons

To demonstrate the PRE effect on relaxation parameters, we chose to monitor the well resolved and minimally overlapped peaks assigned to styrene (~7.2 ppm), lipid-head (~3.2 ppm), CH_2 (~1.3 ppm) and CH_3 (~0.9 ppm) protons.[33] We used a standard inversion-recovery RF pulse sequence and added an excitation sculpting with selective pulses for water suppression as described elsewhere.[34] We determined the T_1 times of these four ^{1}H peaks (**Figures 5-6 and A-1 – A-7**) in the absence and presence of differing concentrations of chelated Cu^{2+} metal ions. In the absence

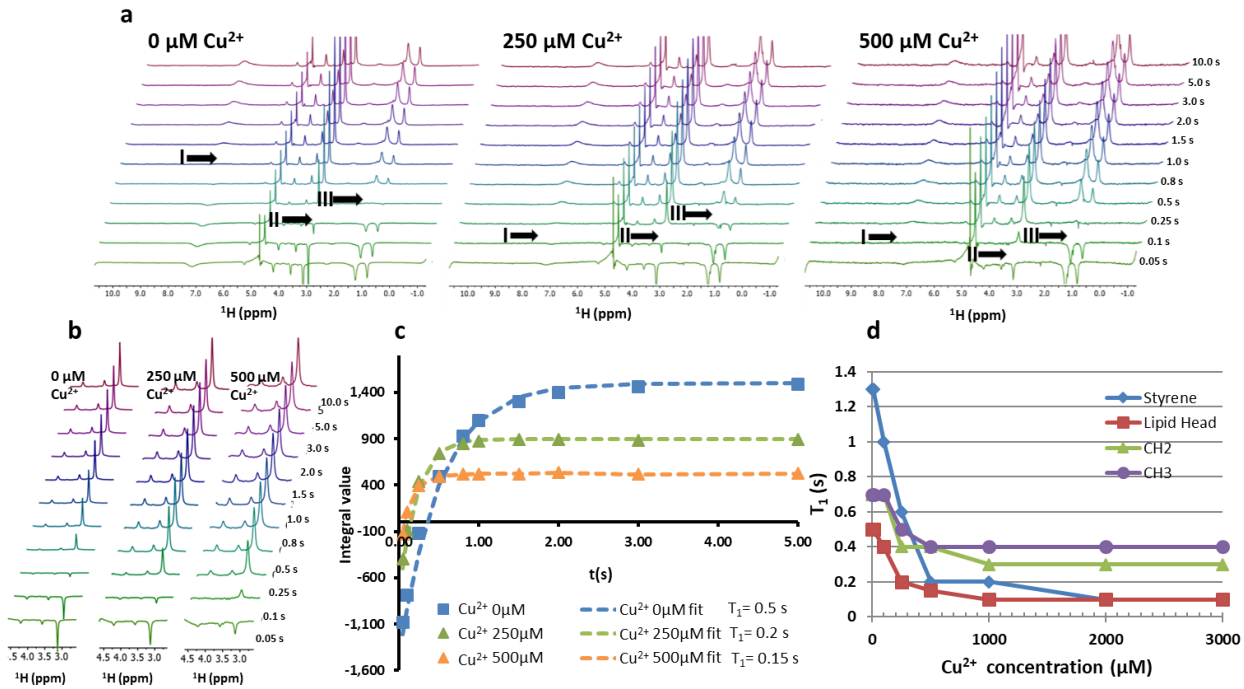

Figure 5-6: Inversion recovery experiments to measure T_1 of protons from SMA-EA-DOTA nanodiscs. **a**) Inversion recovery experiments recorded on a SMA-EA-DOTA nanodiscs at 0, 250 and 500 µM Cu^{2+} concentrations are shown. Roman numerals I, II and III indicate where the intensities of styrene, lipid head and lipid chain peaks, respectively are close to or zero. **b**) Close up of the lipid head region of the inversion recovery spectra. **c**) Inversion recovery data and fit for the lipid head peak at 0, 250 and 500 µM Cu^{2+} concentrations. **d**) T_1 times of styrene, lipid head and lipid chain peaks and their dependence on [Cu^{2+}] concentration.

of Cu^{2+} ions, protons from styrene, lipid head, CH_2 and CH_3 groups exhibited T_1 values of 1.3, 0.5, 0.7 and 0.7 s, respectively (**Figure 5-6**).

Next, we determined T_1 relaxation rates of nanodiscs samples with a Cu^{2+} concentration ranging from 10 µM to 3 mM (**Figures 5-6 and A-1 – A-7**). We observed a slight decrease in T_1 values at concentrations of 10 and 100 µM Cu^{2+}, and a significant drop in T_1 values were observed at >250 µM Cu^{2+}, with T_1 relaxation values approaching saturation at ~0.5 mM Cu^{2+}. The control (SMA-EA nanodiscs-no chelator) showed no decrease of T_1 times upon the addition of copper (**Figure A-8**). SMA-EA was also incompatible with higher Cu^{2+} concentrations due to precipitation of the polymer. The maximum T_1 enhancement with ensured stability was achieved at 2 mM Cu^{2+}, as the calculated DOTA concentration was ~4.0 mM. Removal of non-nanodiscs forming polymer in

solution by SEC reduces the effective concentration of DOTA in the purified polymer nanodiscs, therefore 2 mM Cu^{2+} was chosen for our studies as a maximum copper concentration with ensured chelation. Based on the PRE experiments we found that copper chelated nanodiscs showed the greatest T_1 relaxation enhancement for the styrene moiety, due to the proximity of styrene to the Cu-DOTA-units (**Figure 5-6**). The second most effected region is the quaternary ammonium lipid head CH_3 group. The lesser PRE effect observed, as compared to the styrene, is due to an average much greater distance from the Cu-DOTA-units to the lipid head CH_3. Interestingly, the PRE effect for the lipid head CH_3 protons is comparable to that for the CH_2 and CH_3 protons of the lipid chain which are on average closer to the Cu-DOTA-units compared to the lipid head group. This is most likely due to the fact that the lipid head groups can undergo both intra-discs and inter-discs PRE enhancements as they are solution exposed, whereas the lipid chain protons can only undergo intra-disc PRE due to a lack of solvent exposure.

As a proof of principle of widening the applications of polymer nanodiscs from mainly a membrane mimetic system to also a stable, minimally interacting system for fast NMR acquisition of water-soluble biomolecules, we decided to test the polymer nanodisc PRE effect on a DNA oligonucleotide from the human telomere region (wtTel23, 5'-TAGGG(TTAGGG)$_3$-3', **Figure 5-7**).

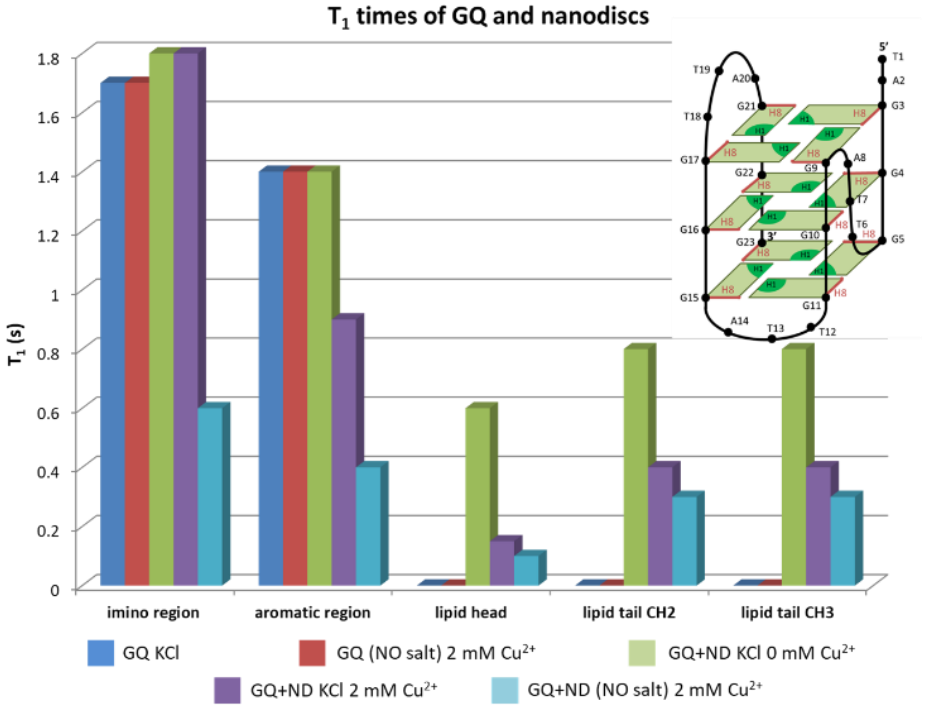

Figure 5-7: T_1 times of signals from the imino and aromatic regions of the G-quadruplex (GQ) and lipid head, CH_2 and CH_3 signals of the nanodiscs in presence or absence of Cu^{2+} and KCl salt. Top, right: a representation of the structure of the wtTel23 G-quadruplex. The black circle shows the position of a residue, green squares represent guanines located in G-quartets, the position of imino protons inside guanine residues is labeled with dark green and the red line shows on which side of the guanine residue the H8 proton is located.

We reasoned that there should be no interactions between the negatively charged polymer and the negatively charged DNA. The wtTel23 sequence is known to form a well characterized G-quadruplex in presence of K^+ ions.[35] The wtTel23 G-quadruplex was folded in the presence of 100 mM KCl and we confirmed that the wtTel23 oligonucleotide used in this study adopted the previously reported hybrid-1 G-quadruplex topology by a comparison of ^{1}H-NMR spectra to published literature (**Figure A-9**).[35] After the addition of the folded wtTel23 to the copper chelated polymer nanodiscs the non-overlapped NMR fingerprint showed no significant change in the ^{1}H-NMR spectrum indicating the retention of hybrid-1 G-quadruplex topology (**Figure A-10**).

A G-quadruplex fold is characterized by stacked G-quartets which are planar arrangements of four guanine residues (**Figure 5-7**). In each G-quartet, the imino protons of guanine residues form a

hydrogen bond with an oxygen atom of a neighboring guanine residue. Critically, the oxygen atoms inside a G-quartet must be stabilized by a cation such as Na^+ or K^+ for the G-quadruplex to be stable. In a G-quadruplex, the G-quartets are arranged in such a way that the imino protons can be considered as the "inside" of a G-quadruplex. The H8 protons and sugar moieties of guanine residues involved in G-quartets as well as residues not involved in G-quartets form the so called solvent exposed "outside" of a G-quadruplex. After the addition of 2 mM Cu^{2+} cleated polymer nanodiscs to the DNA we observed no effect on the T_1 times of imino protons and a ~0.5 s decrease in the T_1 times of the signals in the aromatic region (**Figure 5-7**). The sugar region was overlapped with the signals from the nanodiscs and could not be used for accurate T_1 determination. This T_1 data suggest that the wtTel23 interacts with the nanodiscs by its groove or loop regions and not through stacking on the nanodiscs by the top or bottom G-quartet. Such a model of interactions is also supported by Saturation Transfer Difference (STD) NMR experiments (**Figure A-11**).[36] We observed a clear transfer of magnetization from the lipid head protons to the sugar and aromatic protons of the wtTel23 G-quadruplex and a negligible transfer to the imino protons of the G-quadruplex. Interestingly, upon the removal of excess salt, both the imino and aromatic proton resonances were shown to have a 3-fold reduction in their T_1 times. We believe that the KCl salt reduces the interactions between the G-quadruplex and the nanodisc due to the salt charge screening between the DNA and the lipid heads. This decreased interaction is also reflected in the observed reduction in the PRE effect. Removing the salt increases the strength of the interactions between the nanodiscs and G-quadruplexes and consequently increases the PRE effect (**Figure 5-7**). This interesting result suggests that DOTA functionalized nanodiscs could potentially be used to structurally and dynamically probe surfaces of biomolecules similar to previously applied solvent PRE techniques.[37-41]

5.4 Conclusions

In conclusion, we have demonstrated the functionalization of a metal-chelating polymer and its ability to form nanodiscs, which can be used as a stable, relatively non-interacting system for PRE enhancement of biomolecules for fast NMR acquisition. We show, using inverse recovery experiments, up to a 7x decrease of T_1 rates of polymer-lipid nanodiscs. We also show the compatibility of nanodiscs and structured DNA molecules (G-quadruplexes) and up to 3x reduction in T_1 times. We expect this approach to be valuable in the NMR structural studies of large size RNA that exhibit a very long T_1 values for protons[41]; and could enable multidimensional NMR experimental studies on membrane-associated peptides and proteins that may not be available in large quantity and/or sensitive to heat for long data acquisition. This system coupled with recent developments in our lab to measure RDCs[23] will yield an useful tool for fast NMR acquisition in the study of biomolecules as well as the already known application in membrane protein research. This study also creates potential avenues to use the paramagnetic nature of the chelated polymer nanodiscs for dynamic nuclear polarization (DNP) solid-state NMR experiments[31-32, 43-46] to overcome the sensitivity issues in studying membrane proteins. We expect that the reported novel polymer design would enable multi-labeling to utilize the benefits of PRE, ^{19}F and DNP approaches for distance measurements on membrane proteins by solid-state NMR spectroscopy.

5.5 Acknowledgements: This study was supported by funds from NIH (GM084018 to A.R.).

5.6 References

1. I. G. Denisov, S. G. Sligar, *Nat. Struct. Mol. Biol.* 2016, *23*, 481-486.

2. I. G. Denisov, S. G. Sligar, *Chem. Rev.* 2017, *117*, 4669-4713.

3. S. C. Lee, T. J. Knowles, V. L. Postis, M. Jamshad, R. A. Parslow, Y. P. Lin, A. Goldman, P. Sridhar, M. Overduin, S. P. Muench, T. R. Dafforn, *Nat. Protoc.* 2016, *11*, 1149-1162.

4. M. C. Orwick, P. J. Judge, J. Procek, L. Lindholm, A. Graziadei, A. Engel, G. Grobner, A. Watts, *Angew. Chem. Int. Ed. Engl.* 2012, *51*, 4653-4657.

5. T. Ravula, N. Z. Hardin, S. K. Ramadugu, S. J. Cox, A. Ramamoorthy, *Angew. Chem. Int. Ed. Engl.* 2018, *57*, 1342-1345;

6. T. Ravula, N. Z. Hardin, G. M. Di Mauro, A. Ramamoorthy, *Eur. Polym. J.* 2018, *108*, 597-602.

7. J. M. Dorr, S. Scheidelaar, M. C. Koorengevel, J. J. Dominguez, M. Schafer, C. A. van Walree, J. A. Killian, *Eur. Biophys. J.* 2016, *45*, 3-21.

8. J. Radoicic, S. H. Park, S. J. Opella, *Biophys. J.* 2018, *115*, 22-25.

9. A. F. Craig, E. E. Clark, I. D. Sahu, R. Zhang, N. D. Frantz, M. S. Al-Abdul-Wahid, C. Dabney-Smith, D. Konkolewicz, G. A. Lorigan, *Biochim. Biophys. Acta.* 2016, *1858*, 2931-2939.

10. F. Hagn, M. L. Nasr, G. Wagner, *Nat. Protoc.* 2017, *13*, 79-98.

11. M. C. Fiori, Y. Jiang, G. A. Altenberg, H. Liang, *Sci. Rep.* 2017, *7*, 7432-7442.

12. S. C. L. Hall, C. Tognoloni, J. Charlton, E. C. Bragginton, A. J. Rothnie, P. Sridhar, M. Wheatley, T. J. Knowles, T. Arnold, K. J. Edler, T. R. Dafforn, *Nanoscale* 2018, *10*, 10609-10619.

13. Z. Stroud, S. C. L. Hall, T. R. Dafforn, *Methods* 2018, *147*, 106-117.

14. T. J. Knowles, R. Finka, C. Smith, Y. P. Lin, T. Dafforn, M. Overduin, *J. Am. Chem. Soc.* 2009, *131*, 7484-7485.

15. T. Ravula, N. Z. Hardin, J. Bai, S. C. Im, L. Waskell, A. Ramamoorthy, *Chem. Commun.* 2018, *54*, 9615-9618.

16. S. Lindhoud, V. Carvalho, J. W. Pronk, M. E. Aubin-Tam, *Biomacromolecules* 2016, *17*, 1516-1522.

17. D. J. K. Swainsbury, S. Scheidelaar, N. Foster, R. van Grondelle, J. A. Killian, M. R. Jones, *Biochim. Biophys. Acta.* 2017, *1859*, 2133-2143.

18. A. Oluwole, B. Danielczak, A. Meister, J. Babalola, C. Vargas, S. Keller, *Angew. Chem. Int. Ed. Engl.* 2017, *56*, 1919-1924.

19. T. Ravula, S. K. Ramadugu, G. Di Mauro, A. Ramamoorthy, *Angew. Chem. Int. Ed. Engl.* 2017, *56*, 11466-11470;

20. J. M. Dörr, M. C. Koorengevel, M. Schäfer, A. V. Prokofyev, S. Scheidelaar, E. A. W. van der Cruijsen, T. R. Dafforn, M. Baldus, J. A. Killian, *Proc. Natl. Acad. Sci. U.S.A.* 2014, *111*, 18607-18612.

21. M. Overduin, M. Esmaili, *Appl. Sci.* 2019, *9*, 1230-1245.

22. J. F. Bada Juarez, D. O'Rourke, P. J. Judge, L. C. Liu, J. Hodgkin, A. Watts, *Chem. Phys. Lipids* 2019, *222*, 51-58.

23. T. Ravula, A. Ramamoorthy, *Angew. Chem. Int. Ed. Engl.* 2019, 14925-14928.

24. R. Puthenveetil, K. Nguyen, O. Vinogradova, *Nanotechnol Rev.* 2017, *6*, 111-126.

25. S. Cai, C. Seu, Z. Kovacs, A. D. Sherry, Y. Chen, *J. Am. Chem. Soc.* 2006, *128*, 13474-13478.

26. K. Yamamoto, J. Xu, K. E. Kawulka, J. C. Vederas, A. Ramamoorthy, *J. Am. Chem. Soc.* 2010, *132*, 6929-6931.

27. K. Yamamoto, S. Vivekanandan, A. Ramamoorthy, *J. Phys. Chem. B* 2011, *115*, 12448-12455.

28. V. Kocman, G. M. Di Mauro, G. Veglia, A. Ramamoorthy, *Solid State Nucl. Magn. Reson.* 2019, *102*, 36-46.

29. I. Sengupta, M. Gao, R. J. Arachchige, P. S. Nadaud, T. F. Cunningham, S. Saxena, C. D. Schwieters, C. P. Jaroniec, *J. Biomol. NMR* 2015, *61*, 1-6.

30. G. M. Clore, *Methods Enzymol.* 2015, *564*, 485-497.

31. E. S. Salnikov, F. Aussenac, S. Abel, A. Purea, P. Tordo, O. Ouari, B. Bechinger, *Solid State Nucl. Magn. Reson.* 2019, *100*, 70-76.

32. Q. Z. Ni, E. Daviso, T. V. Can, E. Markhasin, S. K. Jawla, T. M. Swager, R. J. Temkin, J. Herzfeld, R. G. Griffin, *Acc. Chem. Res.* 2013, *46*, 1933-1941.

33. S. V. Dvinskikh, V. Castro, D. Sandström, *Phys. Chem. Chem. Phys.* 2005, *7*, 607-613.

34. M. M. Hoffmann, H. S. Sobstyl, S. J. Seedhouse, *Magn. Reson. Chem.* 2008, *46*, 660-666.

35. C. Lin, D. Yang, *Methods Mol. Biol.* 2017, *1587*, 171-196.

36. M. Mayer, B. Meyer, *Angew. Chem. Int. Ed.* 1999, 38, 1784-1788

37. N. Niccolai, E. Morandi, S. Gardini, V. Costabile, R. Spadaccini, O. Crescenzi, D. Picone, O. Spiga, A. Bernini, *Biochim Biophys Acta Proteins Proteom* 2017, *1865*, 201-207.

38. H. G. Hocking, K. Zangger, T. Madl, *Chemphyschem* 2013, *14*, 3082-3094.

39. C. Hartlmuller, J. C. Gunther, A. C. Wolter, J. Wohnert, M. Sattler, T. Madl, *Sci Rep* 2017, *7*, 5393.

40. C. Hartlmuller, E. Spreitzer, C. Gobl, F. Falsone, T. Madl, *J Biomol NMR* 2019, *73*, 305-317.

41. G. Esposito, A. M. Lesk, H. Molinari, A. Motta, N. Niccolai, A. Pastore, *J Mol Biol* 1992, *224*, 659-670.

42. S. C. Keane, X. Heng, K. Lu, S. Kharytonchyk, V. Ramakrishnan, G. Carter, S. Barton, A. Hosic, A. Florwick, J. Santos, N. C. Bolden, S. McCowin, D. A. Case, B. A. Johnson, M. Salemi, A. Telesnitsky, M. F. Summers, *Science* 2015, *348*, 917-921.

43. P. Niedbalski, C. Parish, Q. Wang, Z. Hayati, L. Song, A. F. Martins, A. D. Sherry, L. Lumata, *J. Phys. Chem. A* 2017, *121*, 9221-9228.

44. E. Ravera, D. Shimon, A. Feintuch, D. Goldfarb, S. Vega, A. Flori, C. Luchinat, L. Menichetti, G. Parigi, *Phys. Chem. Chem. Phys.* 2015, *17*, 26969-26978.

44. J. R. Yarava, S. R. Chaudhari, A. J. Rossini, A. Lesage, L. Emsley, *J. Magn. Reson.* 2017, *277*, 149-153.

45. R. Rogawski, A. E. McDermott, *Arch. Biochem. Biophys.* 2017, *628*, 102-113.

Chapter 6

Conclusions and Outlook

6.1 Summary of Presented Work

The work that has been presented in this thesis can be broken down into 3 main research areas related to polymer lipid nanodiscs. The first is the development of charged hydrophilic groups on the polymer for the formation of nanodiscs with better solubilization stability at low pH and high ion concentrations as shown in Chapters 2 and 3. Chapter 2 describes that an addition of hydrophilic moieties for positive charged or zwitterionic charged polymers allowed for tunability of the nanodiscs solubilization properties. While the addition of an amino group as the hydrophilic moiety allowed for the formation of nanodiscs at acidic pH, the zwitterionic form of the polymer precipitated from solution at neutral pH due to charge-charge interactions. Chapter 3 expounds on what we discovered in Chapter 2 as we developed a polymer with a quaternary ammonium hydrophilic groups. Polymers containing a quaternary ammonium (SMA-QA) showed the ability to form nanodiscs in a wide range of pH and ionic conditions. Nanodiscs formed using SMA-QA also showed a remarkable size control and mono-dispersion.

The second development is the functionalization of a low molecular weight polyacrylic acid (PAA) with various pennant hydrophobic groups that enabled the study and optimization of various hydrophobic groups with regards to polymer-lipid nanodiscs formation as shown in Chapter 4. Our findings presented above show that the addition of hydrophobic groups does greatly

affect the stability of the resulting polymer-lipid nanodiscs. The use of a shorter alkyl butyl chains as the hydrophobic unit leads to a polymer with very poor lipid solubilization properties. Because of the poor properties, the use of butyl-PAA as a nanodiscs forming polymer was determined to be impractical and we discontinued its use for further study. On the other end of the spectrum the longest alkyl chain containing polymer, Hexyl-PAA, had the highest lipid solubilization capability. We found that this is due to the increased amphiphilicity of the polymer, however while Hexyl-PAA had the best solubilization power, it also caused the most lipid bilayer disruption at lower nanodisc sizes as seen by a lowering of lipid melting temperature using DSC. A similar trend was seen with the bulky Neopentyl-PAA as well. Pentyl-PAA was shown to be the optimal polymer for its mix of good solubilization properties, and its enhanced stability at various nanodisc sizes.

Finally, the third is the development of a novel Cu^{2+} chelated polymer for use in paramagnetic relaxation enhancement NMR studies. This system allowed for to faster T1 relaxation rates of the protons of a model biomolecule (DNA g-quadruplex) as shown in Chapter 5. We show that a facile addition of an amino-DOTA to the SMA polymer did not significantly affect the polymer's nanodisc formation properties, but it did allow for the chelation of Cu^{2+}. This metal chelated polymer was able to form polymer-lipid nanodiscs. We showed this metal-polymer system significantly lowered the T_1 times of protons associated to both the polymer styrenes, lipid choline groups, and lipid backbone CH_2 and CH_3. Interestingly we were able to show that the nanodisc system interaction with a DNA G-quadruplex were tunable by varying the amount of salt in solution. We were able to probe this interaction by the T_1 time differences of the DNA protons with and without excess KCl in solution. While we were able to make considerable advances in the field of polymer-lipid nanodiscs by improving on both the hydrophobic and hydrophilic portions of the nanodiscs, and by increasing the NMR applications of SMA by use of metal

chelation for paramagnetic relaxation enhancement, there is still substantial improvements that can be done and subsequent studies with it.

6.2 Potential Future Directions on Polymers and Nanodiscs Systems

In chapters 2, and 3 was presented a useful functionalization of SMA to form different charged polymers with enhanced solubilization stability, and in chapter 4 was discussed the optimization of the hydrophobic moiety on polymer-lipid nanodiscs. One issue that still remains however is there is currently no non-ionic polymers that have been shown to form lipid-nanodiscs. The problem regarding charge is that charge-charge attraction between polymers and the opposite charged proteins can cause protein aggregation, denaturation, or deactivation.[1] These charge-charge interactions can be screened using a high amount of salt (~500 mM) however these conditions are not practicable or biologically relevant. A potentially exciting future development would be the engineering of a neutral charged polymer that forms polymer-lipid nanodiscs. A possible way of achieving this would be following the development of detergents which can

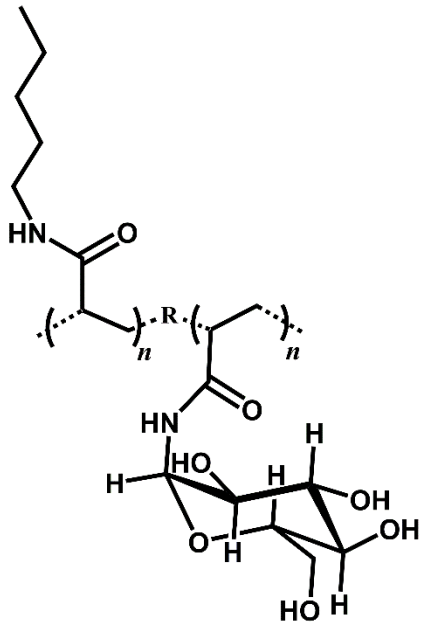

Figure 6-1: potential structure of optimized non-ionic polymer for polymer-lipid nanodiscs

contain a sugars as their hydrophilic moeitys.[2] A polymer that forms nanodiscs using a hydrophobic alkyl moiety and a hydrophilic sugar or polyol based moiety would theoretically provide the optimum system for a majority of membrane proteins (**Figure 6-1**). Using such a polymer should open up various avenues for studying important protein complexes using charge-charge interactions.[1]

6.3 Future Polymer Nanodisc Applications and Conclusion.

Because of its stability and its ability to encapsulate hydrophobic molecules[3] one potential application of polymer-lipid nanodiscs is in drug delivery. Other lipid based drug delivery systems have been developed since the 90s such as liposomes or multi lamellar vesicles.[4] Polymer nanodiscs have characteristics similar to other lipid based platforms. These characteristics are one reason that polymer nanodiscs are a potentially useful drug delivery platform. In addition to the lipid bilayer properties of the nanodiscs the tunability of the polymer belt with various functionalizations may lead to target specific functionalization onto the polymers belt leading to enhanced selectivity of the nanodiscs to different biological targets. The favorable properties of nanodiscs as a lipid based drug carrier system leads to the need for more studies as a drug delivery platform.

Future work on using polymer-lipid nanodiscs system for membrane protein research is ongoing. While studies on membrane protein using nanodiscs have included Cryo-EM[5], NMR[6], FRET[7], and mass-spec[8], there is still a great need for more research into polymer-nanodiscs. While this most likely due to the relative infancy of the polymer-nanodisc field there is still much work to be done studying membrane proteins in the nanodiscs system. NMR is a particularly powerful technique when utilized with nanodiscs. The ability of the nanodiscs, shown in this thesis, to align in the magnetic field allows for future use of the nanodiscs system in solid state NMR as seen with

bicelles.[9] Nanodiscs can also be used not only as a solid state alignment medium but also a partial alignment medium for residual dipolar coupling expermients.[10] With these developments future NMR studies on nanodiscs with biological molecules both in the solid state and solution state need to be done

In order to understand how nanodiscs will effect potential membrane protein targets, further studies on the properties of the nanodiscs themselves need to be done. Because nanodiscs are designed as a membrane mimetic system more insights are needed into how the lipid bilayer of the nanodiscs differ from other lipid bilayer mimetics such as liposomes and bicelles. While chapter 4 uses DSC and solid state NMR to study the stability of the nanodiscs and melting temperature of lipid bilayer, much more work to understand the lipid bilayers' properties is required. In the work presented in this thesis only non-biologically occurring DMPC lipid was used due to its convenient melting point. To understand how a more native like lipid bilayer forms in a polymer-lipid nanodisc system, future studies using naturally occurring lipids such as POPC need to be done leading to future lipid bilayer studies on nanodiscs composing of polymers and cell membrane lipid extracts. These further studies can use not only DSC and NMR but also small angle neutron scattering (SANS), small angle electron scattering (SAXS), and EPR as shown with previous nanodisc and bicelles studies studies.[11-13]

In conclusion, while the work presented in this thesis has demonstrated a marked advancement in the field of polymer-lipid nanodiscs there is still much work to be done in the field. As stated above future chemical optimizations of the polymer still need to be done, along with substantial work needed for the study of polymer nanodiscs formation and lipid bilayer properties. Along with fundamental study on the nanodiscs themselves, the incorporation of a

plethora of unexplored membrane proteins into lipid-nanodiscs opens the path to exciting new studies in the field of protein structural studies.

6.4 Acknowledgements: This study was supported by funds from NIH (GM084018 to A.R.).

6.5 References

1. T. Ravula, N. Z. Hardin, J. Bai, S. C. Im, L. Waskell, A. Ramamoorthy, *ChemComm.* 2018, 54, 9615–9618.

2. S. M. Annela, P. Curnow, P. J. Booth, *BBA-Biomembranes* 2004, 1666, 105-117.

3. T. Ravula[+], N. Z. Hardin[+], S. K. Ramadugu, A. Ramamoorthy, *Langmuir* 2017, 33, 10655–10662.

4. A. Sharma, U. S. Sharma, *Int. J. Pharm*. 1997. 154, 123-140.

5. C. Sun, R. B. Gennis, *Chem. Phys. Lipids*. 2016, 221, 114-119.

6. B. Liang, L. K. Tamm, *Prog. Nucl. Magn. Reson. Spect.* 2018, 105, 41-53.

7. P. Prakash, D. Litwin, H. Liang, S. Sarkar-Banerjee, D. Dolino, Y. Zhou, J. F. Hancock, V. Jayaraman, A. A. Gorfe, *Biophys J.* 2019,116, 179-183.

8. M. Redhair, A. F. Clouser, W. M. Atkins, *Chem. Phys. Lipids* 2019, 220, 14-22.

9. K. Yamamoto, P. Pearcy, A. Ramamoorthy, *Langmuir*, 2014, 30, 1622-1629.

10. T. Ravula, A. Ramamoorthy, *Angew. Chem. Int. Ed. Eng.* 2019, 58, 14295-14928.

11. J. Pencer, T. T. Mills, N. Kucerka, M. P. Nieh, J. Katsaras, *Methods Mol. Biol.* 2007, 398, 231-244.

12. N. G. Brady, S. Qian, B. D. Bruce, *Eur. Polymer J.* 2019, 111, 178-184.

13. A. P. Bali, I. D. Sahu, A. F. Craig, E. E. Clark, K. M. Burridge, M. T. Dolan, C. Dabney-Smith, D. Konkolewicz, G. A. Lorigan, *Chem. Phys. Lipids*, 2019, 220, 6-13.

Appendix

Supporting Information for Chapter 5

A.1 Supplementary Figures

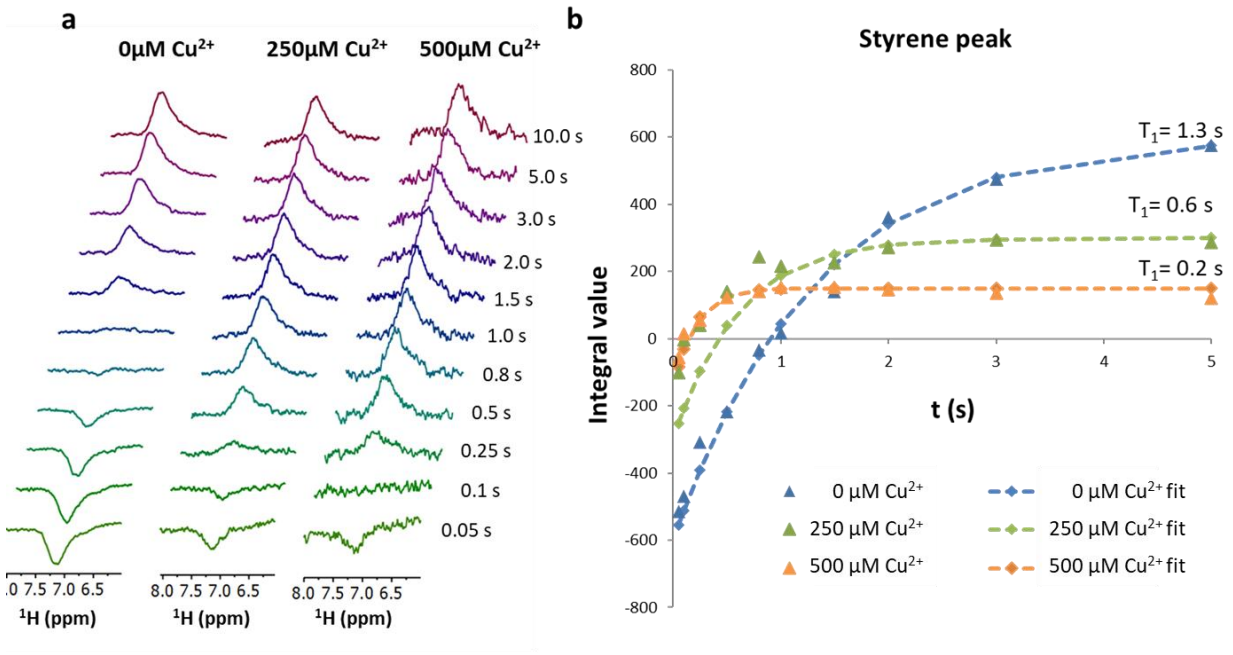

Figure A-1: a) Inversion recovery experimental spectra obtained at different Cu^{2+} concentrations focused on the styrene peak. **b**) Fitting of the styrene peak inversion recovery experiment data and determination of T_1 times. Experiments were conducted at 0, 250 and 500 µM concentrations. The triangles represent the data and the dashed lines are the fits. The spectra were recorded on a 500 MHz NMR spectrometer at 25 °C.

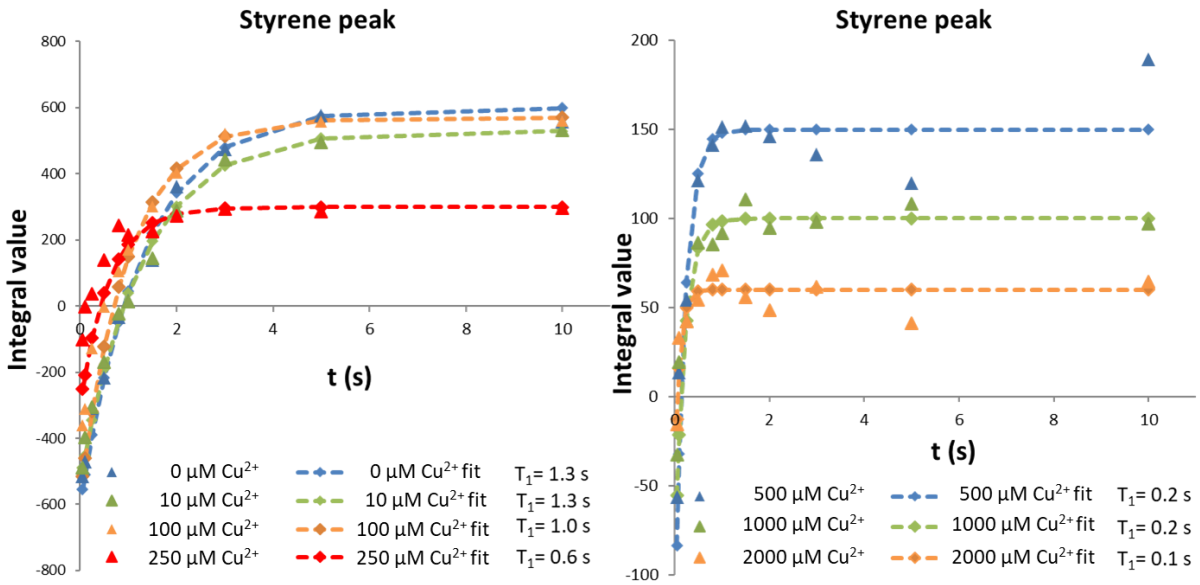

Figure A-2 : Fitting for the styrene peak inversion recovery experiment data recorded on polymer nanodisc samples with concentrations of Cu^{2+} varying between 0 and 2000 µM. The triangles represent the data and the dashed lines are the fits. The spectra were recorded on a 500 MHz NMR spectrometer at 25 °C.

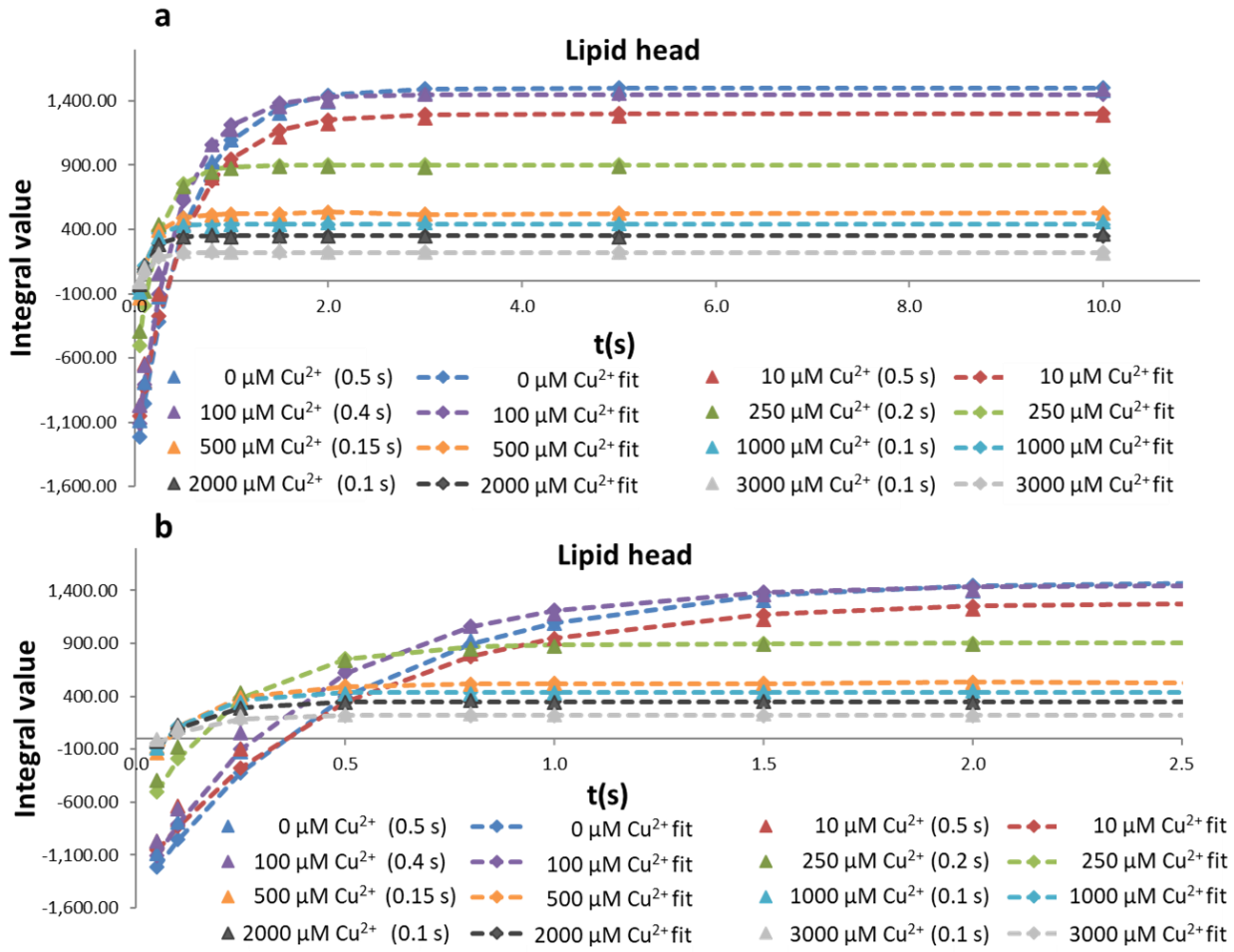

Figure A-3: a) Fitting for the styrene peak inversion recovery experiment data recorded on polymer nanodisc samples with concentrations of Cu^{2+} varying between 0 and 3000 μM. The triangles represent the data and the dashed lines are the fits. **b**) A close-up focus on the data between 0 and 2.5 s so the fitting can be more clearly seen. The spectra were recorded on a 500 MHz NMR spectrometer at 25 °C.

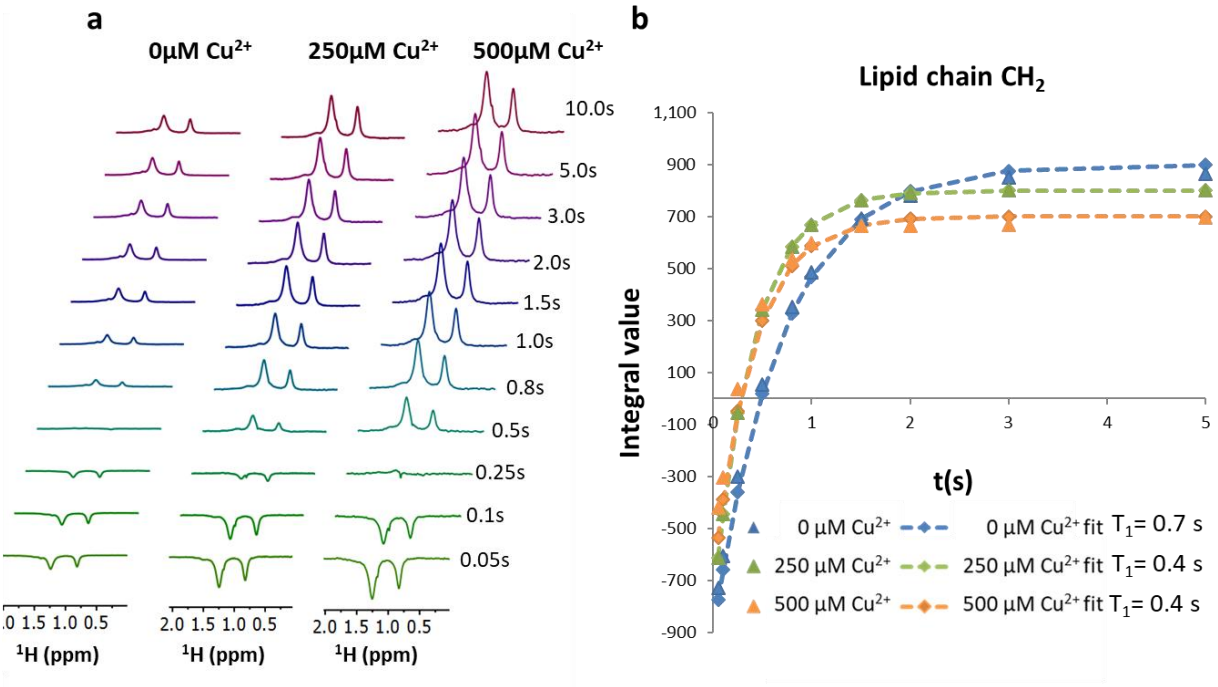

Figure A-4: a) Inversion recovery experiments at different Cu^{2+} concentrations focused on the lipid chain CH_2 peak. **b**) Fitting of the lipid chain CH_2 peak inversion recovery experiment data and determination of the T_1 times. The experiments were conducted using 0, 250 and 500 µM Cu^{2+} concentrations. The triangles represent the data and the dashed lines are the fits. The spectra were recorded on a 500 MHz NMR spectrometer at 25 °C.

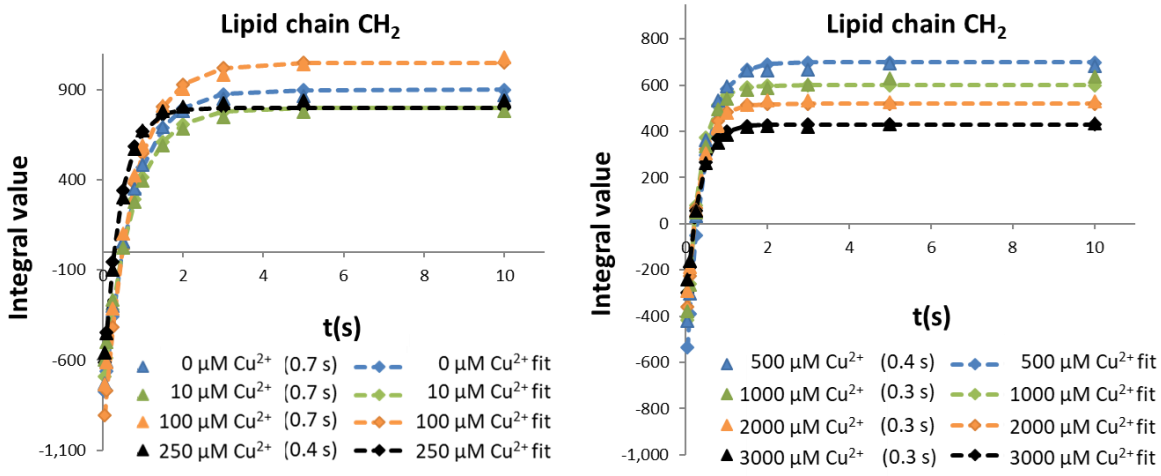

Figure A-5: Fitting for the lipid chain CH_2 peak inversion recovery experiment data recorded on polymer nanodisc samples with concentrations of Cu^{2+} varying between 0 and 3000 µM. The triangles represent the data and the dashed lines are the fits. The spectra were recorded on a 500 MHz NMR spectrometer at 25 °C.

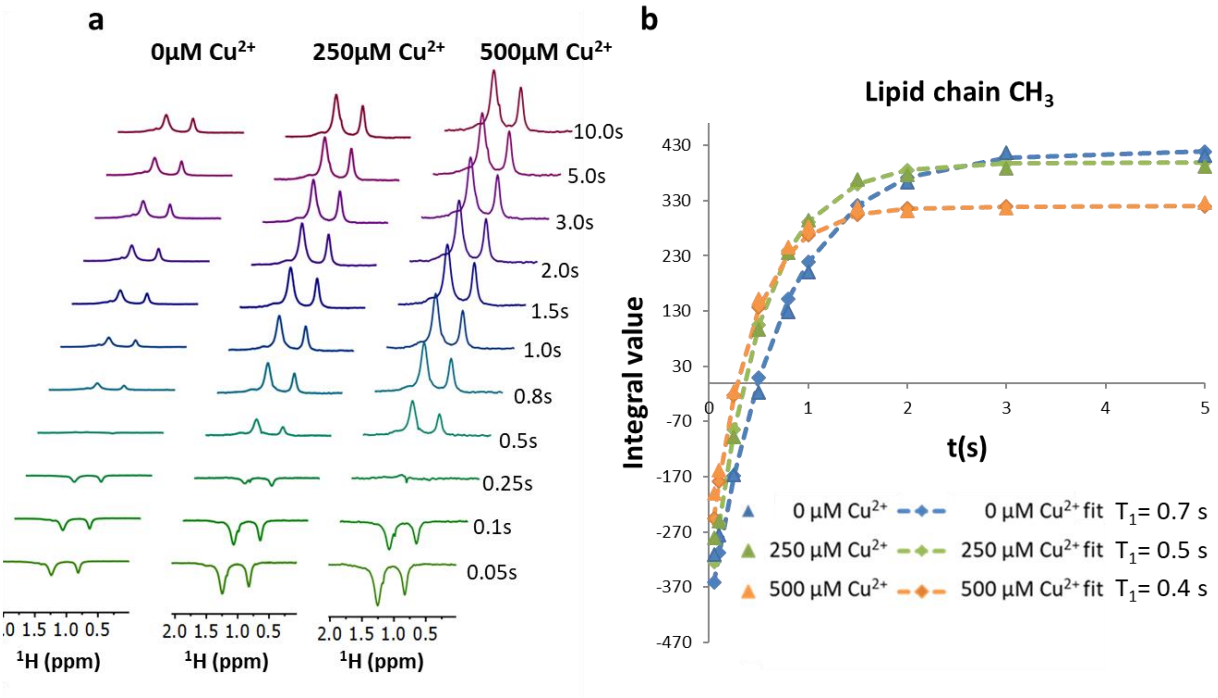

Figure A-6: a) Inversion recovery experiments at different [Cu^{2+}] concentrations focused on the lipid chain CH_3 peak. **b**) Fitting of the lipid chain CH_3 peak inversion recovery experiment data and determination of the T_1 times. The experiments were conducted at 0, 250 and 500 µM concentrations. The triangles represent the data and the dashed lines are the fits. The spectra were recorded on a 500 MHz NMR spectrometer at 25 °C.

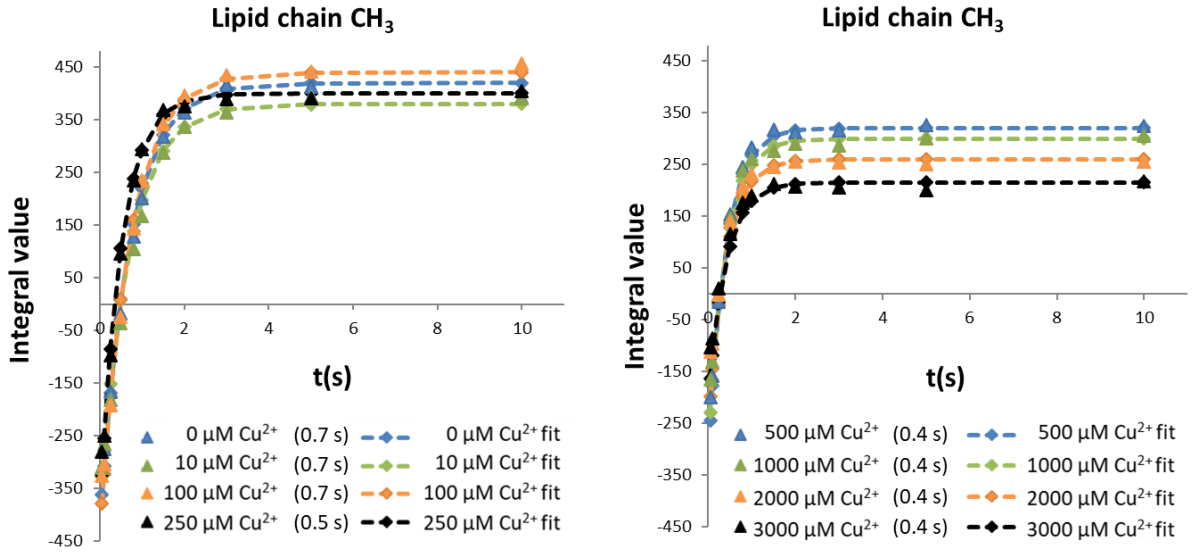

Figure A-7: Fitting for the lipid chain CH_3 peak inversion recovery experiment data recorded on polymer nanodisc samples with concentrations of Cu^{2+} varying between 0 and 3000 µM. The

triangles represent the data and the dashed lines are the fits. The spectra were recorded on a 500 MHz NMR spectrometer at 25 °C.

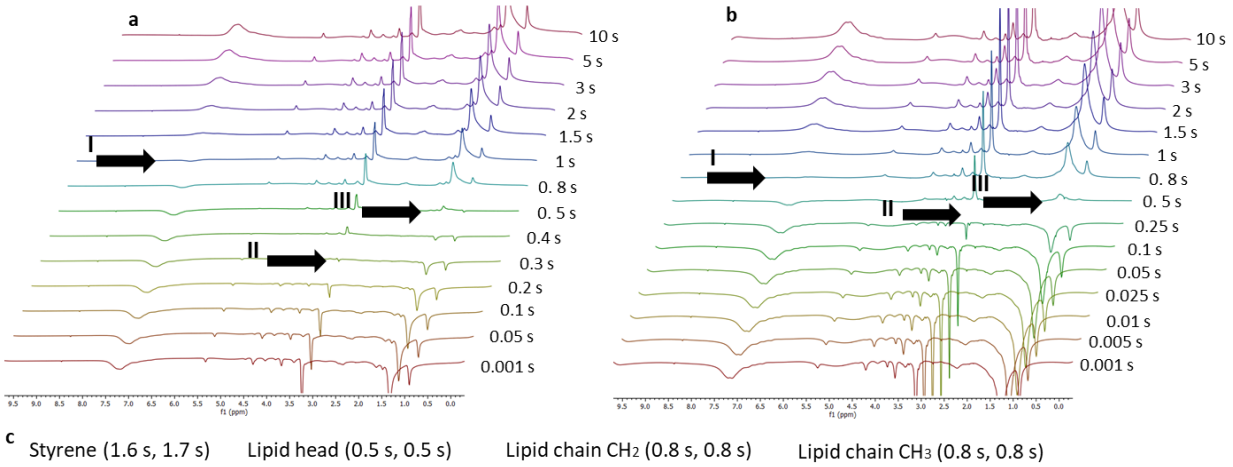

Figure A-8: SMA EA nanodisc without the addition of the DOTA chelator in absence and presence of Cu^{2+} ions. a) The SMA-EA nanodiscs in absence of Cu^{2+} ions b) The SMA-EA nanodiscs in presence of 500 µM Cu^{2+} ions. c) The T_1 values for styrene, lipid head, lipid chain CH_2 and lipid chain CH_3 signals. The first number is the value for the nanodisc in the absence of Cu^{2+} ions. The second number is the value for the SMA-EA nanodiscs in presence of 500 µM Cu^{2+} ions. Roman numerals I, II and III indicate where the intensities of styrene, lipid head and lipid chain peaks, respectively are close to or zero. The spectra were recorded on a 500 MHz NMR spectrometer at 25 °C.

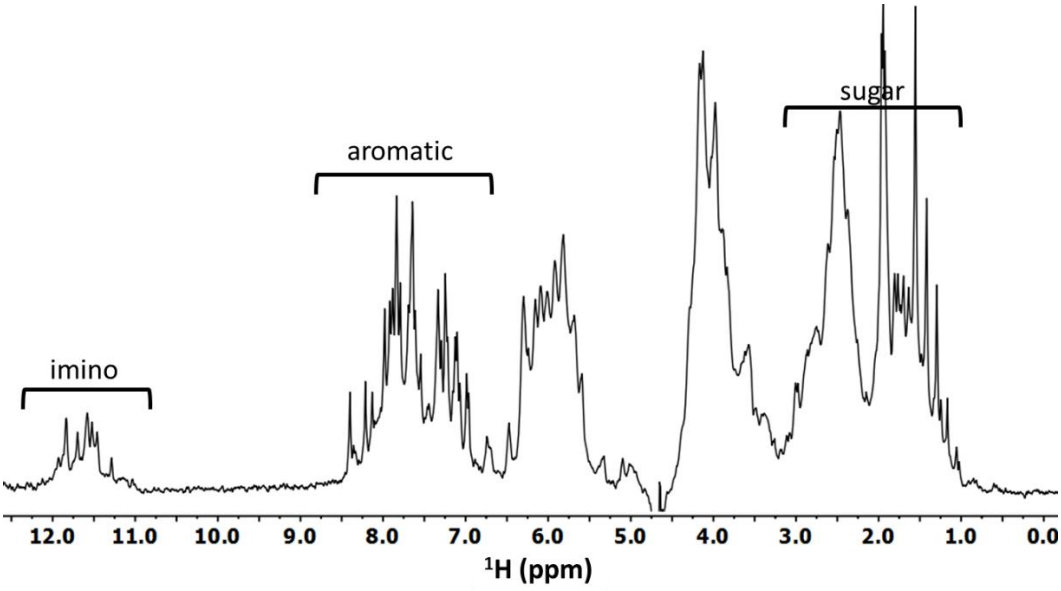

Figure A-9: 1D ^{1}H NMR spectrum of the wtTel23 G-quadruplex. The spectrum was recorded at 0.1 mM oligonucleotide concentration per strand, 100 mM KCl, pH~7.0 and 25 °C on a 500 MHz

spectrometer. The amino, aromatic, and sugar (H2'/H2'') regions are indicated in the above spectra.

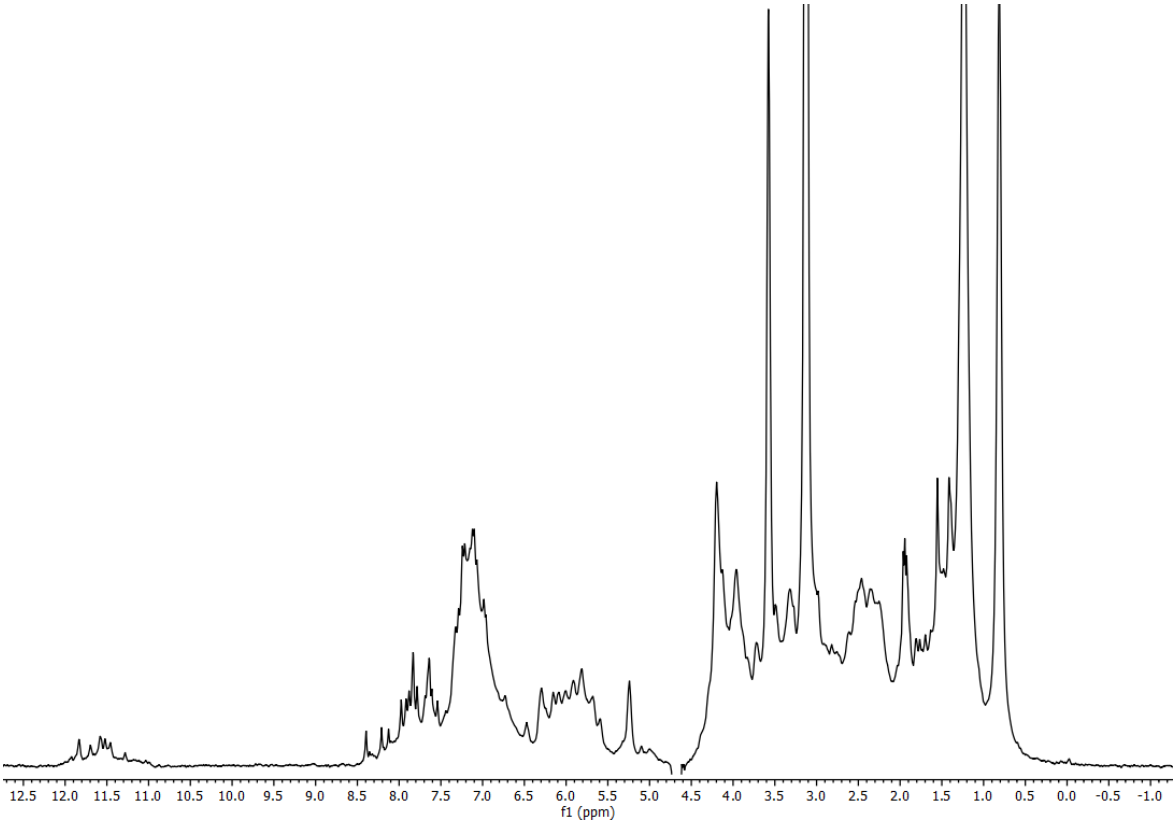

Figure A-10: 1D ^{1}H NMR spectrum of the wtTel23 G-quadruplex in the presence of SMA-EA-DOTA nanodisc. The spectrum was recorded at 0.1 mM oligonucleotide concentration per strand, 100 mM KCl, pH~7.0 and 25 °C on a 500 MHz NMR spectrometer.

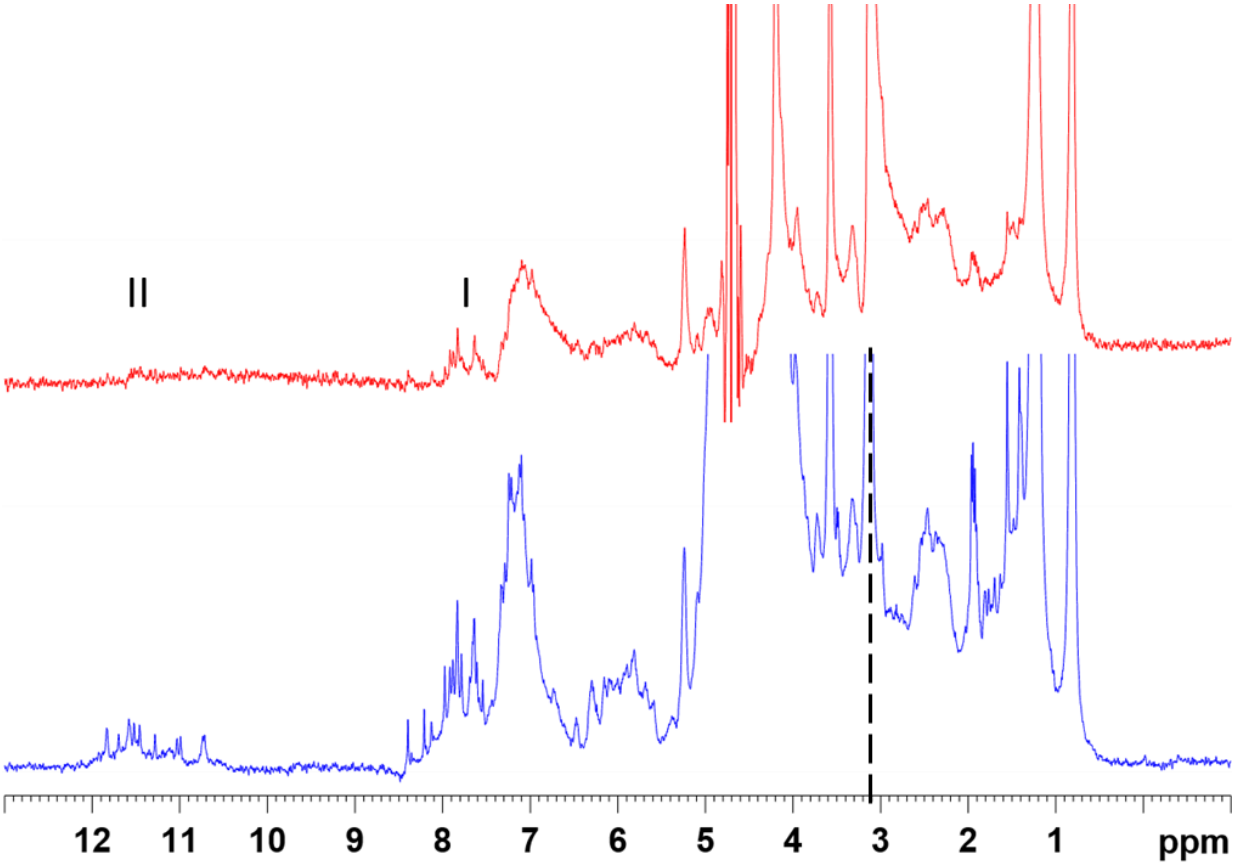

Figure A-11: STD (Saturation-Transfer Difference) NMR spectrum of the wtTel23 G-quadruplex in the presence of the polymer nanodisc. The reference spectrum is shown in blue and the saturation transfer difference spectrum is shown in red. The dotted line indicates the lipid head CH_3 signal that was saturated. The roman numeral I indicates the aromatic signals and the roman numeral II indicates the imino proton signals. The spectrum was recorded at 0.1 mM oligonucleotide concentration per strand, 100 mM KCl, pH~7.0 and 25 °C on a 500 MHz NMR spectrometer. Number of scans = 256, Sweep width = 10000 Hz, offset = 2348.61, 90° pulse = 7.9, Saturation time = 3 s, on resonance excitation = 3.128 ppm, off resonance excitation 40.0 ppm.